FY 1994

February 1995

LBL-PUB--5401

Report on
Lawrence Berkeley Laboratory

Laboratory Directed Research and Development Program

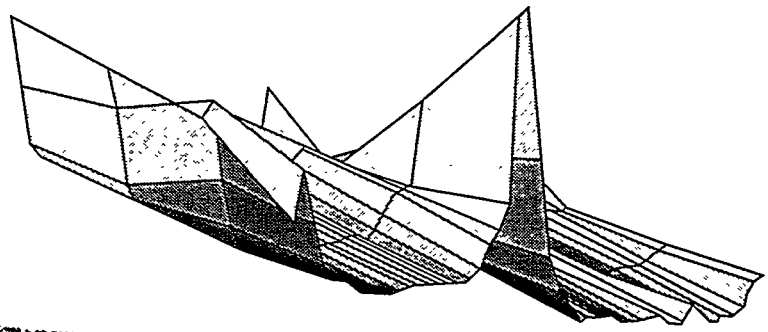

LAWRENCE BERKELEY LABORATORY
UNIVERSITY OF CALIFORNIA
BERKELEY, CALIFORNIA 94720

DLC

DISCLAIMER

DISCLAIMER

Portions of this document may be illegible in electronic image products. Images are produced from the best available original document.

Table of Contents

Introduction

The *Lawrence Berkeley Laboratory (LBL) Laboratory Directed Research and Development Program FY 1994* report is compiled from annual reports submitted by principal investigators following the close of the fiscal year. This report describes the projects supported and summarizes their accomplishments. It constitutes a part of the Laboratory Directed Research and Development (LDRD) program planning and documentation process that includes an annual planning cycle, projection selection, implementation, and review.

The LBL LDRD program is a critical tool for directing the Laboratory's forefront scientific research capabilities toward vital, excellent, and emerging scientific challenges. The program provides the resources for LBL scientists to make rapid and significant contributions to critical national science and technology problems. The LDRD also advances the Laboratory's core competencies, foundations, and scientific capability, and permits exploration of exciting new opportunities. Areas eligible for support include:

- Work in forefront areas of science and technology that enrich Laboratory research and development capability;
- Advanced study of new hypotheses, new experiments, and innovative approaches to develop new concepts or knowledge;
- Experiments directed toward proof of principle for initial hypothesis testing or verification; and
- Conception and preliminary technical analysis to explore possible instrumentation, experimental facilities, or new devices.

The LDRD program supports LBL's mission in many ways. First, because LDRD funds can be allocated within a relatively short time frame, LBL researchers can support the mission of DOE and serve the needs of the nation by quickly responding to forefront scientific problems. Second, LDRD enables the Laboratory to attract and retain highly qualified scientists, and supports their efforts to carry out world-leading research. Finally, the LDRD program also supports new projects that involve graduate students and postdoctoral fellows, thus contributing to the education mission of the Laboratory.

LBL has a formal process for allocation of funds for LDRD. The process relies on individual scientific investigators and the scientific leadership of the Laboratory to identify opportunities that will contribute to scientific and institutional goals. The process is also designed to maintain compliance with DOE Orders, in particular DOE Order 5000.4A. From year to year, the distribution of funds among the scientific program areas will change. This flexibility optimizes the Laboratory's ability to respond to opportunities.

Laboratory LDRD policy and program decisions are the responsibility of the Laboratory Director. The Director has assigned general programmatic oversight responsibility to the Laboratory Deputy Director. Administration and reporting on the LDRD program is supported by the Office for Planning and Communications. LDRD accounting procedures and financial management are consistent with the Laboratory's accounting principles and stipulations under the contract between the University of California and the Department of Energy, with accounting maintained through the Laboratory's Chief Financial Officer.

In FY 1994, LBL was authorized by the Department of Energy to establish a funding ceiling for LDRD based on 3% of the Laboratory's FY 1994 operating budget. This funding level was provided to develop new scientific ideas and opportunities and allow the Laboratory Director an opportunity to initiate new directions. However, budget constraints limited available resources, so only $5.4 M was allocated.

In FY 1994, scientists submitted 158 proposals requesting over $20 M. A total of 52 projects were funded, with awards ranging from $18 K to $488 K. These projects are summarized in Table 1.

Table 1: FY 1994 Laboratory Directed Research and Development Program.

Investigator	Project Title	($)
Accelerator and Fusion Research Division		
Andris Faltens Lou Reginato Peter Seidl	Experimental Investigation of High-Average-Power Applications of Ion Induction Linacs	140,800
Richard Gough	Femtosecond X-ray Pulse Generation	487,700
Chemical Sciences Division		
Robert G. Bergman Bruce M. Novak Tara Y. Meyer S. Joyce Yu Keith A. Woerpel	Exploration of the Interface Between Homogeneous and Heterogeneous Catalysis: Synthesis and Study of Organometallic Catalysts Supported on Novel Polysiloxane Materials with Controllable Solubility Properties	74,900
Charles B. Harris	Ultrafast Dynamics of Electrons at Surfaces	99,400
David K. Shuh	Structure and Chemistry of Nonmetallic Adsorbates at Compound Semiconductor Interfaces Investigated by Synchrotron Radiation Techniques	74,300
Earth Sciences Division		
Harvey E. Doner Mavrik Zavarin Ronald G. Amundson	Application of the Advanced Light Source to the Study of Trace Element Adsorption and Distribution in Soil Carbonates	17,800
Donald DePaolo Mark Conrad Terrance Leighton Bob Buchanan	Characterization and Monitoring of Subsurface Biologic Activity Using Stable Isotope Soil Gas Analysis	78,400
Hoi-Ying Holman Yvonne Tsang	Microbial Transformation of Petroleum Hydrocarbons in Transient Subsurface Environment	99,500
Tetsu K. Tokunaga	X-ray Microprobe Tests of Models for Selenium and Chromium Partitioning in Contaminated Sediments	71,000
Energy and Environment Division		
Haider Taha Tom Wenzel Mark D. Levine	Alternative Strategies to Improve Air Quality in the Los Angeles Basin	100,000
Michael D. Rubin Eicke R. Weber	Defect Characterization of GaN and Fabrication of Blue LEDs	87,600
Engineering Division		
Joseph M. Jaklevic Joycelyn C. Schultz	Development of Microchemical Methods for Biological Assays	94,700

Table 1. Continued.

Investigator	Project Title	($)
Joseph E. Katz Charles S. Fadley Helmuth Spieler	Development of Next-Generation Detectors for Use at the Advanced Light Source	115,300
Environment, Health and Safety Division		
Brian M. Smith Leticia B. Menchaca	Demonstration of Stable Isotope Tracer Methods in Detailed Hydrogeologic Modeling and Monitoring	135,900
Information and Computing Sciences Division		
Bahram Parvin William Johnston Ulrich Dahmen Daniel Callahan Marcos Maestre Robert Liburdy	Visual Servoing for Scientific Applications	142,600
Life Sciences Division		
Teresa Head-Gordon	A Comprehensive Approach to Protein Folding	99,200
Bing K. Jap	Electron Crystallography of Selected Membrane Proteins	80,000
Maria Pallavicini George Brecher Malak Shoukry	Biological Dosimetry and Risk Assessment: Propagation of Genetically Damaged Hemopoietic Stem Cell Progeny	44,600
Mark S. Roos Sam T.S. Wong Thomas F. Budinger	Head Probe for Nuclear Magnetic Resonance Imaging and Spectroscopy at 10 T	50,000
Edwin M. Rubin Jan-Fang Cheng	Creation of Transgenic Mice Containing a Library of P1 Clones Encompassing the Down's Syndrome Region from Chromosome 21	189,900
G. Shyamala	A Transgenic Model for Clinical Testing of Progestins and Analysis of Progesterone Receptor Function	59,800
Diane L. Tribble Edward M. Rubin Elaine L. Gong Mary-Helen Barcellos-Hoff	Variations in Susceptibility to Environmental Oxidants as Studied Using Transgenic Mice	125,400
Materials Sciences Division		
Jeffrey Bokor	Electronic Thermalization in Metals and Semiconductors	169,500
Deborah Charych	Novel Polymeric Thin Films for Entrapment and Detection of Small Organic Molecules	58,900
Shimon Weiss Frank Ogletree Daniel S. Chemla	Time- and Frequency-Resolved Spectroscopy of Single Nanostuctures and Clusters	133,500

Table 1. Continued.

Investigator	Project Title	($)
John Clarke	Electron-Beam Lithographic Fabrication of Submicron Junctions for Coulomb Blockade Arrays	59,000
Ulrich Dahmen	New Directions for *In Situ* Electron Microscopy at High Spatial Resolution	100,400
Charles S. Fadley	Structural Studies of Adsorbates and Magnetic Systems with Circular-Polarized Synchrotron Radiation and Photoelectron Spin Resolution	91,500
Eugene E. Haller Wladyslaw Walukiewicz	Isotope Heterostructures Selectively Doped by Neutron Transmutation	70,100
Dung-Hai Lee	Quantum Hall Plateau Transitions of a Two-Dimensional Electron Gas in Strong Magnetic Fields	18,300
Roya Maboudian	Fundamental Investigations of the Chemical Vapor Deposition of Ge, GaAs, and ZnSe on Si	42,100
Paul L. McEuen	Electron Transport in Nanostructures	74,500
Joseph Orenstein Stuart Parkin	Infrared and Terahertz Spectroscopy of Artificially Structured Magnets	94,400
Norman Phillips	Establishment of the Thermodynamic Temperature Scale in the mK Region	76,700
Zi Q. Qiu	Investigation of Nanometer Magnetism by Using Surface Magneto-Optic Kerr Effect (SMOKE)	25,700
R.O. Ritchie	Fundamental Relationships Between Mechanical Properties and Structure in Diamond Films	40,500
Miquel Salmeron	Atom-by-Atom Chemistry and Processes by Low-Temperature (4 K) Scanning Tunneling Microscope	75,500
Peter G. Schultz John Clarke	Catalytic Atomic Force Microscopy	56,200
Peter G. Schultz Xiao-dong Xiang	Combinatorial Synthesis of High T_c Superconductors	184,800
Neville Smith	Spin-Polarized Photoemission Studies of Magnetic Surfaces, Interfaces, and Films	124,300
Harry W.K. Tom	Time-Resolved Studies of VUV, XUV, and Soft-X-ray Photo-Induced Chemistry at Surfaces	64,600
Nuclear Science Division		
Stuart Freedman	Laser Trapping of Radioactive Atoms	140,300
J. Michael Nitschke	New Concepts in IsoSpin Studies	113,700
Howard H. Wieman Wen G. Gong John W. Harris Jeffery T. Mitchell	Microstrip Gas Chambers for TPC Readout	45,200

Table 1. Continued.

Investigator	Project Title	($)
Physics Division		
Gerald S. Abrams Alessandra Ciocio Patrick LeDu	The Portable DAQ: A Data Acquisition System for Particle Physics Based on Standardized Tools and Techniques	93,500
Alexandre Chorin Paul Concus James Sethian	Chemical/Hydrodynamical Computational Models for Combustion Systems	20,000
Natalie Roe	New Si Microstrip Disk Detector for Vertex Reconstruction of B Meson Decays	80,000
Majorie Shapiro	Evaluation of Trigger Algorithms for an Upgraded Silicon Microvertex Detector	37,000
George F. Smoot	Directions for a Particle Astrophysics Initiative: Additional Observations of the Cosmic Microwave Background	125,000
Structural Biology Division		
Rosalind Kim	Hyperthermophilic Microorganisms	108,000
Yeon-Kyun Shin	A Molecular Description of Transmembrane Signaling	72,700
Multidivisional		
Saly Benson Nancy Brown Joan Daisey Lois Gold	SELECT, Development of a Site Remediation Analysis and Decision Support Software	375,300
TOTAL		5,240,200

Accelerator and Fusion Research Division

Experimental Investigation of High-Average-Power Applications of Ion Induction Linacs

Principal Investigators: Andris Faltens, Lou Reginato, and Peter Seidl

Project No.: 94001

Funding: $140,800 (FY 94)

Project Description

The purpose of this project is to examine the suitability of induction linacs for neutron production for a wide variety of applications, including cancer therapy, a pulsed neutron source for research, materials testing for fusion reactors, advanced fissile power production and breeding, and waste transmutation. The general approach to the majority of these applications is to accelerate protons or deuterons to energies typically between 500 MeV and 2 GeV, impinge them upon a heavy metal target to produce some tens of spallation neutrons per proton or deuteron, and then let the neutrons interact with the remaining material in the target assembly in the desired manner. The highest-average-power proton accelerator in existence is LAMPF, which produces an average beam power of 1 MW with an average beam current of 1 mA. Operation of this machine was for some years limited to lower currents because of beam spill and activation. The desired average currents for the new applications range from a few mA all the way up to 1 A, and peak currents in the pulsed neutron source application of 100 A. Such high peak and average currents are well beyond the experience level of rf accelerators. On the other hand, currents exceeding 1 kA have been routinely accelerated in induction linacs, but the efficiency, reliability, and longevity data are nonexistent. The beam spill and activation issue is different in an induction linac from that in an rf linac because a very large diameter bore can be used in the induction linac without a major reduction in efficiency. To add to the database for the possible future applications of induction linacs, a test stand comprising a new high-efficiency solid-state pulser and new low-loss induction cores was assembled and used to demonstrate achievable system efficiency and pulse repetition rates for the various applications. Afterward, the system was allowed to pulse for a large number of pulses to obtain operational reliability data.

Accomplishments

The intended goals of the induction module pulsing experiment were met. An induction core assembly and a solid-state pulser were assembled and pulsed at a high repetition rate for more than 100 million pulses in an arrangement that demonstrated that more than one-half of the total power used would go into a simulated beam, corresponding to an efficiency that is very good compared to other possible methods of acceleration.

At this time, there are proposals to construct pulsed neutron sources in the U.S. and Europe, and there is interest in neutron production to produce tritium, test fusion reactor wall materials, transmute high-level waste, and burn up excess plutonium. The present research was limited to the technical questions of lifetime, efficiency, and reliability of a modern induction linac for such applications. The equally important question of cost was not addressed; in future work, costs could be reduced by searching for an optimum by adjusting charge per pulse and the rep rate, for a fixed average current, and by adjusting the acceleration schedule, in a manner similar to that done for the Heavy Ion Fusion designs, and by working on the actual hardware. With such work, it is possible that the induction linac will be competitive on cost as well as on the technical requirements.

The experiment comprised a set of induction cores, a resistive load to simulate beam loading, a large capacitor with a series FET switch, an isolation inductor for the bias circuit, a high-voltage power supply with an isolating charging resistor, and a bias current supply. The capacitor was chosen to be large enough to keep the pulse droop to the 1% level. Snubbing circuits were used to decrease the switching transients, and the FET switch itself had zener diodes for this function. The cabling between the pulser and the induction cores was

made with very low inductance to decrease these switching transients.

The diagnostics consisted of current transformers in the drive leads and in the lead going to the simulated beam load, and independent (i.e., non-current-carrying loops) around the induction cores to measure the pulse voltage. There were also dc meters for the bias circuit voltage and current and for the high-voltage-supply current and voltage. The actual experiment was essentially to establish the operating characteristics of the core and pulser assembly, which requires only a few pulses, and then to let the system pulse for a long enough time to establish reliability. The initial tests started with a low voltage on the capacitor and at a low rep rate. As confidence was gained, both were increased. The lowest application of interest requires operation at 50 pulses per second; the first long operating sequence was with a 72-pps rate with a 10-kV output pulse. The essential features of the output waveforms are: risetime 150 ns; flat top 1 μs; falltime 100 ns; core current increasing from 160 A to 320 A, and a "beam" load current of 750 A. It should be noted that the load current of 750 amps greatly exceeds the core drive current. When all of the other losses are included, this operation had an efficiency of 47%. Higher load currents had higher efficiency but started to deteriorate the pulse risetimes and falltimes. The longest run was with a load corresponding to the pulser driving two induction core sets in parallel, so the beam would get twice the pulser output voltage. This run was for a total of 200 million pulses at a 100 pps rep rate.

These tests helped establish that the induction module technology in its present state is ready to operate at much higher rep rates than have been required in recent machines, which are of the order of 1 pps. Part of the measurements included occasional temperature measurements of the core assembly. With natural air convection the only cooling , the hot spots did not exceed 40 °C temperature rise on the surface and an additional calculated 5 °C from the surface to the interior of the core winding. With forced cooling or immersion in an insulating bath that is also able to provide the cooling, much higher repetition rates would be possible. During these tests the induction cores and pulser operated without any failures.

Publication

W. Barletta, A. Faltens, E. Henestroza, and E. Lee, "High Current Induction Linacs," Accelerator Driven Transmutation Technology Conference, Las Vegas, NV, July 1994.

Femtosecond X-ray Pulse Generation

Principal Investigator: Richard Gough

Project No.: 93002

Funding: $487,700 (FY 94)
$477,700 (FY 93)

Project Description

The purpose of this project is to develop a novel tunable source of femtosecond x-rays based on right-angle Thomson scattering using terawatt laser pulses with a tightly focused beam of relativistic electrons. The generated x-rays are strongly forward directed (along the electron beam) and are of femtosecond duration because the interaction time is limited by the transverse dimension of the focused electron beam. Femtosecond x-ray pulses are potentially important to the study of fast chemical reactions in a time-resolved manner, coherent intramolecular dynamics in chemistry, and phonon dynamics in the solid state.

The source characteristics can be calculated from an equivalent magnetic undulator model. Using the measured laser and electron-beam parameters, we expect to generate a 0.43 Å x-ray pulse with a temporal duration of 170 fs containing about 10^5 photons within a 10% bandwidth.

Accomplishments

In FY 94, both the Beam Test Facility and the terawatt laser system have been brought into operation, and we have achieved significant milestones in parameterizing both the electron and

laser beams. Construction of the bend section of the Beam Test Facility transport line was completed on March 25. The first beam was transported through the bend section of the Beam Test Facility one day later. Construction of the transport line, including the installation of the x-ray interaction chamber, 60° bending magnet, and beam dump, was completed by early June. A wide variety of electron-beam diagnostics have been implemented and made operational. These include an integrating current transformer for absolute single-bunch charge measurements, five nondestructive beam position monitors, five fluorescent screens, and two diagnostic stations based on optical transition radiation (OTR). Using OTR, we have been able to measure the electron-beam energy, beam size and divergence, and, hence, the beam emittance on a single-bunch and single-shot basis. In addition, the electron-bunch temporal profile has been obtained from OTR using an online streak camera system.

We have measured electron beam sizes in the x-ray interaction chamber well below 100 μm in both the vertical and horizontal plane and an absolute pointing stability of better than 25 μm.

The laser system has been built and has generated laser pulses with a duration as short as 50 fs and a peak power of 2.5 TW at a repetition rate of 10 Hz. The complete laser system has been moved to the Beam Test Facility. Timing jitter between the laser pulses and the electron-beam bunches has been measured using the OTR diagnostic system to be better than 2.5 ps, which is about one tenth of the electron-bunch length.

Development of spatially, spectrally, and temporally resolving x-ray diagnostic systems is also well under way. This includes evaluation of the intensity and spectrum of the x-ray background and femtosecond x-ray radiation using phosphor screens and Ge detectors, measurement of the x-ray pulse duration with picosecond time resolution using conventional x-ray streak cameras, and development of a cross-correlation technique with potential femtosecond time resolution.

Publications

B. van der Geer, M. de Loos, and W. P. Leemans, "Characterization of the 50 MeV ALS Linac Beam with Optical Transition Radiation," *Proceedings of the 1994 European Particle Acceleration Conference*, London, U.K.; LBL-34973a.

W. Leemans, S. Chattopadhyay, M. Conde, E. Glover, K.- J. Kim, R. Schoenlein, and C.V. Shank, "Status of the LBL Experiment on Femtosecond X-ray Generation through 90° Thomson Scattering," *Proceedings of the 1994 European Particle Acceleration Conference*, London, U.K.; LBL-34971a.

W. Leemans, R. Schoenlein, A. Chin, E. Glover, M. Conde, S. Chattopadhyay, K.-J. Kim, and C.V. Shank, "Femtosecond X-ray Generation Through 90° Thomson Scattering: Status of the LBL Experiment," *AIP Proceedings of the 6th Advanced Accelerator Workshop*, Lake Geneva, WI, June 12–18, 1994, in press; LBL-36369.

Chemical Sciences Division

Exploration of the Interface Between Homogeneous and Heterogeneous Catalysis: Synthesis and Study of Organometallic Catalysts Supported on Novel Polysiloxane Materials with Controllable Solubility Properties

Principal Investigators: Robert G. Bergman and Bruce M. Novak

Postdoctoral Coworkers: Tara Y. Meyer, S. Joyce Yu, and Keith A. Woerpel

Project No.: 92002

Funding: $74,900 (FY 94)
$118,900 (FY 93)
$69,600 (FY 92)

Project Description

Both homogeneous and heterogeneous catalysis are used by the chemical industry for conversion of feedstocks to commercial chemical products. Heterogeneous catalysts offer the practical advantage of catalyst stability and ease of processing. However, the structures of heterogeneous catalysts and the mechanisms of their reactions cannot be studied easily, and therefore it has historically been difficult to design or modify them in a rational way.

Homogeneous catalysts are more difficult to use, but nevertheless are employed in several large-scale processes (e.g., hydroformylation, methanol carbonylation) because they provide selectivity or chemistry not available in heterogeneous systems. They are almost always more highly characterized than their heterogeneous counterparts, and the mechanisms of their reactions are better understood. As a result, homogeneous catalytic processes are typically more amenable to improvement by systematic structural modification.

In view of the complementary advantages of homogeneous and heterogeneous catalysts, for several years there has been intense interest in developing "hybrid" catalysts that combine the useful properties of both types of systems. An important approach to achieving this goal has been the development of systems in which well-characterized homogeneous catalysts are "heterogenized"—i.e., they are covalently attached to robust solid supports.

Silica gel is one of the most important and widely used supports for organometallic catalysts. The goal of this project was the understanding of silica support-catalyst interactions through a continuum approach, wherein the boundary between homogeneous and heterogeneous catalysis systems will be incrementally traversed.

Accomplishments

In one phase of this project, we prepared soluble polysiloxane supports that consisted of polysilicic acid oligomers in which the free silanols were partially capped with trimethylsilyl groups. These polysiloxane supports were treated with both zirconium and iridium substrates to produce bound-metal complexes. Consistent with observations in analogous heterogeneous systems, the zirconium substrates, $Zr(CH_2CMe_3)_4$, $Zr(CH_2Ph)_4$, $(\eta^5\text{-}C_5(CH_3)_5)ZrNp_3$ and Cp_2ZrMe_2, bind to the polysiloxane supports by silanol protonation of one or more alkyl groups. The resulting polysiloxane-bound zirconium species are soluble in hydrocarbon and ethereal solvents, allowing them to be characterized by NMR spectroscopy. Activation of these catalysts by treatment with hydrogen resulted in gellation in the cases of $Zr(CH_2CMe_3)_4$ and $Zr(CH_2Ph)_4$, but use of the more sterically demanding and less labile Cp* ($Cp^* = \eta^5\text{-}C_5(CH_3)_5$) ligand in the Cp^*ZrNp_3 substrate resolved this problem. Preliminary efforts were made to characterize the resulting supported metal hydride complex and to investigate its catalytic activity.

In the second part of the project, we investigated the reaction of $Cp^*Ir(OH)(PMe_3)(Ph)$, a well-characterized organometallic hydroxo complex, with both the soluble polysiloxane polymer and with silica itself. The latter experiments were quite successful, and produced the bound-metal complex Cp*Ir(Osilica)(PMe_3)(Ph), the metal complex binding to the support by exchange of the hydroxide for a silanol group. This class of ligand

exchange was further exploited to cleave the iridium complex from the support by reaction with phenol. Isolation of the cleavage product $Cp^*Ir(OPh)(PMe_3)(Ph)$ confirmed that the complex had resisted irreversible structural changes upon binding.

The supported complex also undergoes clean stoichiometric chemistry with organic reagents. For example, on treatment with acetylene dicarboxylate the supported iridium complex reacts and then releases an organic product with a new metallacyclic ring. This chemistry is summarized in Fig. 1. Thus the starting iridium complexes can be (1) supported on silica, (2) removed in intact molecular form and fully characterized, and (3) converted to a new supported complex that also can be removed in intact molecular form and characterized. To our knowledge this is the first time that it has been possible to utilize the polymeric silica support as an apparently simple and detachable ligand in an organometallic transformation. In addition, in the phenol reaction it appears that substituted phenols with different acidities (pK_a's) remove different amounts of the supported iridium complex from the silica. Preliminary data suggest that this reaction may be useful for mapping silica sites with differing iridium affinities.

Publication

T.Y. Meyer, K.A.Woerpel, R.G. Bergman, and B.M. Novak, "Silica as a Ligand for Transition Metal Centers: Reversible Attachment and Displacement of Iridium(I) from a Silica Support," *J. Am. Chem. Soc.* (in press).

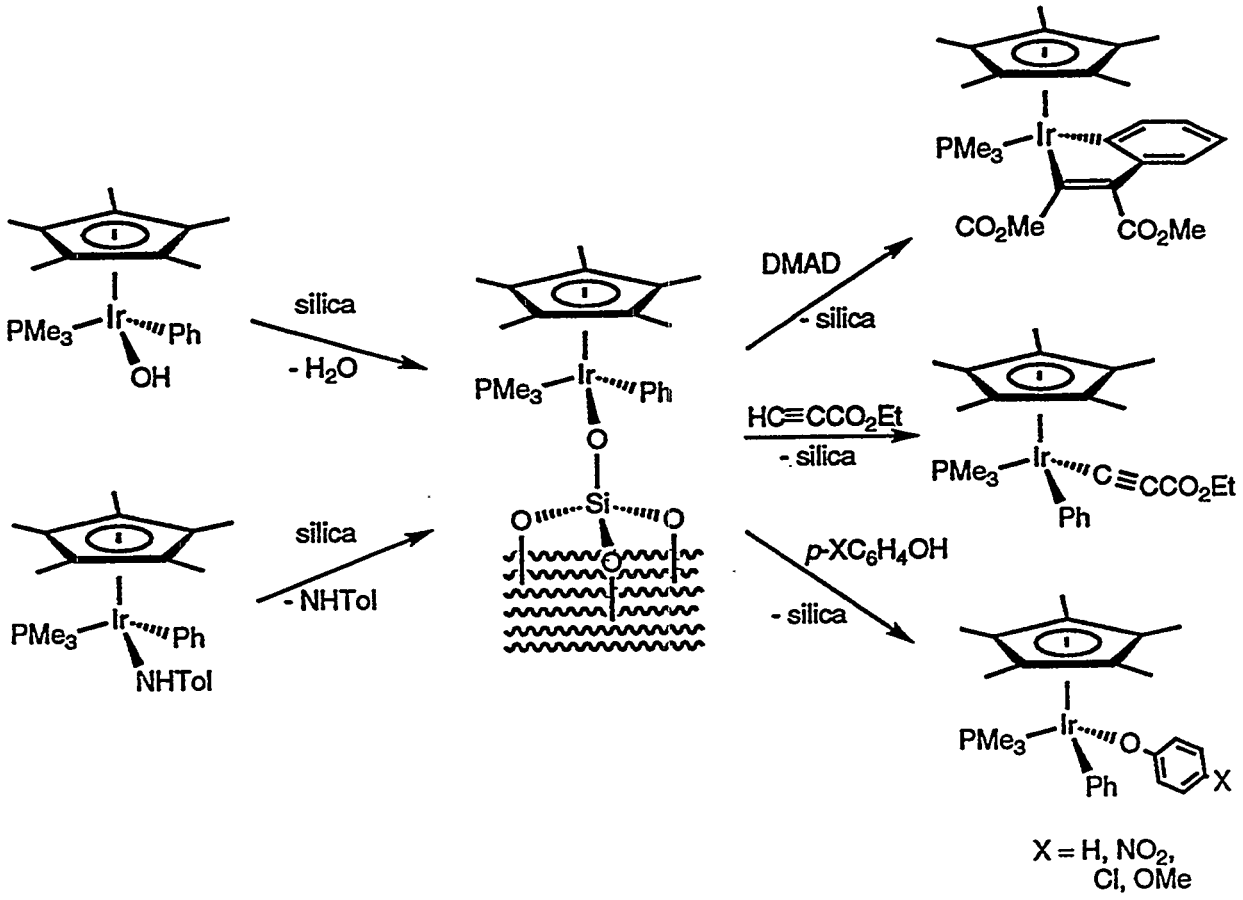

Fig. 1. Chemical reactions observed with the silica-supported (η^5-$C_5(CH_3)_5$)Ir(PMe_3)(Ph) fragment.

Ultrafast Dynamics of Electrons at Surfaces

Principal Investigator: Charles B. Harris

Project No.: 92003

Funding: $99,400 (FY 94)
$100,400 (FY 93)
$125,400 (FY 92)

Project Description

We are developing techniques to examine with unprecedented precision the spectroscopy and dynamics of surface electronic excitations at interfaces. Using angle-resolved two-photon photoemission, one can study the band structure of electronically excited states at surfaces. The use of fiber-optic/grating-pair pulse compression with a picosecond laser system makes possible direct measurement of excited-state lifetimes on the femtosecond time scale. This provides a unique ability to explore excited-state dynamics of electrons at metal-dielectric interfaces.

The electronic dynamics of surfaces are involved in many problems of fundamental interest from two-dimensional magnetism to chemisorption. Directly related areas of technological significance include surface photochemistry, laser-surface interactions such as damage mechanisms in optics, surface recombination that can dominate carrier lifetimes at semiconductor interfaces, and magnetic data storage devices. A surface electronic state is characterized not only by its energy, but also by its momentum parallel to the surface. Energy transfer between states requires that both these quantities be conserved. Thus a complete understanding of excited-state dynamics requires time, energy, and momentum resolution.

The conventional means of determining the band structure of excited surface electronic states is k-resolved inverse photoemission spectroscopy. This technique has been very successful but has limited energy resolution and cannot be time-resolved. Scanning tunneling spectroscopy provides information on unoccupied energy levels with atomic resolution, but also has limited energy resolution and cannot provide time or momentum resolution (except in a few very special cases not of interest to chemistry). The newer method of two-photon photoemission (TPPE) has an order of magnitude better energy resolution than either of the aforementioned techniques and the potential to directly measure lifetimes.

We employ an unusual electron time-of-flight detection scheme that gives high sensitivity and extreme precision in energy measurements. Samples are mounted on a goniometer angle-drive mechanism that was designed and built in our laboratory and is superior to commercially available systems. This apparatus allows parallel momentum measurements and the determination of band structure. Liquid helium cooling of the sample to 45 K enables study of a wide variety of physisorbed and chemisorbed species. Ultrafast time resolution makes this the most sophisticated system of its kind.

Accomplishments

Major strides have been made in the study of rare gas films on metal substrates. These experiments show that angle-resolved TPPE can serve as a powerful and general probe of the transition at an interface from two to three dimensions. We have performed layer-resolved two-photon photoelectron spectroscopy of the conduction band of the Xe/Ag(111) interface for up to nine atomic layers of Xe. For multilayers of Xe/Ag(111), TPPE shows how the 2D states of the interface evolve toward the 3D bulk states of crystalline Xe, and the corresponding effective mass measurement by angle-resolved TPPE tracks the spatial extent of the electron as a function of layer thickness. The binding energies of the three lowest quantum states of the conduction band are plotted as a function of layer thickness in Fig. 2. The n = 1, 2, and 3 bare surface image potential state wavefunctions are plotted to scale, showing that the energy of a particular state is only perturbed when the layer becomes thick enough to spatially overlap with the electron density distribution of that quantum state.

We have recently solved a long-standing puzzle concerning the effect of insulating monolayers on the electrostatic fields near a metal surface. In previous work we found that excess electron binding energies on molecular monolayers (including xenon, cyclohexane, and n-octane) could be explained without invoking the dielectric response of the monolayer. A systematic study of n-alkanes on Ag(111) has now revealed that the binding energy of the image potential electron at the monolayer is indeed correlated with both the

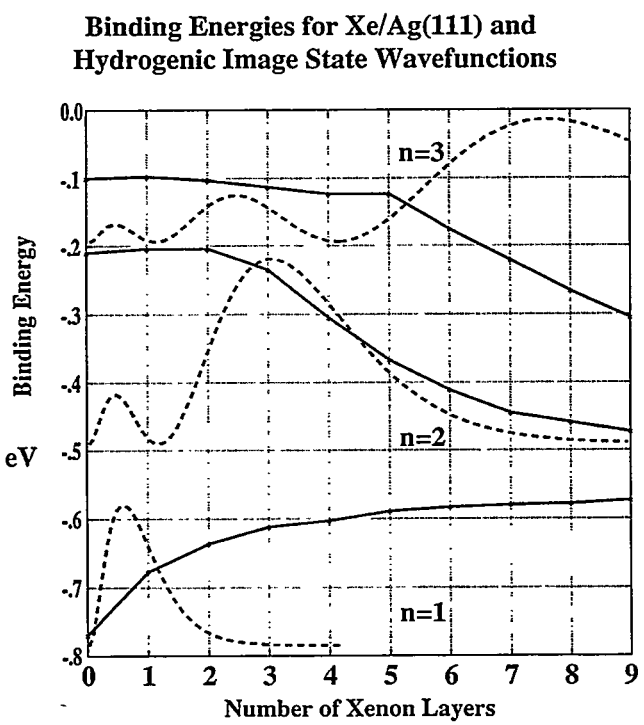

Fig. 2. The solid lines are the experimental binding energies of an excess electron at the Xe/Ag(111) interface for the layer thicknesses indicated. One layer of Xe is approximately 4.1 Å thick. The dashed lines are hydrogenic image potential wavefunctions for a bare metal surface drawn to scale with layer thickness. This illustrates that a particular image potential state, labeled by its principal quantum number n, does not respond to the presence of the adlayer until the layer substantially overlaps with the electron density.

molecular polarizability and the dielectric constant of the associated bulk material, as shown in Fig. 3.

A classical electrostatic continuum model indicates that the potential for the metal-insulator interface is composed of two principal terms: one is the screened image potential interaction between the electron and the metal, while the second is the attractive polarization interaction between the electron and the adlayer. In fact, the attractive interaction between the adlayer and the image electron dominates the screening effect for monolayers with high dielectric susceptibility. Thus a monolayer may either increase or decrease the binding of an image potential electron to the surface. The two effects were roughly in balance for the previously studied monolayers comprising xenon, cyclohexane, and n-octane.

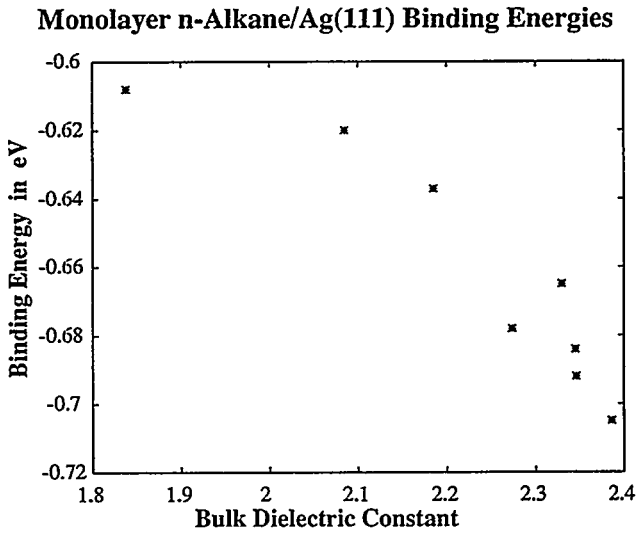

Fig. 3. Plot of n = 1 image potential electron binding energy in the presence of monolayers of various n-alkanes on Ag(111). The x-axis is the estimated dielectric constant for the associated bulk crystalline material. As the dielectric susceptibility of the layer increases, the binding of the excess electron to the layer dominates screening of the electron–metal interaction, leading to stronger net binding

Finally, we have continued the study of 2D localization of electrons at metal–alkane interfaces by confirming the predictions of the model we initially applied to this problem in *Phys. Rev. Lett.* **72**. We have now observed localized electrons in the bilayer of ethane, n-propane, and n-decane. The ethane case is particularly important, since the theory we applied in *Phys. Rev. Lett.* **72** predicts that ethane layers would be the shortest alkane to show localization at the interface.

Publications

R.L. Lingle, Jr., D.F. Padowitz, R.E. Jordan, J.D. McNeill, and C.B. Harris, "Two-Dimensional Localization of Electrons at Interfaces," *Phys. Rev. Lett.* **72**, 2243 (1994).

R.L. Lingle, Jr., R.E. Jordan, J.D. McNeill, and C.B. Harris, "Electrostatic Effects of Insulating Monolayers on Image Potential Electrons," submitted to *Surf. Sci. Lett.*

J.D. McNeill, R.L. Lingle, Jr., R.E. Jordan, D.F. Padowitz, and C.B. Harris, "The Transition from 2-D to 3-D Electronic Structure at the Xe/Ag(111) Interface," in preparation for *Phys. Rev. Lett.*

Structure and Chemistry of Nonmetallic Adsorbates at Semiconductor Interfaces Investigated by Synchrotron Radiation Techniques

Principal Investigator: David K. Shuh

Project No.: 93004

Funding: $74,300 (FY 94)
$76,100 (FY 93)

Project Description

This research project uses two complementary synchrotron radiation (SR) surface characterization methodologies to determine the structural and chemical properties of binary semiconductor material interfaces with simple adsorbates. The results of the SR investigations will provide both fundamental and applied information about the nature of chemisorption on compound semiconductors that are needed to improve existing semiconductor materials-processing technologies. Beamlines capable of supporting the SR techniques employed for this work will become available in the near term at the Advanced Light Source (ALS). A principal consideration is development of both a scientific program and experimental equipment that will take full advantage of the unique ALS facility resources.

The research employs two SR techniques—x-ray standing waves (XSW) and soft x-ray photoelectron spectroscopy (SXPS)—to characterize the adsorbate-semiconductor interfaces in a direct, surface-sensitive manner. XSW is used for determining the structural parameters and SXPS to characterize the chemical behavior of the adsorbate-semiconductor systems. These photon-in electron spectroscopy experiments primarily use dedicated user-accessible endstations at the electron storage rings of the Stanford Synchrotron Radiation Laboratory (SSRL) and the National Synchrotron Light Source (NSLS), although initial activities were conducted at the ALS. In conjunction with the SR experimental program and efforts, a simple surface-science system with limited analytical capabilities continues to be developed to support the SR projects. This modest surface-science capability allows for preliminary research on experimental systems of interest—testing of experimental apparatus—and has been upgraded to serve as a primitive SR endstation.

Accomplishments

XSW Results from the I/GaAs(110) Interface

The I/GaAs(110) interface geometry has been elucidated for the first time using the XSW technique. The chemisorption of halogens on the GaAs(110) chemically etches the semiconductor material and forms surface reaction products with high oxidation states, but the iodine GaAs(110) system is unique in that it does neither at room temperature. The structure of the I/GaAs(110) interface may form similarly to an ideal epitaxially continued layer structure bulk termination or an epitaxial on top structure, both of which may exhibit passivating properties. The XSW measurements have been performed at SSRL Beamline 3-3 (Jumbo). The bulk and iodine back reflection XSW spectra shown in Figs. 4 and 5 were collected in the constant-initial-state mode from photoemission or from the total photocurrent, respectively. The iodine XSW signals were obtained from the difference between photoelectron signals collected at the I $3p_{3/2}$ peak and those from background. The interface structural information is then derived from a two-parameter computer simulation (F and D) of

$$\text{XSW yield} = 1 + R(E) + 2F\sqrt{R}\cos(\nu(E) - 2\pi D), \quad (1)$$

in which R is the reflectivity, ν is the reflectivity phase, F is the coherent fraction, and D is the coherent distance to the Bragg plane of interest. Thus, the amplitude of an XSW spectrum is related to the coherent fraction (F) and the energy position to the phase (D). The reflectivity (not shown) combined with the bulk XSW establishes the experimental sensitivity and resolution, whereas the I XSW yields the structural parameters of the adsorption geometry.

Figure 4 shows the results of the (220) XSW measurements for both the bulk crystal and the I-saturated surface. The bulk coherent fraction is low (0.85) as a result of the beamline optical characteristics, but the planar spacing is exact. The I XSW has a coherent fraction of 0.51, indicating some disorder of the I overlayer, but gives an iodine-GaAs distance of 2.05 Å that is nearly the same as the bulk GaAs (220) spacing of 1.99 Å.

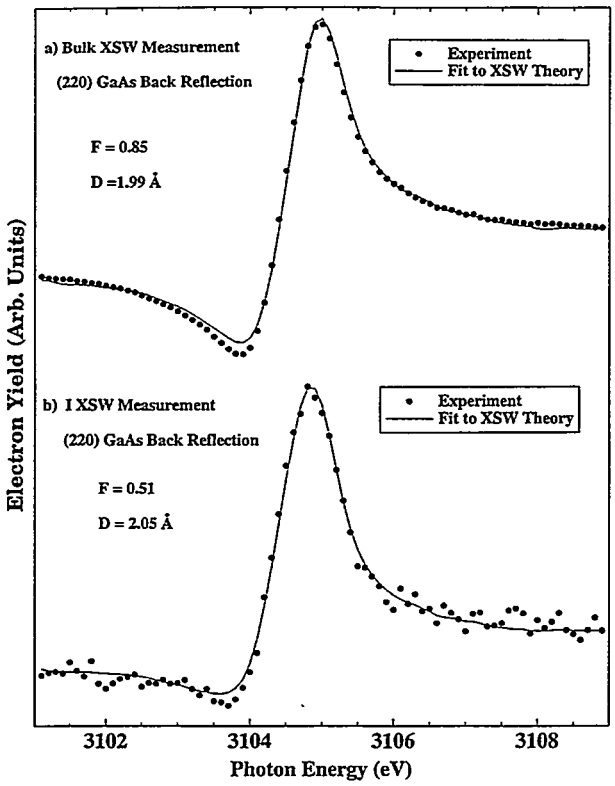

Fig. 4. The (a) bulk and (b) I XSW profile measurements from the (220) back reflection of the I/GaAs(110) interface. The experimental points are represented by the filled circles. The least squares fits to the experimental data, simulated by Eq. (1) and from which the structural parameters have been extracted, are shown by the solid lines.

This is the first successful (220) GaAs reflection experiment that has been obtained on the Jumbo beamline. The (111) XSW experimental reflections are presented in Fig. 5 and have been fit on a trial basis. The coherent fractions are similar to the (220) reflection and yield interface distances that are characteristic of a bulk termination model. This supports the notion that iodine may form an ideal and passivating interface with GaAs(110).

The SXPS investigations will be additionally facilitated by recent membership in the Beamline 8.0 Participating Research Team at the ALS, which will provide dedicated beamtime. Valuable contributions to the commissioning of the beamline and beamline endstation have been made.

Surface Science System and Modification for Use as a Basic SR Endstation

The modest laboratory surface-science system continues to be employed to perform simple measurements and tests of experimental apparatus. The initial efforts to enhance the capabilities of the system permitting its use as a most basic SR endstation have been implemented. Improvement in the analytical capabilities and instrumentation of the system have also been achieved to meet increased experimental characterization requirements. These ongoing laboratory efforts are essential to complementing the SR program, enhancing the productivity of the outside user-based SR efforts, and essential to the prerequisite investigations of experimental systems required for successful experimentation at SR sources.

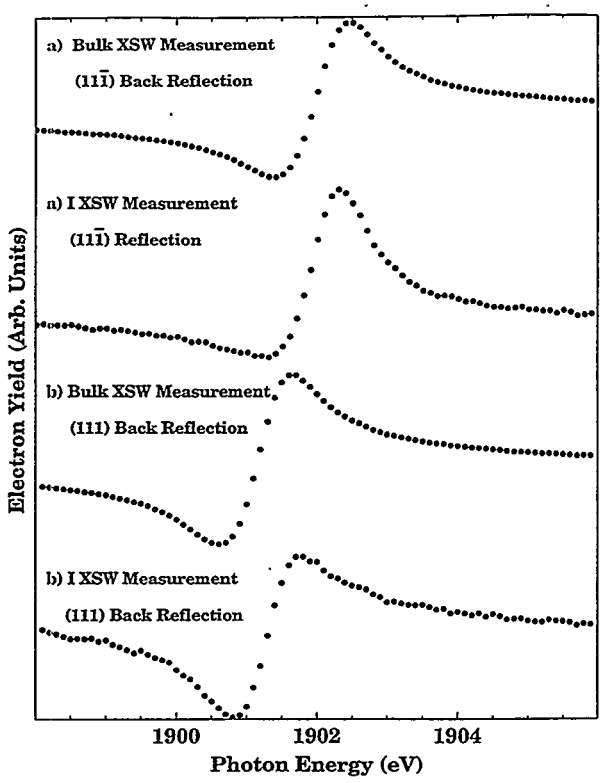

Fig. 5. The bulk and I XSW yields from the measurements of the (a) (111) and the (b) (111) back reflections from the I/GaAs(110) interface, respectively. The experimental data are shown as filled circles.

Publications

D.G. Sutherland, J.A. Carlisle, L.J. Terminello, J.J. Jia, T.A. Callcott, F.J. Himpsel, M.G. Samanat, J. Stohr, D. Ederer, R.C.C. Perera, D.K. Shuh, and W.M. Tong, "Thin Film and Buried Interface Characterization Using 3rd Generation Synchrotron Radiation," in preparation for *J. Vac. Sci. Technol. A.*

W.M. Tong, D.K. Shuh, T. Kendelewicz, and P. Pianetta, "Structure of Iodine on GaAs(110) by X-ray Standing Wave Analysis," in preparation.

J.J. Jia, T.A. Callcott, J. Yurkas, A.W. Ellis, F.J. Himpsel, M.G. Samanat, J. Stohr, D. Ederer, J.A. Carlisle, E.A. Hudson, L.J. Terminello, D.K. Shuh, and R.C.C. Perera, "First Experimental Results from the IBM/TENN/TULANE/LBL Undulator Beamline at the ALS," *Nucl. Instrum. Methods* (in press, 1994).

Application of the Advanced Light Source to the Study of Trace Element Adsorption and Distribution in Soil Carbonates

Principal Investigators: Harvey E. Doner, Mavrik Zavarin, and Ronald G. Amundson

Project No.: 94002

Funding: $17,800 (FY 94)

Project Description

Many environmental problems associated with raw material production, as well as naturally occurring high levels of trace elements, require reliable quantitative prediction of the transport and dispersion of contaminants in surface and ground water systems. Contaminant mobility in a soil system is determined by its partitioning between aqueous and solid phases. Sorption/coprecipitation decrease solute mobility, while mineral dissolution or solute desorption increase solute mobility. Both adsorption and precipitation reactions must be accounted for if solute transport models are to be successful. Calcium carbonate in soil is well known for its influence on the retention of many trace elements both as a primary sorption surface and by its effect on soil pH. Even though extensive research has been conducted on the adsorption and, to a lesser extent, on the distribution and molecular associations of trace elements in pure calcite, only limited work has been done on soil carbonates.

Synchrotron x-ray absorption spectroscopy—such as that now available at the Advanced Light Source (ALS) at LBL and other synchrotron facilities—provides a promising new method for understanding distributions and mechanisms of trace contaminant interaction with mineral surfaces at the molecular level. The focus of this report is on the distribution and elemental association of Ni and Se as a factor for their retention in soil carbonates. Special attention is given to the use of x-ray fluorescence microprobe spectroscopy using the ALS synchrotron facility in identifying these distributions and associations. The ALS synchrotron at LBL has obtained resolutions near 1 μm^2 by use of the Kirkpatrick-Baez mirror system and has a brightness capable of detecting concentrations down to 10^{-15} g μm^{-2}.

Accomplishments

Soils were collected from a terrace formed from marine sediments in the Panoche Creek area of West-Central California. This area is known as a source of several potentially toxic trace elements, such as Se (which is related to the contamination problem in the Kesterson Reservoir) and Ni. In this arid to semiarid environment, the soils often contain calcium carbonate coatings on clasts in the form of pendants. Soils may also contain carbonate nodules up to 1 cm in diameter. Soil and separated carbonate coatings and nodules were analyzed for total Ni and Se following acid dissolution using ICP and hydride-generation AA spectroscopy and found to contain elevated concentrations compared to the total soil. Thin sections of the carbonate coatings and nodules from the soil were prepared and analyzed for Ni, Se, Fe, Ca, Mg, and Si by electron microprobe. Thin sections of the same carbonates were examined for Ni, Se, Fe, and Ca by x-ray fluorescence microprobe using a synchrotron-based x-ray source.

The carbonate coatings contained nearly 1,300 mg Ni kg^{-1} while the <2-mm soil fraction contained 240 mg Ni kg^{-1}. This is an enrichment in the carbonates by a factor of 5. Electron microprobe results suggest that the Ni is associated with Si, although Ni carbonate can not be ruled out. Microprobe x-ray fluorescence showed distinct bands of high and low Ca concentrations in the carbonate coatings every 50 to 70 μm distance from the clast surface, possibly due to changes in environmental conditions over time of formation (Fig. 1). Scans running perpendicular to the clast-carbonate interface indicate a Ni concentration of 1,500 mg kg^{-1} within the clast, which decreases to background levels after 50 μm into the carbonate

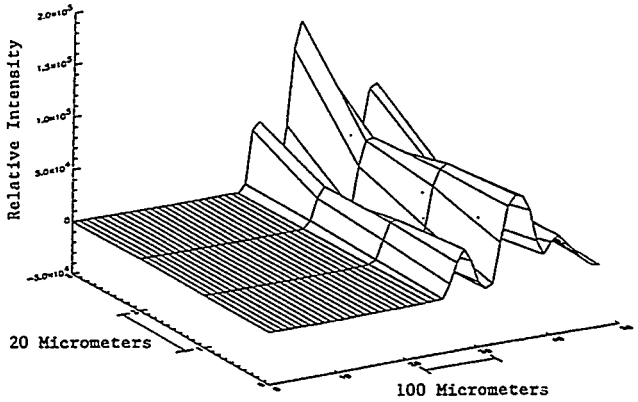

Fig. 1. The distribution of Ca as determined by x-ray fluorescence microprobe in a thin section of a calcium-carbonate-coated clast. The carbonate coating begins at about 240 μm.

(Fig. 2a). This reading was in contrast to the Fe, which showed no elevated concentration in the carbonate (Fig. 2b). Se in the soil carbonate nodules was 10 mg kg^{-1} compared to 3 mg kg^{-1} in the <2-mm soil—an enrichment factor of about 3 in the soil carbonate. The Se concentration was too low in the nodules to be detected by electron microprobe. X-ray fluorescence mapping from the National Synchrotron Light Source in Brookhaven, New York, indicated that Se was heterogeneously distributed in the soil carbonate nodules.

Our results show that spatial analysis of trace element distribution and elemental associations are critically important in understanding the processes involved in the release and retention of trace elements in soil. It is apparent that the elevated Ni concentration in the carbonate coatings originated from the clast itself and not from the soil matrix. Any changes in environmental conditions causing dissolution of the soil carbonates may result in a differential release of Ni and Se. For example, Ni from the soil carbonate may not be released until advanced stages of dissolution due to its location nearer to the clast. Selenium, on the other hand, may be released much earlier, since it appears to have a much more random, heterogeneous distribution.

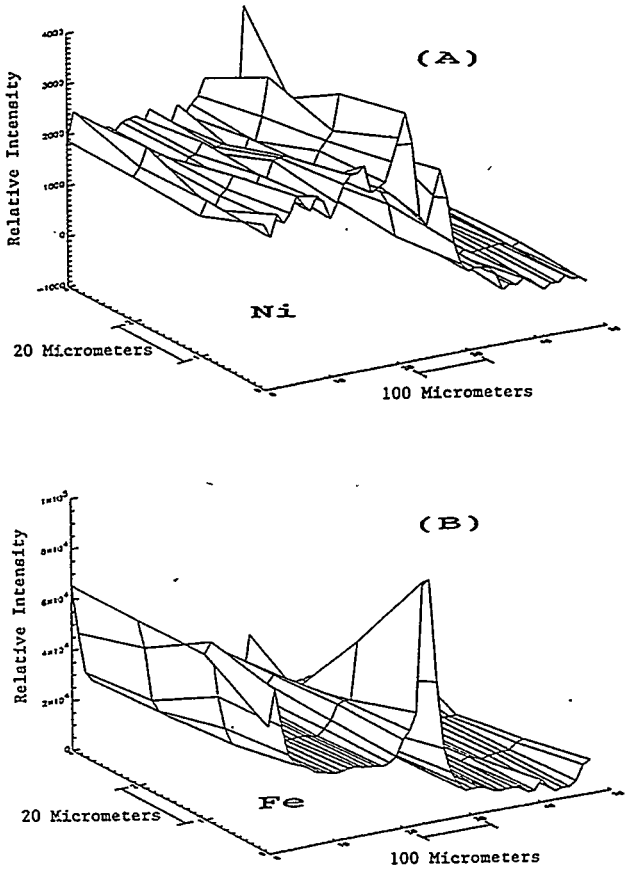

Fig. 2. The distribution of Ni (a) and Fe (b) as determined by x-ray fluorescence microprobe in a thin section of a calcium-carbonate-coated clast. The carbonate coating begins at about 240 μm.

Publications

Harvey Doner and Mavrik Zavarin, "Application of Electron and Synchrotron Microprobe Techniques to the Study of Soil Carbonate Sorptive Properties," NCR-174, Synchrotron X-ray Sources in Soil Science Research Annual Meeting, Argonne National Laboratory, May 24, 1994.

Mavrik Zavarin and Harvey E. Doner, "The Role of Soil Carbonates in the Retention of Ni and Se," submitted to the Third International Conference on the Biogeochemistry of Trace Elements, Paris, France, May 15–19, 1995.

Characterization and Monitoring of Subsurface Biologic Activity Using Stable Isotope Soil Gas Analysis

Principal Investigators: Donald DePaolo, Mark Conrad, Terrance Leighton, and Bob Buchanan

Project No.: 94003

Funding: $78,400 (FY 94)

Project Description

In situ bioremediation of petroleum hydrocarbon compounds is one of the most promising new technologies for environmental restoration. It provides an attractive alternative to costly "pump-and-treat" or "burn-and-bury" techniques that are currently employed to remove hydrocarbon compounds from contaminated ground water and soils. However, there are significant difficulties associated with monitoring the effectiveness of *in situ* bioremediation efforts and determining how these processes can be optimized. Existing monitoring techniques require costly, and frequently inaccurate, drilling strategies. The purpose of this project is to develop a database and methodology for using stable isotope analyses of soil gas samples to monitor subsurface biologic activity.

When bacteria metabolize organic and inorganic compounds they produce a variety of gaseous byproducts. We plan to use measurements of the stable isotopic compositions of these metabolic gases, as appropriate, and their precursor substrates to monitor subsurface biologic activity. Previous workers have measured the $^{13}C/^{12}C$ ratios ($\delta^{13}C$ values) of CO_2 in soil gas samples and found significant variations that were attributed to bacterial activity. However, microbial metabolic processes cause changes, or fractionations, between the isotopic compositions of the substrates and the products. Therefore, to correlate the isotopic effects observed in the field with subsurface microbial activity, it is necessary to know the fractionation effects caused by bacterial metabolism on the isotopic compositions of the gases produced. For this purpose, we have conducted a series of controlled laboratory experiments to measure the fractionation of stable isotopes resulting from bacterial metabolic activity.

Accomplishments

Our initial research has focused on the fractionation of carbon isotopes by bacteria in aerobic environments. We have developed a method for collecting and analyzing the $\delta^{13}C$ values of CO_2 produced by bacteria under controlled conditions in shaker flask experiments. By passing CO_2-free air through a culture containing a carbon source with a known isotopic composition, we collected the CO_2 produced as a byproduct of bacterial consumption of the substrate. We then measured the amount and isotopic composition of the CO_2 to monitor shifts in the $\delta^{13}C$ values associated with the bacterial activity.

For our first set of experiments, we grew the soil bacterium *Bacillus subtilis* on a glucose-defined minimal medium. *Bacillus subtilis* is a well-characterized Gram-positive aerobic bacterium for which extensive genetic and recombinant DNA tools are available. In addition, it has a demonstrated ability to remove heavy-metal contaminants, such as selenium, from solution. During our experiments, the $\delta^{13}C$ value of CO_2 produced by *Bacillus subtilis* was initially about 3‰ lower than the $\delta^{13}C$ value of the glucose substrate (Fig. 3). As the number of cells increased during log phase, the $\delta^{13}C$ values of CO_2 became progressively lower, representing a strongly fractionating process associated with vegetative growth. Once the cultures entered stationary phase, the trend reversed and the $\delta^{13}C$ value of the CO_2 became higher as the glucose remaining in the culture became enriched in ^{13}C.

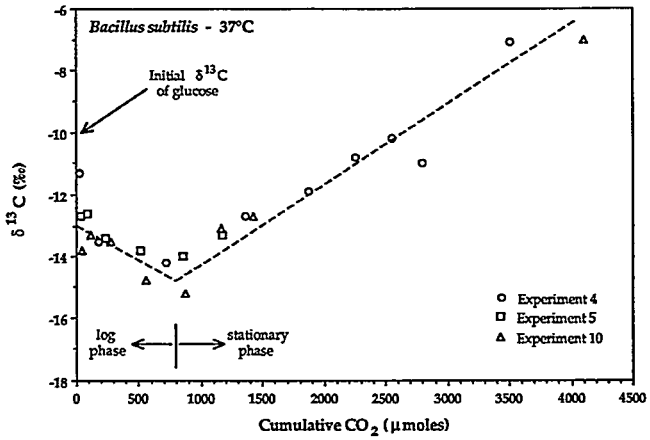

Fig. 3. Carbon isotope composition of CO_2 produced by Bacillus subtilis *grown in a glucose-defined minimal medium.*

We conducted culture experiments with *Bacillus* at both 37 °C and 25 °C. Despite slower growth rates at the lower temperature (~half), we observed virtually identical shifts in the $\delta^{13}C$ values of the CO_2 produced at both temperatures. We also grew *Bacillus* using citrate instead of glucose as the carbon substrate. Citrate is formed as an intermediary compound during metabolism of glucose by bacteria. The growth rates of *Bacillus* on citrate were much slower (~25%), but the carbon isotope composition of the CO_2 evolved in much the same way as it did during the glucose experiments. This implies that the primary source of carbon isotopic fractionation by *Bacillus* occurs after the formation of citrate.

In addition to our experiments with *Bacillus*, we have also done a set of culture experiments with *Psuedomonas putida*. *Psuedomonas* is a Gram-negative soil bacterium that is capable of degrading a wide variety of hydrocarbon compounds. The results of these experiments show that *Psuedomonas* fractionates carbon isotopes much differently than *Bacillus* (Fig. 4). At the beginning of the log phase, the $\delta^{13}C$ values of the CO_2 produced by *Psuedomonas* were about 6‰ lower than that of the substrate. As biomass accumulated during log phase, the $\delta^{13}C$ values of the CO_2 increased rapidly. Unlike *Bacillus*, however, there was no obvious change in the magnitude of carbon isotopic fractionation by *Psuedomonas* when it shifted metabolic mode from log to stationary phase. The results of these experiments suggest that it may be possible to use changes in the carbon isotopic compositions of soil gas CO_2 to differentiate changes in the metabolic mode of different types of soil bacteria capable of degrading different kinds of pollutants.

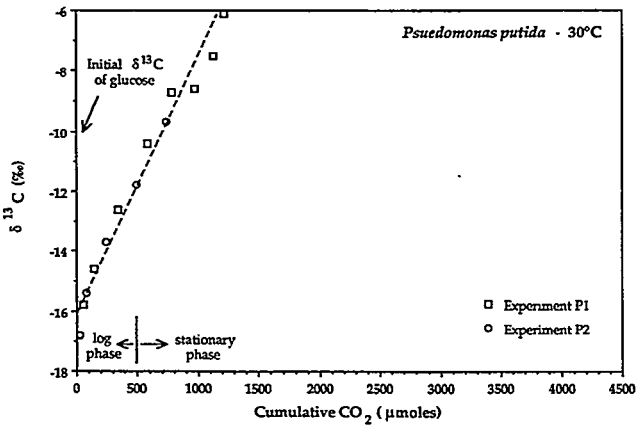

Fig. 4. Carbon isotope composition of CO_2 produced by Psuedomonas putida *grown in a glucose-defined minimal medium.*

Publications

M.E. Conrad, T. Leighton, and B.B. Buchanan, "Carbon Isotope Fractionation by *Bacillus subtilis*," *Geolog. Soc. of Am. Abstracts with Programs* **26** (7), A-510 (1994).

M.E. Conrad, T. Leighton, and B.B. Buchanan, "Fractionation of Carbon Isotopes by Bacteria During Aerobic Metabolism," in preparation.

Microbial Transformation of Petroleum Hydrocarbons in Transient Subsurface Environment

Principal Investigators: Hoi-Ying Holman and Yvonne Tsang

Project No.: 94004

Funding: $99,500 (FY 94)

Project Description

Soil-water content has been shown empirically to affect the rate of degradation of petroleum products by indigenous microorganisms in the vadose zone. The kinetics of degradation under different soil-water content were evaluated by measuring $^{14}CO_2$ produced and released by microbes as they metabolized *n*-[1-^{14}C]hexadecane, [*methyl*-^{14}C]toluene, [*ring*-^{14}C]toluene, [1-^{14}C]naphthalene, [9-^{14}C]phenanthrene, and [*side ring*-^{14}C]anthracene. Measurements from the batch kinetic experiments showed that the degradation of ^{14}C-labeled petroleum compounds depends strongly on soil–water content. The dependency, however, is compound-specific.

Changes in soil–water content are accompanied by changes in the redox potential of soil, motility and biomass of microorganisms, and the availability and transport of gases and nutrients in soil. In this study, we measure the effect of soil–moisture content on the extent and progress of degradation of petroleum hydrocarbons in the vadose zone.

Our results help to characterize the natural biodegradation processes and provide information crucial for the design of enhanced biodegradation of petroleum compounds in the subsurface environment.

This study consists of three different types of microcosm experiments: a batch mineralization experiment, a biometer experiment, and a microcosm experiment conducted inside a partially saturated soil column. In the first year of the project, we completed the batch mineralization experiment and finished fabricating the experimental apparatus for biometer experiments. Microbial observations were also made throughout the batch mineralization experiment to examine effects of water content on soil microbial communities. ^{14}C-labeled substrates were used to quantify the kinetics of mineralization of petroleum products. $^{14}CO_2$ produced and released by microbes was trapped and counted by a liquid scintillation counter.

Accomplishments

Data show that the mineralization of petroleum hydrocarbons depends markedly on soil-water content. Figs. 5 and 6 show the percent conversion of ^{14}C-labeled compounds as a function of time t after the ^{14}C-labeled compounds were injected into soil samples at t_0 = 360 hours. Solid lines on these figures represent the fit of the first-order equation to the data. Each data point in the figure represents the mean of triplicate experiments. Triplicate measurements about each data point were generally within 20% of their mean value.

Figure 5a shows that the abiotic mineralization (sterile controls) is insignificant compared to the biotic mineralization of [*methyl*-^{14}C]toluene. The amount of $^{14}CO_2$ produced from [*methyl*-^{14}C]toluene by microorganisms increases with soil-water content. Increasing the soil-water content from air dry to 50% of the maximum field capacity resulted initially in a six-fold increase in the amount of $^{14}CO_2$ production, and a larger than ten-fold increase at later times. Above 50% soil water, the $^{14}CO_2$ production from [*methyl*-^{14}C]toluene ceased to increase with water content. Similar results were observed in mineralization assays using [*ring*-^{14}C]toluene as the substrate (Fig. 5b). Notice that the first-order fit to the measurement was excellent for all soil-water concentrations.

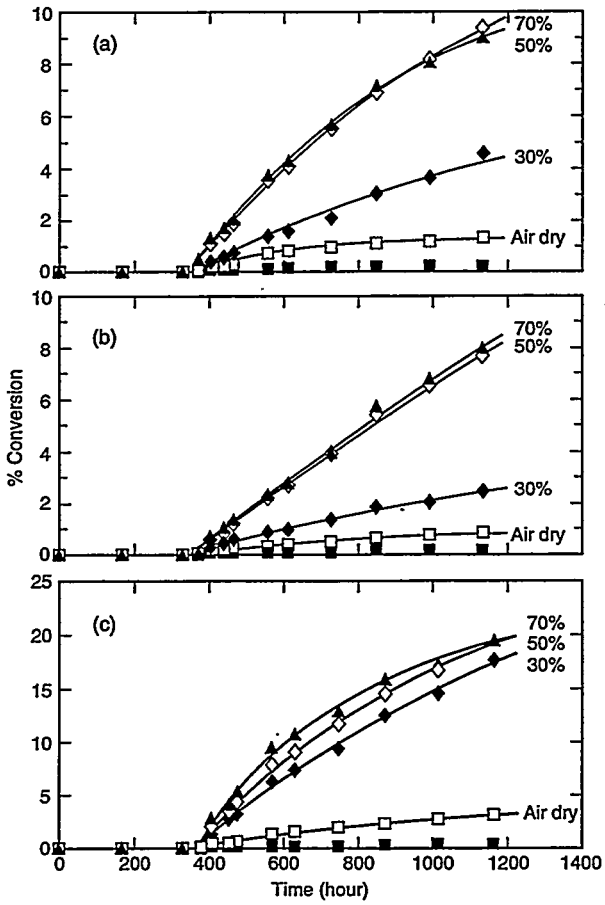

Fig. 5. Time courses of mineralization of ^{14}C-labeled petroleum hydrocarbons, by abiotic processes (■), and by indigenous microorganisms in silty loam vadose soil: (a) [methyl-^{14}C]toluene, (b) [ring-^{14}C]toluene, (c) [1-^{14}C]naphthalene. Soil–water contents are (□) air dry, (♦) 30%, (◇) 50%, and (▲) 70%. (–) is fit of the first-order model to the data.

Biodegradation of toluene begins with oxidation of either the methyl group or the aromatic ring. It is generally believed that these two degradation pathways are accomplished by different microbial populations. The production of $^{14}CO_2$ from both the [*ring*-^{14}C]toluene and [*methyl*-^{14}C]toluene in our experiments, as well as the similarities between their cumulative mineralization curves, imply that (1) microbial populations participating in these two different oxidizing processes are both present in our soil samples, and (2) these different populations respond to the change of soil-water content in a very similar fashion.

Figure 5c shows that the mineralization of [1-^{14}C]naphthalene followed a similar trend of increasing mineralization with soil–water content

until the water content exceeded 50%. The first-order fit to the data is also good.

Results for [9-^{14}C]phenanthrene and [*side ring*-^{14}C]anthracene generally showed a larger $^{14}CO_2$ production at moderate moisture contents (Figs. 6a and 6b). Unlike toluene and naphthalene, the trend between the $^{14}CO_2$ production and soil-water content has been ambiguous. The first-order model could provide a good fit to the mineralization data only when water content was low. At higher water contents, the model deviated from the data. The poor fit of the first-order model to the $^{14}CO_2$ produced at early time from [9-^{14}C]phenanthrene occurred when water content was 70%; for [*side ring*-^{14}C]anthracene the water content was at 50% and 70%.

Data in Fig. 6c for *n*-[1-^{14}C]hexadecane appear to show an entirely contrary trend of less mineralization at higher soil-water contents: the drier the soil, the more *n*-[1-^{14}C]hexadecane is completely biodegraded. However, the percentage of mineralization is so low (less that 1%) for all soil-moisture contents that this relationship may not be meaningful.

To assess effects of volatilities of aromatic hydrocarbons on the extent of mineralization, mineralization data shown in Figs. 5a through 6b were also compared between compounds. Results show the amount of $^{14}CO_2$ produced from volatile hydrocarbons was less than that from nonvolatile organics, suggesting a competing process of volatilization and biodegradation in our soil.

In conclusion, the data demonstrate that soil water can accelerate the degradation of petroleum hydrocarbons in soil by at least an order of magnitude. For mono- and di-aromatic hydrocarbons, production of $^{14}CO_2$ from degrading the hydrocarbons increases dramatically with soil-water content up to about 50% of maximum field capacity. This relationship breaks down at higher soil-water contents. For larger hydrocarbons such as polycyclic aromatic hydrocarbons, the production of $^{14}CO_2$ increases markedly in the presence of soil water, but no simple relation between $^{14}CO_2$ production and soil-water content is evident. For long-chain aliphatic hydrocarbons, the early mineralization is retarded by the presence of soil water.

The first-order model succeeded in describing mineralization kinetics of mono- and di-aromatic hydrocarbons for all soil-water contents. For polycyclic aromatic hydrocarbons, the model can represent their mineralization processes for only the soil-water contents below 50%.

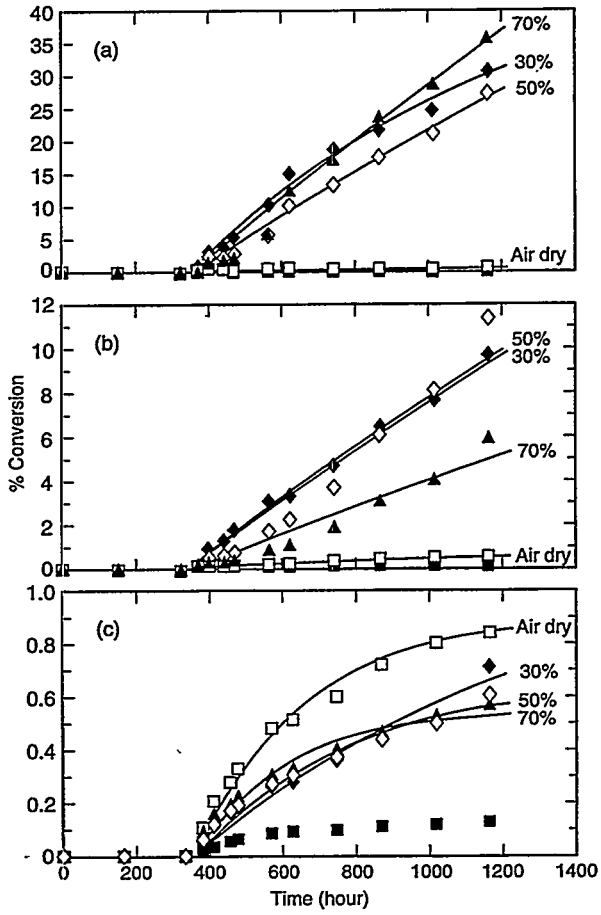

Fig. 6. Time courses of mineralization of ^{14}C-labeled petroleum hydrocarbons, by abiotic processes (■), and by indigenous microorganisms in silty loam vadose soil: (a) [9-^{14}C]phenanthrene, (b) [side ring-^{14}C]anthracene, (c) n-[1-^{14}C]hexadecane. Soil–water contents are (□ air dry, (♦) 30%, (◇) 50%, and (▲) 70%. (–) is fit of the first-order model to the data.

Publication

H.-Y. Holman and Y. Tsang, "Influence of Soil Moisture on Biodegradation of Petroleum Hydrocarbons," submitted to the *In Situ* and On-Site Bioreclamation International Symposium, San Diego, 1995.

X-ray Microprobe Tests of Models for Selenium and Chromium Partitioning in Contaminated Sediments

Principal Investigator: Tetsu K. Tokunaga

Project No.: 93006

Funding: $71,000 (FY 94)
$70,000 (FY 93)

Project Description

X-ray absorption spectroscopy (XAS) and the synchrotron x-ray fluorescence microprobe (SXRFM) have been demonstrated to be useful techniques in improving understanding of selenium contamination in sediments. Selenium (Se) is a potentially toxic, naturally occurring trace element. Its mobility and toxicity are strongly dependent on oxidation state. XAS studies conducted at the Stanford Synchrotron Radiation Laboratory (SSRL) with I.J. Pickering and G.E. Brown, Jr., provided the first direct evidence for the red, elemental form of Se, Se(0), in contaminated sediments collected at Kesterson Reservoir, California. In another part of this study, XAS permitted real-time tracking of Se reduction from soluble Se(VI) to Se(IV) to insoluble Se(0) in sediments. Research conducted with S.R. Sutton and S. Bajt at the National Synchrotron Light Source (NSLS) with the SXRFM revealed the existence of highly heterogeneous, small-scale distributions of selenium in contaminated sediments collected at Kesterson Reservoir.

A diffusion-based model of Se(VI) transport into localized reducing zones of sediments around decomposing plant tissue, where reduction to Se(IV) and Se(0) takes place, was developed. X-ray microprobe maps of total Se distributions in laboratory sediment simulations of the contamination process were supportive of this model. However, the previous work relying on fluorescence spectra generated with white radiation lacked valence-specific information. Recent runs at the NSLS beamline X26A using monochromatic microbeams on similar sediment systems permitted extraction of oxidation state data necessary for more quantitative testing of the model. The technique used for this purpose, micro-XANES, combines the spatial resolution of conventional SXRFM with the valence-sensitivity of x-ray absorption near-edge spectroscopy (XANES).

Another trace element with strong valence-dependent environmental consequences is chromium (Cr). In its hexavalent form, Cr(VI), chromium is a soluble, strong oxidizer, and possible carcinogen. When reduced to Cr(III), this element is insoluble in most environments, and much less bioavailable. Recent SXRFM analyses of Cr-contaminated sediments were conducted at the Advanced Light Source (ALS) with Al Thompson and Karen Chapman. While the SXRFM results permit mapping of total Cr concentration distributions, experiments using monochromatic sources are needed to obtain valence-specific data. Therefore, ALS white-beam SXRFM studies were complemented with further NSLS micro-XANES analyses of Cr. Major features of the recent studies are summarized in the following section.

Accomplishments

In ongoing studies at the NSLS, the valence-dependence of Se K-edge absorption energies was used to preferentially detect Se(0), Se(IV), Se(VI), and total Se in flooded sediments. Previous experience gained through XAS conducted at SSRL indicated that these three inorganic Se species were most likely to occur. Regions within soils adjacent to decomposing plant roots were scanned in front of monochromatic synchrotron x-ray beams tuned to preferentially excite K electron transitions for Se(0), Se(IV), and Se(VI). Deconvolution of the data provided maps of relative concentrations of these Se oxidation states in sediments surrounding a decomposing plant root. These micro-XANES maps show accumulation of Se(0) and some Se(IV), at the expense of Se(VI) reduction, in good agreement with model predictions developed during the previous year.

The most recent research has involved SXRFM and micro-XANES of Cr in contaminated sediments. In analyses at the ALS SXRFM, sediment samples from the San Francisco Bay estuary exposed to waste waters were found to contain highly heterogeneous distributions of Cr contamination at scales less than 1 mm. This result is similar to that previously found for Se-contaminated systems. In both cases, most of the contamination was localized within a small portion of the sediment volume. Laboratory experiments on local redox-driven diffusive accumulations of Cr in sediments

were analyzed with the x-ray microprobes at both the ALS and NSLS. At the ALS, the SXRFM has been used to track diffusion of Cr(VI) through small distances within sediments in response to localized reducing environments. At the NSLS X26A, micro-XANES maps of Cr(III), Cr(VI), and total Cr were obtained in real time, tracking both diffusion and localized reduction of Cr(VI). The experiments also showed the importance of relative mobilities of Cr(VI) and potential reducing agents. At low concentrations, where most of the Cr(VI) is retained by sorption onto sediment grain surfaces, diffusion toward local reducing sites is relatively ineffective. When reducing agents are relatively mobile, in-place reduction of adsorbed Cr(VI) to Cr(III) becomes possible, with insignificant redistribution of Cr.

The highly localized nature of the Se and Cr distributions in sediments may have important implications on long-term persistence of trace element contaminants. Such localization may limit later reoxidation and transport required for *in situ* removal of trace element contaminants. These x-ray microprobe observations also raise new questions concerning spatial scales to which contaminant concentrations are assigned.

Additional information has also been obtained from part of an earlier XAS study conducted in collaboration with SSRL. This experiment simulated Se exchanges between ponded waters and underlying sediments and provided samples showing the previously mentioned Se reduction sequence in sediments. Further analyses of data collected during these hydrostatic ponding experiments showed that diffusive transport between surface waters and sediments, supplemented with reduction, can quantitatively account for Se partitioning within these systems. The earlier work completed at SSRL has also received interest from a U.S. Bureau of Reclamation group investigating remediation options for Se contamination in wet lands of the Kendrick area of Wyoming. XAS analyses of sediments from this area are planned for early 1995.

Publications

T.K. Tokunaga, S.R. Sutton, and S. Bajt, "Mapping of Selenium Concentrations in Soil Aggregates with Synchrotron X-Ray Fluorescence Microprobe," *Soil Sci.* **158** (1994).

I.J. Pickering, G.E. Brown, Jr., and T.K. Tokunaga, *X-Ray Absorption Spectroscopy of Selenium-Contaminated Soils: 1993 Activity Report* (Stanford Synchrotron Radiation Laboratory, Stanford, CA, 1994).

T.K. Tokunaga, S.R. Sutton, and S. Bajt, *Intra-Aggregate Selenium Concentration Heterogeneities: Synchrotron X-Ray Fluorescence Microprobe Studies of Kesterson Reservoir Soils and Laboratory Simulations: 1993 Activity Report* (National Synchrotron Light Source, Brookhaven National Laboratory, Upton, NY, 1994).

T.K. Tokunaga, I.J. Pickering, and G.E. Brown, Jr., "X-Ray Absorption Spectroscopy Studies of Selenium Transformations in Ponded Sediments," submitted to *Soil Sci. Soc. Am. J.* (1994).

I.J. Pickering, G.E. Brown, Jr., and T.K. Tokunaga, "Quantitative Speciation of Selenium in Soils Using X-Ray Absorption Spectroscopy," submitted to *Environ. Sci. Technol.* (1994).

T.K. Tokunaga, G.E. Brown, Jr., I.J. Pickering, S.R. Sutton, and S. Bajt, "Selenium Transport Between Ponded Waters and Shallow Sediments," in preparation.

T.K. Tokunaga, S.R. Sutton, and S. Bajt, "Micro-XANES Analyses of Selenium and Chromium Transport and Redox in Soils," in preparation.

Energy and Environment Division

Alternative Strategies to Improve Air Quality in the Los Angeles Air Basin

Principal Investigators: Haider Taha, Tom Wenzel, and Mark D. Levine

Project No.: 94005

Funding: $100,000 (FY 94)

Project Description

The latest plan to reduce ozone in the Los Angeles air basin in California calls for extreme reductions in current levels of the ozone precursors, oxides of nitrogen (NOx) and reactive organic gases (ROG). These reductions are on the order of 75 percent of current emission levels. A significant portion of these reductions is to come from the development and deployment of unspecified technologies to reduce emissions from both mobile and stationary sources. We have developed the capability to investigate ozone reduction strategies that may require smaller overall emission reductions, at possibly lower cost, than the current plan for Los Angeles.

It is generally thought that reducing the emissions of ozone precursors—oxides of nitrogen and reactive organic gases (NOx and ROG)—would improve air quality by reducing ozone concentrations in major air basins. However, the impacts of emission control measures on ozone air quality are not straightforward. Implementing the current strategies of uniform reductions in basin-wide emissions of NOx and/or ROG may actually result in increasing or decreasing local ozone concentrations, depending on the level and mix of existing emissions and meteorology, each of which varies from one area to another within an air basin. There is a need to improve our understanding of ozone formation as it relates to location-specific conditions within air basins.

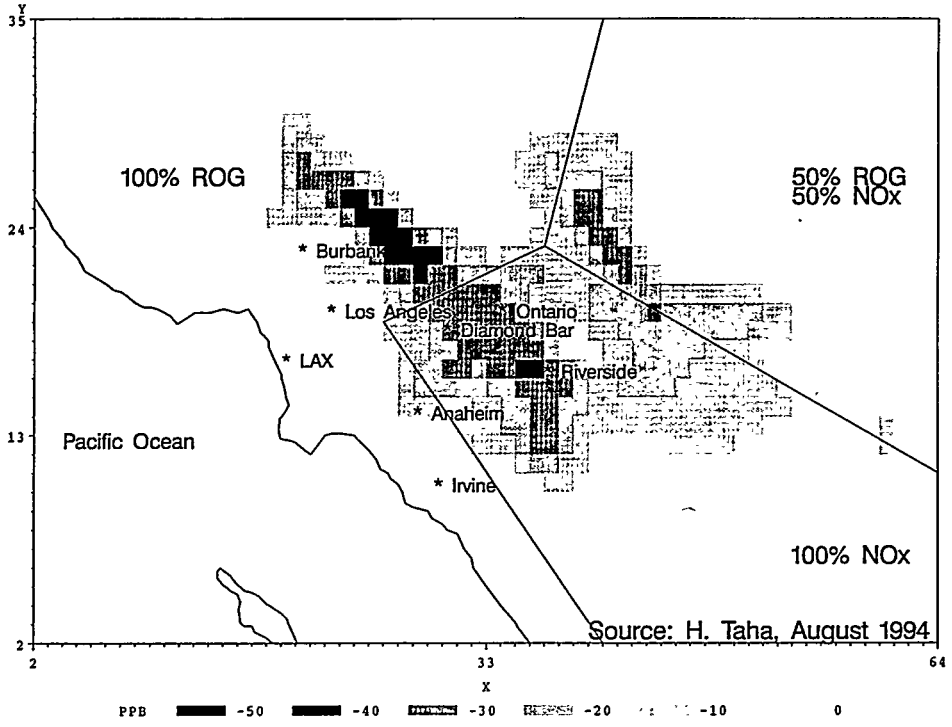

Fig. 1. Ozone concentration differences (in ppbv) for a space-varying ROG/NOx control measure with respect to a base case at 3 pm on August 27, 1987. The control level is 30 percent and the resulting largest decrease in ozone concentrations is of the order of 50 ppbv. The straight lines delineate the subbasin boundaries and the percentages within each show how the 30 percent control level is to be partitioned between NOx and ROG.

In this study, we use mobile source emission factor models (EMFAC) coupled with three-dimensional mesoscale meteorological (CSUMM) and photochemical (UAM) models to compare the effectiveness of alternative strategies to reduce precursor emissions and improve air quality in the L.A. Basin. A specific approach has been to investigate the air-quality impacts of implementing space-varying ROG/NOx control ratios instead of uniform reductions in NOx and ROG, as is proposed in current regulations. For this analysis, we divided the basin into three or four subbasins (e.g., West Basin, East Basin, San Bernardino, and Riverside) and for each subbasin a different ROG/NOx reduction ratio for stationary sources was used. If a ratio appropriate to each subbasin is chosen, improvements in air quality can be achieved by minimal reductions in emissions.

Accomplishments

During FY 94, we first obtained several programs and models previously not available to LBL, installed them, and adapted them to our computing environment. These models allow us to simulate the effect of policies and meteorological conditions on mobile and stationary source emission rates, which in turn are used to simulate the L.A. Basin's photochemistry and ozone formation. For example, we can adjust the mobile source emission factor model to simulate the effect of the introduction of electric vehicles on emission rates and basin air quality. Our simulations of the August 26–28, 1987, episode indicate that removing all vehicles from the L.A. Basin would not reduce ozone levels enough to meet the national standard. Consequently, we have begun to investigate alternative strategies that focus on all sources of emissions.

One strategy that would involve practically eliminating one of the ozone precursors (NOx) was selected since natural biogenic sources account for about 10 percent of all ROG emissions in the basin. However, research indicates that a high level of NOx reduction, on the order of 95 percent, would be required to meet federal clean air standards. A second strategy would be to reduce NOx and ROG emissions to different levels in different areas of the basin. A regulation based on space-varying ROG/NOx ratios would require only modest control levels to achieve significant results. For example, a control level of 30 to 50 percent in selected areas of the basin may achieve the same improvement in air quality as 75 percent control of both precursors (the current plan) or 95 percent reduction of NOx emissions. Furthermore, there appears to be no local increase in ozone under this strategy.

Publication

H. Taha, T. Wenzel, and M.D. Levine, "Alternative Strategies to Improve Air Quality in the Los Angeles Air Basin," in preparation.

Defect Characterization of GaN and Fabrication of Blue LEDs

Principal Investigators: Michael D. Rubin and Eicke R. Weber

Project No.: 92011

Funding: $87,600 (FY 94)
$90,000 (FY 93)
$75,000 (FY 92)

Project Description

The purpose of this project is to develop processes for growing GaN and related materials using molecular-beam epitaxy (MBE). These wide-bandgap materials can then be used to fabricate devices that emit ultraviolet or blue light. Potential applications include flat-screen displays, high-density optical storage, and efficient illumination.

The strong chemical bonds in GaN have many advantages in properties but make intrinsic single-crystal films difficult to obtain. GaN tends to form with high concentrations of nitrogen vacancies because of the low-solubility and high-equilibrium vapor pressure of nitrogen. Poor lattice and thermal-expansion matches with practical substrates cause other types of defect generation. Our approach to this problem lies in a combination of advanced materials processing techniques and defect characterization.

Accomplishments

Growth of GaN using MBE occurs under metastable growth conditions so that activated nitrogen is required to drive the forward synthesis

reaction. The stoichiometry of our films has been improved by using a directed nitrogen ion beam to drive the forward reaction and by operating at temperatures and pressures where the decomposition kinetics are slow. When the nitrogen is excited with a plasma or ion-beam source, species with relatively high kinetic energies are generated. Impingement on the growth surface by these species can result in subsurface damage to the growing film, as well as an enhancement in the rate of the reverse decomposition reaction.

The kinetic energy of the impinging nitrogen ions during growth affected the optical and structural properties of GaN films. Strong band-edge photoluminescence (PL) is found when a kinetic energy of ~10 eV is used. Luminescence is not detectable, however, when the kinetic energies exceed 18 eV. Also, conductive SiC substrates were found that result in more homogeneous cathodoluminescence (CL) than insulating sapphire substrates. This effect is attributed to sample surface charging in the case of sapphire substrates and subsequent variation in the incident ion flux and kinetic energy across the growth surface. The quality of GaN films grown by MBE is presently limited by damage from the impingement of high-energy species on the growth surface.

Film quality has been greatly improved by the use of a low-energy, high-current monoenergetic ion beam. Film quality is now limited, however, by the contamination caused by sputtering from the tungsten filament and stainless steel walls of the ion source, as determined by secondary ion mass spectroscopy (SIMS). Consequently, a new type of plasma source was designed specifically for this application. The new source is a modification of the hollow-anode type. This type of source will retain the advantages of a monoenergetic beam with a much lower level of contaminants. The two-stage design produces an exceptionally high level of excited ionized and atomic nitrogen. Furthermore, the prototype was constructed of materials such as high-purity Al and AlN, which are not considered contaminants.

Until recently, researchers have assumed that the nitrogen vacancy acting as a donor is the dominant defect in undoped material. Several experimental observations indicate that a much more complicated defect chemistry involving substitutional sites and complex formation occurs.

Electron paramagnetic resonance (EPR) studies have been performed on a GaN film grown on sapphire and on a rare bulk crystal from Unipress. The thin-film sample showed a complex multiplet spectrum. The intensity decreases with temperature and is highly dependent on magneteic field orientation. The bulk material showed a spectrum with a high and isotropic g-value, indicative of a defect that has a strong interaction with the lattice.

Publications

T.C. Fu, N. Newman, E. Jones, J.S. Chan, X. Liu, M. Rubin, N.W. Cheung, and E.R. Weber, "Influence of Nitrogen Ion Energy on the Quality of GaN Films Grown with Molecular Beam Epitaxy," submitted to *Appl. Phys. Lett.* (1994).

R.G. Wilson, M. Rubin, et al., "1.54 Micron Photoluminescence from Er-implanted GaN and AlN," *Appl. Phys. Lett.* **65**, 992 (1994).

J.S. Chan, N. Newman, T. Fu, M. Rubin, and N. Cheung, "RF Magnetron Sputtering of AlN," to be published in *Handbook of Thin-Film Process Technology*, D.A. Glocker and S.I. Shah (eds.), Institute of Physics Publishing (1994).

J.S. Chan, N. Newman, T. Fu, M. Runin, and N. Cheung, "MBE Growth of AlN," to be published in *Handbook of Thin-Film Process Technology*, D.A. Glocker and S.I. Shah (eds.), Institute of Physics Publishing (1994).

N. Newman, et al., "Fundamental Materials Issues in the Growth of GaN by Molecular Beam Epitaxy," to be published in the *Proc. Mat. Res. Soc. Symp.*, San Francisco, CA (April 1994).

K. Yung, J. Yee, J. Koo, M. Rubin, N. Newman, and J. Ross, "Stimulated Emission from an MBE GaN Film in a Vertical-Cavity Single-Pass Configuration," *Appl. Phys. Lett.* **64**, 1135 (1994).

M. Rubin, N. Newman, J.S. Chan, T.C. Fu, and J.T. Ross, "P-Type Gallium Nitride by Reactive Ion-Beam MBE with Ion Implantation, Diffusion, or Coevaporation of Mg," *Appl. Phys. Lett.* **64**, 64 (1994).

J. Chan, T. Fu, N.W. Cheung, J. Ross, N. Newman, and M. Rubin, "Comparison of AlN Films Grown

by RF Magnetron Sputtering and Ion-Assisted Molecular Beam Epitaxy," *Mater. Res. Soc. Symp. Proc.* 300 (1993).

J. Ross, M. Rubin, and T.K. Gustafson, "Single-Crystal Wurtzite GaN on (111) GaAs with AlN Buffer Layers Grown by Reactive Magnetron Sputtering," *J. Mater. Res.* **8,** 2316 (1993).

N. Newman, J. Ross, and M. Rubin, "Thermodynamic Processes Involved in the Growth of Epitaxial GaN Thin Films," *Appl. Phys. Lett.* **62,** 1242 (1993).

J. Ross, M. Rubin, and T.K. Gustafson, "Crystalline Growth of Wurtzite GaN on (111) GaAs," *Proc. Mat. Res. Soc. Symp.* **242,** 457 (1992); LBL-32258.

Engineering Division

Development of Microchemical Methods for Biological Assays

Principal Investigators: Joseph M. Jaklevic and Jocelyn C. Schultz

Project No.: 93008

Funding: $94,700 (FY 94)
$46,900 (FY 93)

Project Description

The aim of this project is to develop methods for performing biochemical procedures in submicroliter quantities arrayed in multiple reaction cells and to develop a high-speed DNA sequencer based on the use of ultrathin (50–150 μm) slab gels. The result of such a program will be the capability to perform biochemical assays in large numbers at reduced costs and/or at faster rates. The methods will have applications in emerging biotechnological areas such as genome sequencing and large-scale clinical assays.

To miniaturize biochemical procedures, large arrays of small-area reaction cells can be fabricated using standard photolithographic nanofabrication methods. Successive masking and processing steps can be used to create physical wells in an appropriate substrate or, alternatively, a patterned surface treatment can be used to create hydrophobic barriers around individual reaction cells. Dispensing in nanoliter quantities can be achieved with droplet-on-demand ink-jet dispensers. Our work to date has focused on developing these dispensers for our applications.

Using ultrathin polyacrylamide gels in automated fluorescence sequencers is a means to greatly speed up DNA sequencing through miniaturization. The efficiency of heat transfer in ultrathin gels (50–150 μm) permits the use of electric fields larger than those used in standard-thickness (0.35–0.5-mm) electrophoresis gels, and thus DNA separation speeds can be increased ~8 times. In our system, a 488-nm laser beam passes transversely through the width of the gel to excite all of the DNA lanes simultaneously. A linear array of lenses and fiber-optics collects the fluorescence from the excited chromophore attached to the DNA fragments. A cooled charge-coupled device (CCD) solid-state array detects the light. A similar system is being developed in our group for use with standard-thickness gels. The high spatial resolution of this fiber-optic detector offers the possibility of densely spacing the DNA lanes across the width of the gel, thus maximizing the number of samples that can be run at one time. The eventual coupling of the thin-gel format to microfabricated arrays for preprocessing of the DNA templates could constitute a significant improvement in sequencing technology.

Accomplishments

Submicroliter Dispenser

Our first droplet-on-demand dispenser, built using a piezo-ceramic transducer that was on hand, dispensed subnanoliter droplets as soon as we obtained electronics that allowed us to apply fast risetime voltage pulses. To optimize and quantify the dispenser's performance, we assembled an apparatus that allowed strobed microscopic viewing of the droplet stream (typically at 250 Hz). Droplets of 0.2-nl volume (75-μm diameter) with a velocity of 2 m/s could be dispensed with an 80-V pulse.

A second-generation droplet-on-demand ink-jet dispenser was then designed, built, and tested. Custom-made piezo ceramics were used and other design changes that we anticipated would improve performance were incorporated. Droplets of 0.4-nl volume (90-μm diameter) with a velocity of 3 m/s could be dispensed with only a 50-V pulse, and the dispenser could operate consistently for more than an hour. The droplets shot out at least 15 mm from the dispenser orifice in a straight path. The different dispensing characteristics indicate a better coupling of the piezo motion into forward motion of the liquid in the second-generation dispenser. It was also verified that the dispenser could reliably generate single droplets on demand.

Ultrathin Slab Gels for High-Speed Automated DNA Sequencing

A complete automated fluorescent sequencer based on an ultrathin gel format was assembled. This apparatus includes optics that direct the laser beam, an LBL-built water-cooled gel frame and electrophoresis cell, a linear lens array that images the fluorescent light onto an LBL-built fiber-optic array, and the optics necessary to image the other end of the fiber-optic array on the CCD detector. A compact arrangement of two prisms and a mirror, placed after the last focusing lens, allows us to finely adjust the position of the laser beam through a window at the side of the gel plates and into the gap between the plates.

The focused laser beam waist and focus position were measured to verify that the laser beam behaves as expected. The relative position of the linear lens array and the fiber-optic array was optimized for best image resolution. Laser transmission through water filling a 100-μm gap between the quartz gel plates (6 mm thick, 15 cm wide) was 60–65%. This transmission dropped to 40% when the gap between the plates was filled with polyacrylamide sequencing gel, presumably due to a greater scattering of the laser beam by the gel material compared to pure water. Efficient light transmission relies on the high reflectivity of the laser beam at grazing incidence on the quartz/gel interface. As a measure of the electrical integrity of the electrophoresis cell, up to 4,500 V could be applied between the two electrodes of the fully assembled electrophoresis cell with the polyacrylamide sequencing gel filling the gap between the quartz plates and the cooling water on.

By the end of FY 94, all preliminary testing had been completed and the next step was to sequence a DNA standard: load DNA samples at one end of a polyacrylamide gel and monitor the DNA fragments as they pass by the detector at the other end. Preliminary data collected during the first month of FY 95 indicate that good signal-to-noise ratio and resolution of a DNA fragment band can be obtained with this instrument. Future work will focus on optimizing all experimental parameters (gel and running buffer composition, DNA preparation, sample loading procedures, electrophoresis voltage and cooling water temperature) for the fastest sequencing throughput.

Publication

W.F. Kolbe, J.C. Schultz, and J.S. Zelver, "Fluorescent Sequencer Development," presented at the DOE Human Genome Program Contractor-Grantee Workshop IV, Santa Fe, NM, November 13–17, 1994.

Development of Next-Generation Detectors for Use at the Advanced Light Source

Principal Investigators: Joseph E. Katz, Charles S. Fadley, and Helmuth Spieler

Project No.: 94006

Funding: $115,300 (FY 94)

Project Description

We are developing next-generation high-spatial-resolution and high-speed detectors for electrons and photons that are essential for taking full advantage of the high-brightness radiation that is now available from sources such as the Advanced Light Source (ALS). A vast array of experiments on solid samples, surfaces, and gas-phase or cluster-beam targets will benefit from faster detectors of the type we are exploring. When developed, such detectors would find wide use at the ALS and elsewhere in fields such as photoelectron spectroscopy, diffraction, and holography; x-ray absorption and fluorescence spectroscopy; surface analysis using electron and ion probes; laser spectroscopy; and atomic and molecular physics.

The present situation is that no multichannel detectors exist that will count at sufficiently high rates to accommodate the fluxes expected at the ALS (or indeed even from the highest power laboratory x-ray or UV sources). Without faster detectors, it will be necessary in many experiments to close down the slits to artificially reduce the ALS source brightness to avoid detector saturation!

In this project, we are making make use of integrated circuit (IC) technology developed at LBL primarily for the Silicon Detector Collaboration

(SDC) particle physics detectors to create a next-generation multichannel detection system that will be significantly superior to any that is currently available. In Table 1, we compare the characteristics of the detector currently under development at LBL with the best commercially available detector. The table makes it clear that our design should count 100 times faster overall (1.2×10^9 vs. 1.2×10^7) and possess about seven times more channels (768 vs. 116). A layout of the prototype presently being constructed is shown in Fig. 1. It makes use of 12 two-chip sets. Each set contains 64 data channels. The "SDC" chip in each set provides a fast low-noise preamplifier-shaper discriminator for each channel and is an IC originally developed for the SDC at the Superconducting Super Collider (SSC). The double-buffered counter chip (DBC) was specifically developed in this project but is also useful for particle physics applications; each of these chips includes 64 16-bit counters with a buffered multiplexed readout. The 16-bit counters allow for over 20 ms of data accumulation at a maximum input rate of 1.5 MHz per channel before overflow; data transfer to the output buffer at the end of each counting interval will require less

Table 1. LBL Next-Generation Detector compared to best commercially available detector.

	Best Available	LBL Next Generation
Single collector size (mm × mm)	7 × 0.16	10 × 0.05
Overall active area (mm × mm)	7 × 20	10 × 40
No. of collectors	116	768
Max. count rate per collector	100 kHz	1.5 MHz
Max. total elec. count rate (Cts./s)	1.2×10^7	1.2×10^9
Max. microchannel plate count rate (Cts./s)	2.5×10^8	2.5×10^9
Microchannel plate electron gain	$10^6 - 10^7$	$10^4 - 10^5$
Max. energy resolution for a 20-cm analyzer	$4/10^4$	$1.2/10^4$
Dead time per readout	1/128	$<1/10^5$

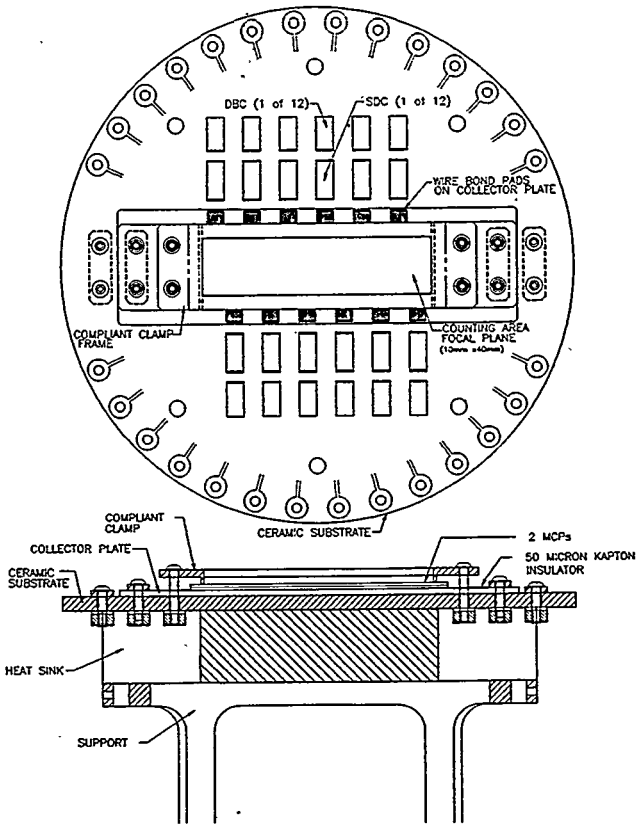

Fig. 1. Plan views of the LBL Next-Generation Detector showing the UHV-compatible design to integrate a pair of hot MCPs, 768 electrodes on the collector plate, 12 IC sets of two chips each on a ceramic substrate, and the heat sink support structure.

than 100 ns, leading to a dead-time fraction of $<1{:}10^5$. For many cases, this high speed will permit the taking of spectra in a single rapid snapshot approach without any scanning of the analyzer deflection parameters; a single spectrum could thus be obtained in as little as 10^{-2} to 10^{-3} seconds, compared to the minutes now required.

Accomplishments

- *Electron trajectories and statistics during amplification and counting*: To design the collector electrode structure, detailed Monte Carlo simulations of electron trajectories between the output of the microchannel plate (MCP) and the collection electrodes have been carried out. This work established the voltages and working distances required to avoid resolution loss due to spreading of the electron cloud.

- *Detector and IC mounting*: The design and construction of a scale model of an assembly compatible with ultrahigh vacuum (UHV) and consisting of high-speed "hot" MCPs, collectors, and IC electronics on a ceramic substrate was completed. This design is shown in Figs. 1 and 2. The model is presently being used to assist in the design and evaluation of fixtures required to assemble the hot MCPs, collector electrodes, and integrated amplifiers and counters. The need for special fixtures is clear in view of the requirement to wire-bond the collectors to the SDC inputs (768 connections on 50-micron pitch). By now, detailed drawings of both the collector plate and the 50-micron spacer have been sent out for fabrication.

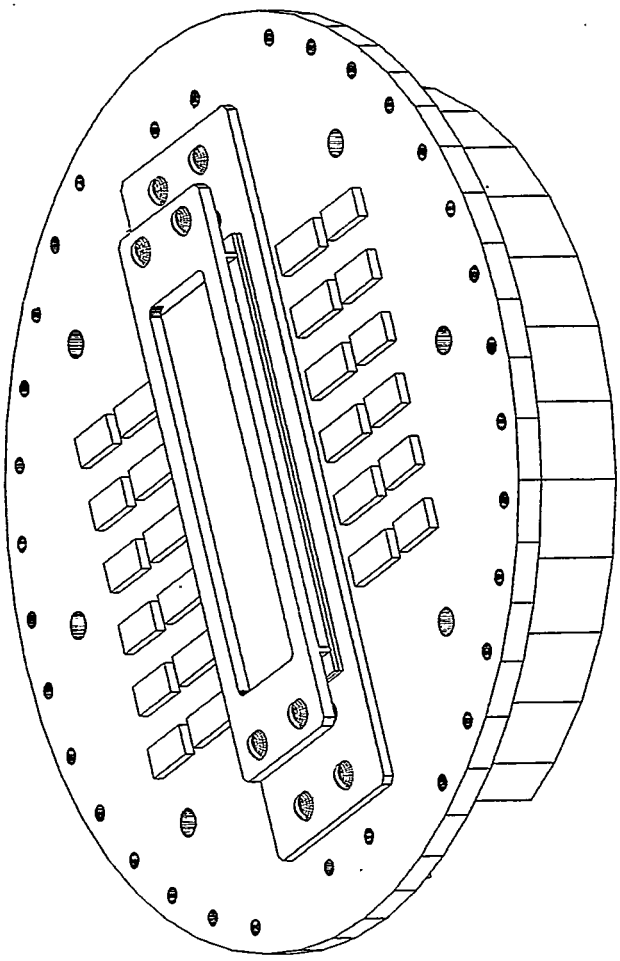

Fig. 2. Perspective view of the LBL Next-Generation Detector.

- *IC design*: The design of the DBC chip has been completed, successfully fabricated, and tested. In doing this, a test circuit printed circuit board for both the SDC and DBC chips was fabricated and tested. It has also been demonstrated that noise coupling from the DBC to SDC is not sufficient to degrade the performance of the SDC low-noise preamplifier-shaper-discriminator.

- *Ceramic substrate*: A good start was made on the design and layout of a ceramic substrate to support the SDC and DBC chips along with the hot MCPs and collector plate. As an important step toward completing this design, a test ceramic substrate supporting only the hot MCPs and collector plate, along with only a few electrode connections, had initial design and fabrication. The test substrate will be used to determine the hot MCP gain, gain distribution, electron cloud size, and heat dissipation.

- *UHV test chamber*: To test the new detector, a dedicated UHV chamber is required; we have assembled such a chamber, including ion pumps, associated valves, and mounting cart. A dedicated roughing pump is to be acquired for this system. All electrical connections to the detector will be via a 25-pin, nonmagnetic, 3.5-kV feedthrough. Fabrication of a UV lamp system (a photon source) to both scrub and test the hot MCPs has been completed.

- *External electronics and computer control*: The external electronics required for this detector include a power supply system to float at analyzer focal plane voltage, up to –2 kV. All of the floating supplies must be current-limited. Both current and voltage monitors are required, along with UHV vacuum interlocks. Such a well-regulated low-noise supply system for the detector is now under construction. To read out the 768 16-bit data words from the DBCs at a 10-MHz bit-serial rate, a digital-signal processor data system hosted in a PC is under development. The control computer system will also be able to set both the SDC and DBC thresholds and monitor MCP operating characteristics such as voltage, current, and temperature.

Environment, Health and Safety Division

Demonstration of Stable Isotope Tracer Methods in Detailed Hydrogeologic Modeling and Monitoring

Principal Investigators: Brian M. Smith and Leticia B. Menchaca

Project No.: 94007

Funding: $135,900 (FY 94)

Project Description

This study focused on the stable isotopes of hydrogen, oxygen, and strontium in waters at the Lawrence Berkeley Laboratory (LBL). Its principal objectives included: (1) demonstrating stable isotopic methods for possible future incorporation into LBL's Environmental Monitoring Program, (2) seeking opportunities to apply the methods to other contaminated federal and industrial sites, (3) seeking new alliances with businesses, universities, and regulatory agencies to prepare for future transfer of the methods to the private sector, (4) developing a model to allow rock properties to be estimated from isotopic data, and (5) installing a high-throughput gas preparation system to enhance the Laboratory's capabilities to further develop and apply the new techniques.

With the advent of RCRA- and CERCLA-driven programs to cleanse the environment of contaminants, it has become important to understand in detail the hydrology of thousands of local sites throughout the U.S. and other developed countries. Understanding the complexities of water flow and contaminant transport within small regions requires hydrogeologic tools and techniques that are widely applicable, environmentally innocuous, and sufficiently mature to be acceptable to regulatory agencies.

The stable isotope ratios of oxygen ($^{18}O/^{16}O$) and hydrogen (D/H) provide the most direct means for identifying water sources, because these isotope ratios are properties of the molecules comprising the waters themselves, rather than properties of any dissolved constituents. The vapor pressures of the different isotopic molecules of water are inversely proportional to their masses; $H_2{}^{16}O$ (mass = 18) has a significantly higher vapor pressure than $D_2{}^{18}O$ (mass = 22). Thus, water vapor formed by evaporation of liquid water is enriched in ^{16}O and H, while the remaining water is enriched in ^{18}O and D. The fractionation factor at any given temperature is the ratio of the vapor pressures, provided equilibrium between vapor and liquid is maintained. Waters formed under different climatic conditions will differ in isotopic composition.

Two of the stable isotopes of Sr, ^{87}Sr and ^{86}Sr, provide a different kind of hydrologic information. The isotope ^{87}Sr is produced by radioactive decay of ^{87}Rb over millions of years. Accordingly, $^{87}Sr/^{86}Sr$ ratios vary between rock units of differing age or composition. While H and O isotopic ratios of water are not affected by low temperature interactions with rocks, waters tend to take on the Sr isotope ratios of the rocks through which they pass. Therefore, the ratio $^{87}Sr/^{86}Sr$ of the dissolved Sr in ground water provides an indication of ground water flow path and of chemical reactions between the water and the host rock or soil.

Accomplishments

Surface waters and ground waters at LBL were analyzed for H and O isotopic ratios. During the study period, rain, springs, wells, vadose zone, hydraugers and tap water had $\delta^{18}O$ values of –2 to –14; –6 to –6.5; –6 to –7; –7 to –8, –6 to –8 and –12 to –13 (‰ vs. V-SMOW), respectively. The large stable isotopic variation found in local rainfall is explained by the combined effects of storm source and local meteorological conditions. Precipitation under low local ambient temperature from storms originating in the Gulf of Alaska had the lowest $\delta^{18}O$ values, while tropical storms combined with warm local temperatures produced the highest values. Many individual storms had stable isotopic compositions far different from local ground water, providing a natural isotopic tracer for such processes as infiltration and mixing of ground waters with surface waters.

Isotopic mass balance equations were developed and used to estimate stream flow response to rainfall events in Strawberry Creek. Following every rain event, $\delta^{18}O$ values in the stream changed positively, toward the isotopic signal of ground water and independently of the isotopic signal of the rain. This indicates that stream flow increments following rain events result mainly from an increase in ground water influx (base flow) and direct rainfall and runoff effects are subordinate.

We used the observed variations in the isotopic ratios of well water following the rainy season to identify areas of rapid surface recharge at LBL. Well water $\delta^{18}O$ ratios in some areas showed negative shifts of between 0.5‰ and 2‰ during or after the rainy season. These isotopically shifting areas correspond to sites of known contaminated groundwater and coincide with inferred faults. Most wells at LBL showed no significant $\delta^{18}O$ variation during the year. The marked contrast between tap water and ground water isotopic ratios enabled the detection of leaking facility water pipes and sanitary sewers. These were evidenced by areas of anomalously low $\delta^{18}O$ values (–8 to –9.5‰), resulting from the mixing of ground water (–6 to –7 ‰) with facility water (–12 to –13 ‰) piped in from higher elevations.

Groundwater samples were analyzed for $^{87}Sr/^{86}Sr$ using thermal ionization mass spectrometry (TIMS) and clear patterns were observed that relate to the geological formations present at the site. Within each of the three rock formations, the ground water inherits characteristic $^{87}Sr/^{86}Sr$ ratios from the rock. Where water flows from one unit into another, the $^{87}Sr/^{86}Sr$ ratios evolve toward values typical of the new rock type over distances on the order of tens of meters. The exact distance over which this occurs gives an indication of how fast the water is flowing; faster flow draws out this equilibration zone over long distances. In the B53 area, the component of downward flow into the Orinda Formation siltstone from the overlying rock unit was found to be small, as the $^{87}Sr/^{86}Sr$ ratio in the water evolved to typical Orinda Formation values over less than 15 meters. Actual downward flow velocities are less than 1m/year, based on mass-balance of the Sr exchanged between the water and rock. Ideally, we would obtain data from many points along the rock unit boundaries, but the present array of monitoring wells at LBL does not provide the opportunities to do so. However, the technique developed here may be applied to other sites and can be used further at the LBL site as the drilling program progresses.

The δD and $\delta^{18}O$ values and tritium in plant transpiration vapor from *Eucalyptus globulus* and *Genista monspessulana* were analyzed. Stable isotope methods were developed to determine the water sources for the two species. The $\delta^{18}O$ of transpired water source for *E. globulus* was –6.5‰, while that from *G. monspessulana* was –7.5‰ (see Fig. 1). These correspond to midrange ground water and vadose zone isotopic values, respectively. Tritium concentrations in plant transpiration water are nearly identical to subsurface values and reflect the proximity to the National Tritium Labeling Facility stack. Application of this technique is twofold: in monitoring tritium contamination in soil and ground water without the need for extensive drilling, and in studies of subsurface water migration in areas of tritium contamination.

This applied research has resulted in increased analytical capabilities at the Center for Isotope Geochemistry, and in new partnerships with other DOE sites and with the California regulatory community. Three Work For Others proposals have been funded for FY 95, including new applications of our methods at all California DOE sites. Currently, we are developing a CRADA proposal to further diffuse this technology to the private sector.

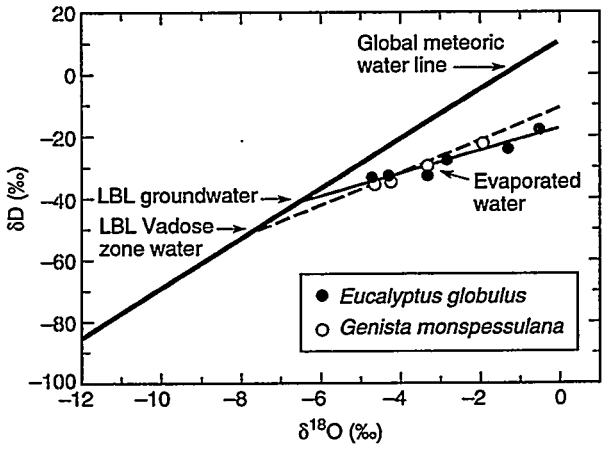

Fig. 1. Stable isotope composition of plant water sources are inferred through the analysis of evapotranspired water; a similar approach may be used to estimate subsurface tritium concentrations.

Publications

B.M. Smith, L.B. Menchaca, M. Conrad, and T. Johnson, "The Application of Stable Isotope Methods to Site Characterization and Environmental Monitoring at the Lawrence Berkeley Laboratory, California," to be submitted to *Environmental Science and Technology*.

L.B. Menchaca, B.M. Smith, and M. Conrad, "A New Method for Determining Vadose Zone and Groundwater Tritium Concentrations from Evapotranspired Plant Water," to be submitted to *Nature*.

L.B. Menchaca, B.M. Smith, and M. Conrad, "Plant Transpiration as a Monitor of Subsurface Water Migration," to be submitted to *Oecologia*.

Information and Computing Sciences Division

Visual-Servoing for Scientific Applications

Principal Investigators: Bahram Parvin, William Johnston, Ulrich Dahmen, Daniel Callahan, Marcos Maestre, and Robert Liburdy

Project No.: 94008

Funding: $142,600 (FY 94)

Project Description

The routine use of video image sequences in laboratory science (that is, video as data) has considerable potential as a powerful data collection tool. However, the current state of the art has not permitted this potential to be realized for two reasons: (1) our inability to collect, store, and analyze digital video streams in a reasonable amount of time, and (2) the lack of systems methodology to use the results of the analysis to alter the parameters of the experiment as a function of the image content.

The first obstacle is that individual scientific experiments often generate many thousands of images per video sequence. Currently, this video is converted to digital data and analyzed in an off-line mode using interactive techniques—a process that is tedious, time consuming, and subjective. The second obstacle is that existing systems tend to be stand-alone, disallowing dynamic manipulation of experimental parameters based on the analysis of *image content*. The proposed research is significant in that:

1. It will dramatically reduce the cycle time for conducting certain types of experiments and potentially increase the efficiency of data acquisition in dynamic studies.
2. It integrates LBL's existing work in image understanding and high-speed distributed computing into a unique set of applications for supporting laboratory science.
3. It closes the loop between on-line measurements based on image content and process control, thereby:
   a. Providing a platform for biologists and material scientists to open up new frontiers in microengineering and micromanipulation.
   b. Achieving a new milestone in visual-servoing, an increasingly important field combining computer vision, control theory, and high-speed computing for science and automated manufacturing.

To this end, the Imaging Technologies Group, in collaboration with the National Center for Electron Microscopy and the LBL Life Sciences Division, identified three laboratory problems for prototype applications: (1) *in situ* electron microscopy experiments, (2) a novel approach to DNA sequencing, and (3) a study of the effects of electromagnetic fields (EMFs) on individual living cells. In each of these cases, the on-line collection and analysis of digital video is a key element, together with subsequent control based on content analysis of the video.

Accomplishments

From a system integration perspective, the design philosophy has been to provide an environment where any scientific instrument that can generate a few tens of megabits per second can use the high-speed network and access a multiprocessing environment for on-line application. However, the enabling technologies for achieving the on-line processing and manipulation are robust computational techniques operating on video streams, which has been the major focus of our research. We claim the necessary computational techniques have been designed and partly implemented to address the three applications named above. A brief description follows.

It has been our experience that object detection by exclusively "low-level" (image-pixel-based) processing is bound to fail in the presence of noise, variation in contrast, shading, and the inherent limitation of the model on which a particular low-level operator is based. These limitations lead to ambiguities for detection and localization of an object in the field. The novelty of our approach is in incorporating "high-level" (vision-based)

models to provide geometric constraints for bounding the problems. These constraints are inferred by extracting *perceptually significant* features from the image. For a set of laboratory problems, we have constructed a "feature" dictionary to enable detection and tracking of a particular set of geometric structures. These include (1) convex ribbons corresponding to precipitates in electron microscopy, (2) concave ribbons corresponding to DNA molecules, and (3) circular geometry corresponding to cells in the calcium oscillation studies.

The generic architecture of our system is shown in Fig. 1, where the object models could be 1, 2, or 3, above. Note that each of the three applications has identical building blocks, but they each use a different object model. An operational example of the DNA application, together with the intermediate results, is shown in Fig. 2.

Other accomplishments include (1) a distributed implementation of circular object detection demonstrating real-time performance; (2) development of algorithms for closing the loop for manipulation of *Polybeads* with an electric field;[1] (3) specification and purchase of data acquisition components; and (4) construction of a fiber link between Buildings 72 and 50B for high-speed connection of an optical microscope video-capture system to large-scale storage and computing systems.

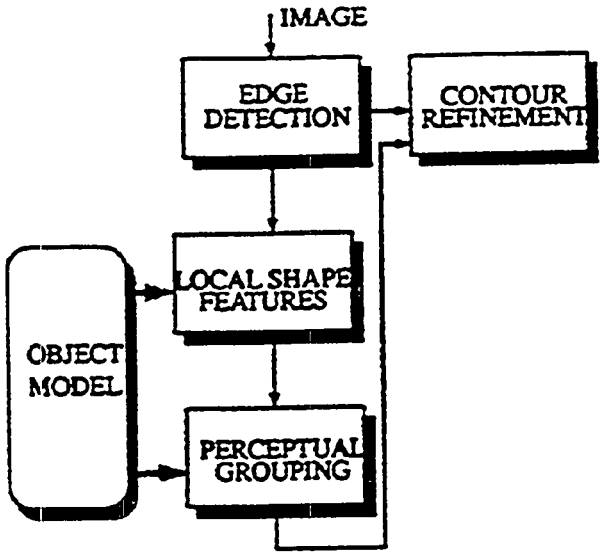

Fig. 1. Image-understanding architecture for visual-servoing applications.

Fig. 2. Steps in extraction of DNA molecules: (a) edges and local symmetries for multiple molecules; (b) global symmetries; (c) inferred polygons; and (d) refined contours.

[1]Polybeads are spherical crystals that are used to calibrate optics of a microscope; their shape emulates DNA segments once they have been sectioned.

Life Sciences Division

A Comprehensive Approach to Protein Folding

Principal Investigator: Teresa Head-Gordon

Project No.: 92021

Funding: $99,200 (FY 94)
$98,800 (FY 93)
$10,800 (FY 92)

Project Description

A holistic approach to protein folding has been undertaken in the last year by designing specific computational studies that impact on the following two areas: (1) the understanding of the hydrophobic effect as a possible driving force for early folding kinetics, and (2) prediction of protein secondary structure using neural networks. Nonlinear optimization in conjunction with hydrophobic studies and new neural network algorithms provide the theoretical scheme for predicting protein structure solely from amino acid sequence.

With respect to the hydrophobic effect and its relation to folding kinetics and protein stability, the early stages of protein folding could be entirely dictated by hydrophobic interactions (whereby hydrophobic groups come together to minimize their interaction with water), and secondary structure formation could be a simple direct structural consequence of the hydrophobic collapse of the polypeptide. Such a scenario implies that the aqueous environment is the primary driving force for early folding and that the details of amino acid sequence are not critical. Trapped early kinetic intermediates of proteins (characterized by hydrogen-exchange labeling and proton NMR) containing predominately helix or predominately sheet indicate that compactness occurs on the same time scale as secondary formation in the former type and precedes sheet formation in the latter.

Furthermore, the temperature dependence of protein stability shows marked similarity to hydrocarbons as revealed by transfer microcalorimetry experiments (the hydrocarbon model of Robert Baldwin at Stanford). These transfer experiments reveal that large changes in heat capacity (and not the large entropy change at room temperature) is the signature of hydrophobia in both systems, which implies that the roles of enthalpy and entropy change as a function of temperature.

These experimental attributes of protein kinetics and thermodynamic stability are united by our lack of clarity on the molecular origin of the hydrophobic effect. X-ray and neutron diffraction experimental techniques are unable to help because of the insolubility of hydrophobic groups in water, and the problem is too computationally demanding, even for empirical molecular dynamics simulations using well-established force fields, for theoretical approaches.

With respect to neural networks, protein structure prediction methods promote the idea that the secondary and tertiary structure is somehow encoded in the amino acid sequence. The empirical determination of this mapping between sequence and structure has been approached in a variety of ways, although none has been entirely successful. We have developed a constrained optimization strategy known as the antlion method that uses neural networks as guidance to determine a native tertiary structure using only the amino acid sequence as input. We have successfully applied this method to the prediction of the structure of melittin, the 26-residue bee venom polypeptide. The key to extending the antlion method to predictive studies of larger proteins with a richer tertiary structure is the development of reliable neural networks.

The successful application of neural network algorithms for prediction of protein structure is stymied by three problems: (1) the scarcity of the database of known protein structures; (2) poorly devised network architectures, which make the input-output mapping opaque; and (3) a global optimization in the multiple minima space of the network variables. As a consequence, the current protein structure predictive capacity of neural networks is no better than sequence homology modeling and statistical analyses of the databank of structures—methods which have not in themselves yielded reliable prediction algorithms.

Accomplishments

In the studies of the hydrophobic effect as a possible driving force for early folding kinetics, a new water model was developed that allows us to investigate via rapid simulation the molecular nature of the hydrophobic effect. For the first time we can evaluate properties such as heat capacity with meaningful error bars in the case of hydrocarbon dissolution and attach a molecular description to understand the macroscopic thermodynamics. Further calculations as a function of temperature will allow us to assess the validity of the hydrocarbon model for understanding protein stability. Free energy reaction coordinates for representative sidechains using this model will allow us to interrogate the plausibility of the hydrophobic effect being the primary driving force of early kinetics. We have also discovered the reason why the hydrophobic effect is proportional to surface area (optimization of large hydrogen bond rings along the solute surface), an explanation that is consistent with the observed temperature dependence of the thermodynamics of hydrophobic dissolution.

For prediction of protein secondary structure using neural networks, our proposed theoretical framework for solving the protein structure prediction problem involves the use of highly developed constrained optimization techniques that isolate the native structure minimum as the only minimum of the (originally complex) hypersurface. The algorithmic components—protein force fields and optimization codes—are largely in place, but we still require the input of robust constraints predicted by neural networks to uniquely isolate the native structure minimum. However, based on the three problems cited above, neural network prediction of constraints is below threshold for successful constraint optimization.

Through funding from the Air Force Office of Sponsored Research, we propose to correct these problems by focusing on well-thought-out network designs. We have recently completed trial neural networks that learn secondary structure better than networks with arbitrary topology. We are currently scaling up these networks to directly tackle secondary structure prediction.

Publications

T. Head-Gordon and F.H. Stillinger, "An Orientational Perturbation Theory for Pure Liquid Water," *J. Chem. Phys.* 98, 3313–3327 (1993).

F.H. Stillinger and T. Head-Gordon, "Perturbational View of Inherent Structures in Water," *Phys. Rev. E* 47, 2484-2490 (1993).

T. Head-Gordon, "An Efficient Solvent Model for Study of Hydrophobic Phenomena," *Chem. Phys. Lett.* 227, 215–220 (1994).

T. Head-Gordon, "A New Solvent Model for Hydrophobic Association in Water," to appear in *J. Am. Chem. Soc.*

T. Head-Gordon, "Characterization of Water Structure Around Hydrophobic Groups," submitted to *Proceedings of the National Academy of Sciences* (1994).

R.C. Yu and T. Head-Gordon, "Neural Network Design and Application to Protein Secondary Structure Prediction," accepted for publication in *Phys. Rev. E* (1995).

Electron Crystallography of Selected Membrane Proteins

Principal Investigator: Bing K. Jap

Project No.: 94009

Funding: $80,000 (FY 94)

Project Description

Our work in electron crystallography on membrane proteins has focused on the following objectives: (1) to obtain a high-yield expression system for obtaining milligram quantities of the Cystic Fibrosis Transmembrane Conductance Regulator (CFTR) protein for two-dimensional (2D) crystallization; and (2) to initiate research on the structure determination of GpIIb/IIIa integrin. We are currently obtaining preliminary results in

the molecular structure determination of these two clinically important membrane proteins. Our long-term research objective is to provide the detailed structural insight necessary to develop a molecular explanation for the diseases associated with their defects. This information is expected to be crucial in the development of drugs for combating the diseases.

Initially, we planned to use the bacculovirus expression system to overexpress the CFTR, but we were unable to get this expression system. We believe it would be beneficial to develop a high-level expression system for overproducing membrane proteins with histidine tails that can be used to greatly simplify their purification. The establishment of such an expression system will certainly be crucial to our membrane protein structure and function program. The capability to overexpress membrane proteins would allow us to carry out structural studies of clinically important membrane proteins, starting from their cDNA.

To construct the expression system of CFTR, we needed the cDNA clone of CFTR, which we obtained from Dr. L.-C. Tsui, Department of Genetics and Medical Biophysics at the University of Toronto. We have also established a collaboration with the group of Dr. George Chandy at the University of California, Irvine, to obtain a high-level expression of CFTR using the vaccinia virus expression vector, as they have done for the potassium channels. This expression system has several advantages. It has been demonstrated, at least for the potassium channel, that milligram quantities of active protein can be obtained in a variety of host cells. For the case of the potassium channel, a histidine tail was engineered on the protein, which dramatically eased the purification of this protein with the use of Ni^{2+}-chelate chromatography. A similar technique was used in the expression of our CFTR protein.

Accomplishments

We successfully obtained the recombinant of the CFTR and the vaccinia virus. The cloning of the CFTR was done in two stages. The first stage involved the cloning of the CFTR to a transfer vector with a $(His)_6$ tag; our major effort was directed toward obtaining this clone. The second stage involved performing the recombination of the transfer vector with the vaccinia virus.

Although the recombination is a straightforward technique, it is time consuming. It involves the selection of a properly combined vaccinia virus and CFTR clone that includes several rounds of infection and selection of potential clones. We have obtained recombination of the CFTR clone and vaccinia virus and are currently purifying the recombinant vaccinia virus.

We have now established the tissue culture and radioactivity facility, which enables us to continue our work on the purification of the recombinant virus. Once the recombinant virus is purified, the expression system will be evaluated in producing active CFTR protein that is properly inserted into the cell membrane. This insertion involves the infection CV-1 cells (African green monkey kidney cells) or CHO cells (Chinese hamster ovary cells) with our expression system and characterization of the expressed CFTR protein. We expect to begin the purification and crystallization of CFTR this coming year. The purification protocol for this protein will be established, yielding milligram quantities of active CFTR protein, and will be used to perform the crystallization trials forming 2D or 3D crystals.

This project supports a new researcher, Dr. Peter Walian, working on the crystallization of a member of the integrin family of adhesion proteins, GPIIb/IIIa. This research is being done in collaboration with Joel Bennett, M.D., of the University of Pennsylvania School of Medicine.

Biological Dosimetry and Risk Assessment: Propagation of Genetically Damaged Hemopoietic Stem Cell Progeny

Principal Investigators: Maria Pallavicini, George Brecher, and Malak Shoukry

Project No.: 94010

Funding: $44,600 (FY 94)

Project Description

Biological health-effect risks from environmental toxicant exposure are often monitored by

measuring genetic damage present in cell subpopulations in peripheral blood. Peripheral blood cells derive from a rare subpopulation in bone marrow, designated "stem cells." It is estimated that 1/50,000 bone marrow cells may be a stem cell. Stem cells have the capability to self-renew and contribute to the production of blood cells (hemopoiesis) for the lifetime of the organism. Thus, measurement of long-term stable genetic damage in peripheral blood reporter subpopulations (often lymphocytes are used) following environmental exposure to radiation or carcinogens/mutagens is used to estimate absorbed dose (e.g., dose received by stem cells *in vivo*). Two underlying assumptions are made in estimating systematic dose from measurements using reporter cells in peripheral blood: that the frequency of genetically variant circulating cells is (1) equivalent to the frequency of variant stem cells and (2) proportional to the extent of systemic genetic damage. Several studies suggest, however, that these assumptions may not be entirely valid.

Several factors may contribute to an apparent uncoupling between the frequency of genetically aberrant lymphocytes and genetically damaged stem cells. Genetically aberrant lymphocytes may arise from both damaged hemopoietic stem cells as well as from immature lymphocyte subpopulations that survived radiation. Since neither the frequency nor the residence of long-lived lymphocytes is known, it is unclear whether the presence of long-lived lymphocytes alters frequency measurements of aberrant cells in the circulation. Variation in the radiosensitivity of lymphocyte subpopulations *in vivo* and their lengthy lifespan may contribute to their continual presence in sequestered sites for many years after exposure. The frequency of aberrant lymphocytes in peripheral blood may be altered by clonal expansion of lymphocyte subpopulations in response to immunologic stimuli (e.g., specific antigentic stimulus, viral and bacterial infection, arthritis). We propose to increase understanding of the dynamics of hemopoiesis by determining the relationship between radiation dose, stem cell genetic damage, and propagation of genetically damaged cells throughout the hemopoietic system.

Accomplishments

The first step in determining whether genetically damaged reporter populations in blood reflect damage incurred by the stem cells is to measure genetic damage in isolated stem cells following exposure to agents anticipated to pose biologic health-effect risks. We developed techniques to isolate primitive hemopoietic subpopulations highly enriched in stem cells. Although stem cells cannot be identified morphologically, assays exist in mice to measure stem cell content of marrow populations. In mice and humans high-dose radiation exposure eradicates the hemopoietic system and induces lethality unless blood cell production is restored. Transplantation of approximately 50,000 bone marrow cells into a lethally irradiated mouse will rescue hemopoiesis and the donor cells will maintain blood production for the lifetime of the organism. It is estimated that at least one stem cell is present in the 50,000-cell rescue inoculum.

A series of methodological approaches were evaluated to isolate marrow populations containing stem cells from transgenic mice. The transgenes present in the mouse marrow cells allowed us to use DNA-based approaches to monitor the ability of transplanted cells to contribute to hemopoiesis in transfused recipients. To date, we have shown that we can restore hemopoiesis in irradiated mice by transplantation of 50 isolated cells. The transfused 50-cell inoculum contains stem cells capable of generating blood cells for at least nine months. The technique uses flow cytometry to discriminate and sort the rare subpopulation, which is labeled with antibodies and fluorescent dyes targeted toward proteins on the cell surface and intracellular structures. The ability to isolate stem cells will facilitate analysis of genetic damage in this rare subpopulation, which is capable of regenerating the entire hemopoietic system.

Assessment of genetic damage in blood cells and stem cells requires assays to detect alterations in the genome of the target subpopulation. Cells with severe chromosome abnormalities are unlikely to survive for extended periods. Stable long-term genetic alterations are those compatible with cell survival and are more likely to result in biologic health effects because this population is maintained for the lifetime of the organism.

Chromosome translocations provide an estimate of stable genetic damage because cells carrying translocations are maintained for extended periods. Developments in fluorescent-tagging of chromosomes using fluorescence *in situ* hybridization with chromosome-specific probes allow visualization of translocations in mitotic cells. Fluorescent chromosome-specific probes are widely available for human chromosomes; however, measurements of translocations in murine cells have been hampered by the limited availability of murine chromosome-specific DNA probes. Recently, Dr. Ulli Weier in the Life Sciences Division at LBL generated fluorescent DNA probes to specifically label (i.e., paint) mouse chromosomes 1, 2, 3, and X. The DNA paint probes allow visualization of translocations involving these chromosomes in murine cell subpopulations.

We have used the mouse DNA paint probes to visualize translocations involving these chromosomes in murine cell subpopulations. We are in the process of determining the sensitivity of translocation detection to monitor genetic damage induced by low-dose radiation exposure. Detection of chromosome damage following low-dose exposure is desirable to more closely mimic environmental exposure of humans. Simultaneous detection of translocations in peripheral blood reporter populations and isolated stem cells will establish the relationship between frequency of genetically damaged stem cells and their progeny in peripheral blood.

Combinations of methodologies to isolate hemopoietic stem cells and measure stable genetic damage should lead to a better understanding of how progeny from genetically damaged stem cells are propagated throughout the hemopoietic system during lifetime hemopoiesis and should increase understanding of the significance of peripheral blood-based assays for risk assessment. Furthermore, the ability to isolate stem cell populations from transgenic mice provides unique opportunities for future studies to extend sequence information from the human genome project to identify genes that modulate stem cell differentiation and proliferation.

Head Probe for Nuclear Magnetic Resonance Imaging and Spectroscopy at 10 T

Principal Investigators: Mark S. Roos, Sam T.S. Wong, and Thomas F. Budinger

Project No.: 93012

Funding: $50,000 (FY 94)
$48,100 (FY 93)

Project Description

The objective of this project was to develop rf coil technology critical to ^1H NMR spectroscopic imaging of objects the size of the human head at 10 T. This technology will be a major component in a future generation of NMR spectrometer that will have substantial improvements in sensitivity over current machines. The primary applications of such instruments are for *in vivo* biomedical research.

Last year, volume coils operating at up to 430 MHz were designed, fabricated, and tested to determine their suitability for NMR studies. Direct characterization of the probes was not possible because large-bore NMR magnets operating at fields of 8 to 10 T do not yet exist. However, the relevant performance parameters, including the signal-to-noise ratios (SNR) for NMR experiments, global power deposition, and field homogeneity can be deduced from benchtop measurements. We measured these parameters in spherical and cylindrical phantoms designed to validate theoretical predictions and to roughly approximate the geometry of the human head. This project has provided the technology essential for *in vivo* NMR at 10 T and has experimentally verified predictions for the performance of these instruments.

The study was begun by constructing prototype coils based on the birdcage design with additional distributed capacitance. We found that it was difficult to obtain sufficiently high resonance frequencies with this design and that the inductance

of the end rings is undesirable. A capacitively shortened waveguide resonator was then investigated that has been employed as a body coil operating at 170 MHz for 4-T whole-body MR by Siemens.

Accomplishments

A prototype head resonator was constructed with two segmented inner conductors on a 30-cm former in a 35-cm cylindrical shield. As built, this structure resonates at up to 460 MHz and produces a linearly polarized B field in its interior. We were unsatisfied with the complexity of construction and difficulty in tuning this design, and in the second project year focused on a cavity resonator design proposed by Dr. Thomas Vaughan of the University of Alabama (UA) at Birmingham, who agreed to collaborate on this project. This resonator consists of 8 to 16 individually tunable cylindrical elements in a cylindrical cavity. An additional advantage of this resonator is that its modes and their associated current distributions are well understood. One resonator was constructed at UA and one at Lawrence Berkeley Laboratory (LBL), and both were tested at LBL.

The cavity resonator was tuned at up to 400 MHz under a variety of load conditions, and the internal B field was surveyed using a survey apparatus that employs a loop detector with a zero-bias Schottky barrier diode (Hewlett-Packard HSCH-3486) rectifier connected to an integrating capacitor. The capacitor voltage is measured with high-impedance plastic leads (Polymer Corp., Reading, Pennsylvania) to avoid disrupting the fields. The field was surveyed with the coil empty, and with a saline-filled cylinder inserted into the coil to simulate a head. Survey results are in qualitative agreement with theoretical predictions (Fig. 1), but substantial difficulties were encountered in driving the loaded (but not the empty) cavity in a manner that preserved the desired symmetry of the field. A four-point drive employing a quadrature hybrid and two 180-degree splitters was eventually adopted.

The field surveys and measurements of the resonator quality factor (Q) under loaded and unloaded conditions demonstrate the feasibility of constructing a head probe for NMR imaging and spectroscopy at 10 T that will realize the gains in signal-to-noise ratio expected from operation at

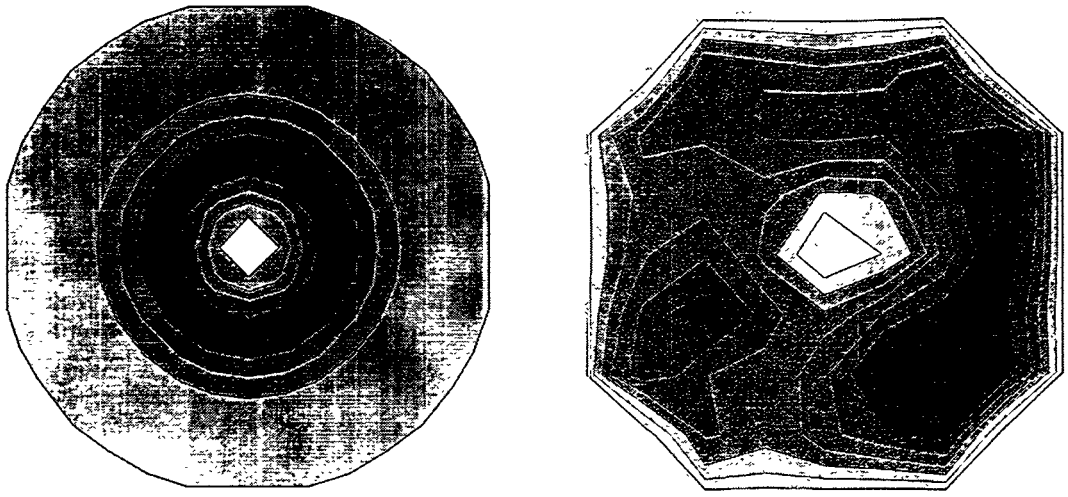

Fig. 1. Magnetic field distribution on the center transverse plane when saline with half-normal conductivity (0.45%) is placed in the coil. On the left is the prediction of the theory describing a lossy dielectric cylinder and current elements of finite length in an infinite cylindrical shield. On the right is the corresponding experimental result, a survey of the coil operating at 350 MHz. The area of field plotted for both theory and experiment is 16 cm by 16 cm. The magnitude of the component of the circularly polarized magnetic field transverse to the axis of the cylinder is plotted.

higher field. It is important to keep in mind that the uniformity of the field within a sample will be determined primarily by its conductivity and dielectric properties in this frequency range, and that substantial variation will exist. Whether it will be possible to model these variations well enough to make corrections and allow quantitative spectroscopy remains to be demonstrated, but most surface coil spectroscopy today is already performed using uncorrected, nonuniform fields.

Publications

N. Zhang, "Effects of Capacitive Shortening on the Resonance Frequency of the Birdcage Coil," *Proc. Soc. Mag. Res.* 1114 (1994).

N. Zhang, M.S. Roos, S.T.S. Wong, and J.T. Vaughan, "An Experimental Study of a Head Coil for Proton Imaging and Spectroscopy at 8–10 T," *Proc. Soc. Mag. Res.* 1102 (1994).

Creation of Transgenic Mice Containing a Library of P1 Clones Encompassing the Down's Syndrome Region from Chromosome 21

Principal Investigators: Edward M. Rubin and Jan-Fang Cheng

Project No.: 94011

Funding: $189,900 (FY 94)

Project Description

The goal of these studies was to create multiple lines of transgenic mice, each containing a large distinct segment of human DNA from the Down's syndrome (DS) region of chromosome 21. The multiple lines of transgenic mice created through microinjection of P1 and YAC DNA clones mapped to this region would serve as an assay to assess the effect that the *in vivo* overexpression of these defined human sequences have on the organism. A variety of phenotypic characteristics normally associated with increased dosage of this region in individuals with DS (e.g., heart disease, hematological abnormalities, developmental abnormalities) will be assessed. The mice created as part of this study will serve as a repository for understanding the *in vivo* biological properties of this region of the genome.

Accomplishments

P1 and YAC clones isolated from the DS region of chromosome 21 (DS21) were prepared in a form suitable for introduction into mouse zygotes. These sequences have been introduced into mouse zygotes and several lines of transgenic mice containing each of the human sequences were created. Overlapping P1s and YACs have been used to minimize the risk of a gene being interrupted at the end of a P1 clone. Following the creation of this DS21 *in vivo* library, the individual lines of mice will be assessed for various phenotypic features associated with DS. When phenotypic effects are observed in the P1- or YAC-containing transgenic animals, truncated forms of the P1 or YAC clone will be constructed and examined in a second set of transgenic animals to determine the sequence(s) responsible for the identified phenotype.

Clone-Based Map of 21q22

This region encompasses much of the Down's syndrome region at 21q22.2 and includes the markers CBR and PCP-4 between which mapping studies have indicated the *weaver* gene lies. The physical map we have developed consists of a complete YAC contig and a P1 contig that extend over part of the YAC contig. There are 5 YACs and 8 P1s spanning approximately 2 Mb of DNA. Except for the YAC 285E6, the other 4 YACs have been previously reported to be nonchimeric and nondeleted as suggested by the long-range restriction maps derived from both lymphocyte DNA and YACs. This YAC contig completely covers the region between CBR and PCP-4; however, the YAC 745H11 is unstable, producing smaller fragments during growth. This YAC was therefore not used in constructing transgenic mice. The omission of YAC 745H11 left a gap between YACs 230E8 and 141G6 that was filled using P1 clones.

Creation of a Library of Transpolygenic Mice

Pups resulting from zygote microinjection with YAC and P1 DNA were screened using the PCR; primers designed to detect sequence-tagged sites (STSs) from the human and vector sequences were employed. For each YAC, two to ten independent lines of transpolygenic mice harboring a full-length insert were created. In addition, for each YAC clone between 8 to 13 lines of mice containing incomplete segments of the YAC inserts were created. The P1 phage DNA was injected as pools of two overlapping phage DNA mixed together in equal concentration and the DNA was thus microinjected as three different pools. At least one line of mice was created for each P1 phage that bridged the gap in the YAC contig.

Expression of Transgenes

To investigate whether the human YAC DNA integrated into the mouse-genome-displayed expression of the resident genes, one transcription unit was examined for each YAC using reverse-transcription PCR (RT-PCR). The STS CBR is contained within the gene for human carbonyl reductase, which is considered to be a housekeeping gene. The STS resides within YAC 230E8 and a line of mice containing this YAC expresses the carbonyl reductase gene fairly uniformly in all tissues examined. The STS D21S267 is contained within a transcription unit that has been shown to be expressed predominantly within the human brain. This STS is found within YACs 141G6 and 152F7 and two lines of mice, each containing one of these YACs, express the gene containing this STS; moreover, expression of the human gene is particularly strong in the mouse brain. Thus each YAC transgene was demonstrated to express at the appropriate location.

Publication

D. J. Smith, Y. Zhu, J.-L. Zhang, J.-F. Cheng, and E. M. Rubin, "Construction of a Contiguous 2 Mb YAC/P1 Library of Human Chromosome 21q22.2 in Transgenic Mice," submitted to *Genomics* (1994).

A Transgenic Model for Clinical Testing of Progestins and Analysis of Progesterone Receptor Function

Principal Investigator: G. Shyamala

Project No.: 94012

Funding: $59,800 (FY 94)

Project Description

The objective of this project is to create transgenic mice expressing "A" and "B" forms of human and murine progesterone receptor. To this end, as a first step, we had to make cDNA constructs of these various forms of the receptor suitable for expression in a transgenic setting. Our original intention was to create these constructs using the constitutive CMV promoter and mammary-specific WAP promoter. However, prior to the initiation of the project we realized that while this strategy would be sufficient to create the transgenic mice, the females may encounter problems during pregnancy due to overexpression of one form of the receptor. The problems may arise because pregnancy is under complex and exquisite regulation by progesterone, which mediates its effects through the receptor. Such regulations in pregnancy would create difficulties in establishing a founder line of mice. Accordingly, we decided to use a binary system for the creation of these mice, which prevents the expression of transgene until an F-1 hybrid is generated. Fig. 2 describes the plasmids necessary for constructing the binary system.

Accomplishments

1. To make the UASG-TATA-luciferase construct, we obtained a plasmid (pCa Spe R3) from Mike Strathman of the Lawrence Berkeley Laboratory Human Genome Center. We first inserted the coding region and 3′ poly A sequences of the luciferase gene into this vector and removed the P-elements of the original plasmid, thereby resulting in the generation of pUAS-TATA-Luc.

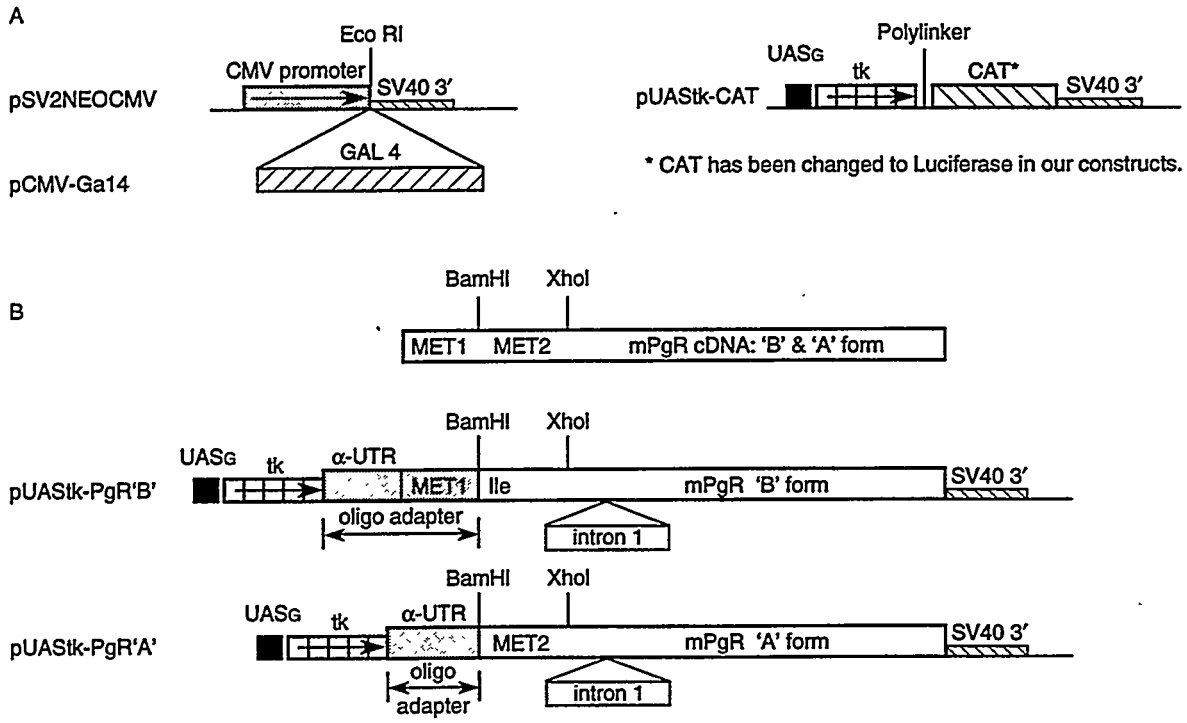

Fig. 2. Schematic representation of plasmid constructions for the binary system. A: Insertion of the GAL 4 gene into the CMV promoter expression plasmid, and diagram of the UAS_G binding sites (3-4) inserted 5′ to tk-CAT. The curved arrow indicates the transactivation of the UAS_G by GAL 4 leading to CAT expression. B: Construction of the mPgR "B" and "A" expression plasmids. Modified mPgR clones are inserted into UAS-tk-CAT, replacing CAT. Both constructs contain the first intron isolated from the genomic clone. The mPgR "B" plasmid has the second MET (ATG) modified to Ile (ATC). The mPgR 5′ UTR region has been removed and replaced with the α-globin 5′ leader. The oligo used to add the leader has both the leader sequence and the first 25 bp of the mPgR cDNA and is ligated with the Bam HI site in mPgR. The mPgR "A" plasmid has only MET2 by cleavage of mPgR with Bam HI. The α-globin 5′ leader is then inserted between the promoter and this Bam HI site.

2. For creation of CMV-GAL-4 plasmid, the plasmid pGATB that has the GAL-4 site was also provided by Mike Strathman. For insertion of GAL-4 into the unique ECoR$_1$ site of pSV$_2$ NEO CMV, the GAL4 gene carried on a HindIII fragment was modified to EcoRI and cloned into pUC19. This gene was then cloned into a vector, whereby it was expressed from the CMV promoter.

3. The two plasmids (UAS_G-TATA-Luc and CMV-GAL-4) were transfected into 3T3 cells to monitor the function of the GAL4 gene product. The UAS-TATA-luciferase plasmid alone or cotransfected with the CMV vector gave baseline levels of luciferase. The combination of UAS-TATA-Luc yielded a seven-fold induction of luciferase activity, demonstrating that the GAL4 construct was functional. The results of the cotransfection also demonstrated that the UAS-TATA-Luc construct had a functional UAS element, such that this UAS-TATA promoter could be used with confidence to express the PgR "A" and "B" gene constructs.

4. The GAL-4 expression construct, having been tested for its functionality *in vitro*, was ready for transfer into the mouse genome. Accordingly, this construct was given September 1994 to Dr. Eddy Rubin for transfer into mice.

5. For isolating of the first intron of murine PgR, a lambda clone (G-1) encoding the first intron of murine progesterone receptor was subcloned and subjected to Southern blot analysis to

identify restriction fragments that contained intron sequences. One subclone was found to contain intron sequences since it was 250 bp larger than the corresponding cDNA fragment. However, we were expecting the first intron to be greater than 1 kb in length based on the chicken genomic sequence. Thus this clone most likely did not contain the entire intron. This was confirmed by sequence analysis of this clone, which revealed the 5′ boundary of the intron but not the 3′ end. We obtained 250 bp of intron sequences but required the 3′ junction for proper splicing. Since we now knew the exact location of the intron, we made oligo nucleotide primers to the cDNA/intron junction to be used in a PCR reaction and amplified the intron sequences. The oligos were designed to contain restriction sites at their ends for ease of subcloning, and also spanned convenient restriction sites within the cDNA for ease of substituting the intron region into cDNA clones. PCR reactions were performed using the PgR lambda genomic clone G-1 as substrate. A unique ~1.5 kb PCR product band was observed and was specific for the presence of both primers and for the presence of PgR DNA. This PCR product was gel-purified, subcloned into pUC19, and analyzed for its sequence, which revealed the presence of the full-length intron.

6. For construction of pUAStk-PgR "A" we had to use three independent steps: (1) the insertion of the first intron of PgR into the PgR cDNA, which in turn involved two independent steps; (2) the fusion of this construct within the UAS-TATA promoter; and (3) fusion of the UAS-TATA-PgR with the poly (A) site. Once this construct was made, its authenticity was established by restriction analyses. This construct was also given during September 1994 to Dr. Eddy Rubin for transfer into mice.
7. Toward constructing pUAStk-PgR "B" we had to initially generate a site-specific mutation at the second ATG. For this, the 5′ end of the PgR cDNA, which had been previously cloned into the Bluescript vector, was used to prepare single-stranded DNA. For this, the plasmid was transformed into the *dut-1, ung-1* strain and super-infected with helper phage in the presence of uridine to generate single-stranded DNA containing uracils in thymine positions. This DNA was used as a substrate for *in vitro* second-strand synthesis originating from a primer with a single mismatch and the second ATG. The site-specific mutation was then confirmed by sequence analyses.

Variations in Susceptibility to Environmental Oxidants as Studied Using Transgenic Mice

Principal Investigators: Diane L. Tribble, Edward M. Rubin, Elaine L. Gong, and Mary-Helen Barcellos-Hoff

Project No.: 94013

Funding: $125,400 (FY 94)

Project Description

Radical-mediated oxidative modifications have been implicated in the development of numerous chronic and degenerative diseases including atherosclerotic heart disease and cancer. Recognition of the ubiquitous pathophysiological consequences of oxidative processes provides a unifying framework for the study of environmentally induced diseases since a diverse array of disease-promoting environmental agents act as oxidants in biological systems. A primary goal of this project is to characterize the effects of selected environmental oxidant stressors on the development of atherosclerosis in susceptible mice, and to use such atherosclerosis-promoting conditions to investigate the protective effects of gene coding for human apolipoprotein A-I (apo A-I_h) and copper-zinc superoxide dismutase (CuZn–SOD), which have been shown to inhibit oxidant-induced sequelae *in vitro*.

We are employing ionizing radiation and hypoxia/reoxygenation as prototypic environmental oxidant stressors. Biological responses to both of these exposure conditions are diverse, but are suggested to be mediated in large part through the formation of reactive oxygen species. Irradiation is performed using a 250-keV x-ray machine with a single dose of 8 Gy collimated to limit exposure to the upper thorax. Hypoxia is imposed by housing animals in a hypobaric chamber (0.50 atm) for repeated cycles alternating with normoxia. Exposures and atherosclerosis-inducing diets (15% fat, 1.25% cholesterol, and 0.5%

sodium cholate) are initiated at 10 weeks of age. Atherosclerotic lesion formation is measured after 18 weeks by quantitative lipid staining of serial sections of the proximal aorta. To assess possible mechanisms of disease acceleration and inhibition, variations in susceptibility to atherosclerosis are being examined in relation to plasma lipoprotein cholesterol levels, indices of tissue oxidative injury and selected metabolic alterations putatively involved in atherogenesis, with emphasis on the role of lipoprotein oxidation and activation of transforming growth factor-β1 (TGFβ). Where possible, we are complementing these *in vivo* studies with parallel *in vitro* experiments addressing specific mechanistic questions.

Accomplishments

Exposure to a single dose of radiation was found to enhance the development of atherosclerosis in fat-fed C57Bl/6 mice as indicated by a three-fold greater mean lesion area in irradiated animals than in nonirradiated littermates ($5096 \pm 1875\ \mu^2$ vs. $1640 \pm 445\ \mu^2$, respectively) ($p < 0.05$). These results are consistent with previous observations that carotid atherosclerosis is potentiated in individuals having received radiation for treatment of head and neck cancers. Mechanisms underlying the atherosclerosis-promoting effects of radiation are not known, but are suggested to involve direct oxidative damage to components of the vasculature and oxidant stress-induced alterations in the expression of critical regulatory proteins, including growth factors and adhesion molecules. Characterization of early and late changes in the vasculature of irradiated mice is currently under way and is expected to improve understanding of specific atherogenic alterations potentiated by radiation exposure.

Irradiation had no effects on plasma lipid or lipoprotein levels, either in fat-fed or chow-fed controls. Notably, however, promotion of lesion formation was observed only in animals receiving the high-fat diet, suggesting that radiation-induced alterations are not sufficient alone, but rather facilitate atherogenesis only in conjunction with a conducive lipoprotein milieu. Previous studies in the laboratory of Dr. Rubin have shown that animals transgenic for apo A-I_h, the primary structural protein in high-density lipoproteins (HDL), are particularly resistant to diet-induced atherogenesis. Such effects may be due to the participation of HDL in reverse cholesterol transport and possibly to HDL-mediated inhibition of oxidative sequelae. In future studies, we will investigate whether the disease-enhancing effects of irradiation are inhibited in apo A-I_h transgenics.

Among the reactive oxygen species implicated in atherogenesis and possibly relevant to radiation/induced disease enhancement is superoxide anion O_2^-. To evaluate the pathogenic importance of superoxide anion O_2^- in diet-induced atherogenesis, we compared atherosclerosis susceptibility in fat-fed CuZn-SOD_h-transgenic animals versus nontransgenic littermate controls. CuZn-SOD_h-transgenic mice, initially developed by Epstein and colleagues, contain a 14-kb segment encompassing the entire human CuZn-SOD gene and all necessary regulatory sequences. These mice have been studied in some detail with regard to altered response to tissue-specific oxidant stressors, although most of these studies have involved acute rather than chronic toxicity, and none have looked at disease outcomes. For our studies, the SOD-transgene was bred for over five generations into the C57Bl/6 background. After 18 weeks on the atherogenic diet, these animals exhibited ~2.5-fold higher aortic SOD activity (units/mg protein) than nontransgenics (46.7 ± 20.5 vs. 20.1 ± 9.5, $p < 0.001$). There were, however, no measurable group differences in lesion formation.

The lack of an obvious protective effect of CuZnSOD does not rule out the involvement of O_2^- mediated oxidation events in the development of atherosclerosis nor the inhibition of such processes by SOD overexpression. It does, however, suggest that if inhibition of atherogenic oxidative processes occurs, the protective effects are obscured by other consequences of SOD overexpression (e.g., enhanced H_2O_2 production). The existence of multiple and possibly counteractive effects is not unexpected given the numerous possible consequences of SOD overexpression and the multifactorial nature of atherosclerosis. It is also possible that the atherosclerosis-inducing (dietary) conditions are not optimal for expression of SOD protection. We are currently investigating whether SOD protection is apparent in animals exposed to radiation as well as hypoxia/reoxygenation, which potentiates O_2^- formation via xanthine oxidase.

These studies will indicate the involvement of oxidative processes in the toxic effects of selected environmental hazards and will improve understanding of genetic factors influencing susceptibility to oxidant-induced diseases.

Publications

D.L. Tribble, F. vanVenrooij, E.L. Gong, and A. Nichols, "Use of a Nonexchangeable Probe to Monitor Particle-Specific Oxidation Kinetics in Mixed Systems: Evidence That HDL Inhibits LDL Oxidation by $FeCl_3$ Without Simultaneous Oxidation," *Circulation* **90**, I-136 (1994).

E.L. Gong, M.H. Barcellos-Hoff, J. Verstuyft, E.M. Rubin, and D.L. Tribble, "Atherogenic Effects of Radiation Exposure in Fat-Fed C57Bl/6 Mice," submitted for presentation at the annual meeting of the Radiation Research Society, April 1995.

Electronic Thermalization in Metals and Semiconductors

Principal Investigator: Jeffrey Bokor

Project No.: 93014

Funding: $169,500 (FY 94)
$180,900 (FY 93)

Project Description

Our goal is to obtain quantitative data on hot-electron relaxation mechanisms and rates in a variety of metals and semiconductors. This information can be used to optimize electronic device performance in the nanoscale regime and to design laser photochemical processes on metal surfaces. We will also explore a new approach to stimulating chemical processes on surfaces using strong-field THz electromagnetic pulses to initiate hot-electron-triggered reactions. This method offers the remarkable possibility of inducing surface chemical reactions involving the breaking of electronic bonds using radiation in the mm-wave region of the electromagnetic spectrum.

Time-resolved photoemission spectroscopy will be used as the principal technique for directly measuring laser-excited hot-electron energy distributions and the time evolution of these distributions as they thermalize and equilibrate by various energy-loss and momentum-exchange processes. A new technique for electron heating will be studied. The technique involves the use of THz bandwidth electromagnetic pulses radiated from large-area ultrafast photoconducting antennae.

In conjunction with this experimental effort, theoretical models capable of describing the results will be developed and the relevant scattering parameters will be determined.

Accomplishments

We have developed new instrumentation for time-resolved studies of carrier dynamics in semiconductors. Central to this new capability is a Ti:sapphire-based femtosecond laser system, including a 1-kHz repetition rate regenerative amplifier. The laser system has been procured, installed, and is now operating in our laboratory. It is being used together with two experimental techniques for determining the detailed dynamics of carriers in semiconductors.

To take advantage of the improved characteristics of the new laser (high repetition rate, and shorter pulse width) for time-resolved photoelectron spectroscopy, modifications to the experimental apparatus have been made. The time-of-flight photoelectron spectrometer data acquisition electronics were improved to operate at the higher laser repetition rate. Also, a new harmonic generation scheme has been implemented for producing the ultraviolet fourth harmonic of the Ti:sapphire laser frequency that preserves the 100-fs pulse width. This 200-nm wavelength beam is used as the photoelectron spectroscopy probe. The upgrade of the apparatus for time-resolved photoelectron spectroscopy of carrier dynamics in semiconductors is now complete and experiments are under way.

We are also studying the response of electrons in semiconductors to high-field THz electromagnetic pulses. The field strength that can be produced in a free-space propagating THz pulse is well into the nonlinear regime of carrier velocity versus electric field. This leads to a nonlinear optical response of the semiconductor to the THz optical field. Preliminary experiments carried out at low repetition rate (10 Hz) have validated the basic approach. We have also carried out theoretical calculations of the frequency dependence of the nonlinear absorption and studied its sensitivity to the fundamental parameters we wish to determine, namely, the carrier momentum and energy relaxation times. These calculations give us additional confidence in our method. Finally, we have engineered and built the first high-field THz generator system that is capable of operating at kHz repetition rates.

Novel Polymeric Thin Films for Entrapment and Detection of Small Organic Molecules

Principal Investigator: Deborah Charych

Project No.: 94014

Funding: $58,900 (FY 94)

Project Description

The sense of smell (olfaction) can be thought of as a remarkable series of chemical sensors whose sensitivity and resolving power nearly reach the molecular level. One model of olfaction implicates adsorption of odor molecules onto the lipid layer of olfactory cell membranes, producing a change in membrane potential and generating a nervous pulse. The goal of this work is to construct new materials that mimic this process to a certain extent but will allow detection of small odorous molecules via a color change, rather than a change in membrane potential. We propose to build polymeric lipid assemblies of molecules that can adsorb solvent molecules and signal the adsorption by undergoing a visible chromatic transition. The color change arises from changes in conformation of the conjugated polymer backbone, which makes up one of the components of the lipid layer assembly.

Currently, the detection of organic pollutants in water involves primarily gas chromatography mass spectrometry (GC-MS). These methods, while highly accurate, are not conducive to on-site field analysis because of high analytical turnaround time, high cost, and the need for technically experienced personnel. Our proposed device would signal the presence of above-threshold amounts of an organic pollutant by a simple color change from blue to red. The red color signifies the presence of the contaminant. The methodology is based on our previous findings that chemically functionalized polydiacetylene thin films act as simple colorimetric biosensors. These films were derivatized with a carbohydrate ligand, which specifically bound bioorganisms such as viruses. The specific binding of the virus to the derivatized polymer resulted in a change in the polymer's absorption spectrum, visualized as a blue-to-red color transition. The intensity of the resulting red color corresponded to the quantity of virus, measurable by visible absorption spectrophotometry. These results have allowed the screening of a range of biological and nonbiological targets using the direct colorimetric assay.

Accomplishments

To assess the feasibility of binding and detecting small organic molecules using the colorimetric technique, we first explored the direct colorimetric detection of small protein molecules (MW 60–150 kD) to compare with our previous data obtained with large multivalent virus particles (particle diameter approximately 1,000 Å). We synthesized the specific binding ligands toward an IgG antibody and toward the protein streptavidin (dinitrophenol and biotin ligands, respectively). Binding of these proteins to the thin films did not elicit the blue-to-red transition. Further studies involving AFM, Raman, and FTIR spectroscopy, as well as protein-coated latex beads, indicated that the mechanism of the color transition involves torsional strain on the polymer's conjugated backbone, brought on by either multipoint binding, lipid-lipid intercalation, or both.

With this knowledge in hand, solvent intercalation into the lipid membranes was investigated. According to the lipid hypothesis of olfaction, different lipids of different compositions can give different responses to odor molecules. Single-component thin membrane films of 10,12 pentacosadiynoic acid (PDA) were prepared and polymerized to the blue state by UV exposure (254 nm). The blue-to-red color transition was indeed found to be induced by solvent adsorption to the membrane. It was determined that the thin films are more sensitive to water-immiscible solvents than to water-miscible solvents in water. For the miscible alcohols, it was found that the response increases dramatically going from ethanol to isopropanol, perhaps because of a greater extent of solvent intercalation into the membrane. Moving to the water-immiscible solvents, measurable responses were already obtained at 0.05 wt% (500 ppm). Within this series, a similar trend is observed with increased alcohol chain length, as well as with increased extent of chlorination. A wide variety of water-immiscible solvents were examined at their water-saturation concentrations, as shown in Fig. 1. (Note, per Table 1, that each concentration is different.) The y-axis represents the colorimetric

Table 1. Saturation concentrations in water of various solvents.

Solvent	Saturation concentration in water (wt%)	Solvent	Saturation concentration in water (wt%)
hexane	0.0011	1-hexanol	0.077
cyclohexane	0.0055	1-butanol	7.45
diethylether	6.0	CCl_4	0.077
toluene	0.051	$CHCl_3$	0.815
benzene	0.179	CH_2Cl_2	1.3
1-octanol	0.054		

response, or the extent of blue-to-red conversion. The numbers above the bar represent an upper limit to the detection in ppm. For many of these solvents, it is clear that concentrations well below 500 ppm can be detected. As a comparison, solvent sensors based on SAW devices reliably detect 1,000 ppm of THF and 2,000 ppm of dichloromethane. Sensors based on conducting polymers reliably detect 100 ppm of methanol and acetone but require an expensive impedance analyzer to measure the kinetic response of the polymer's electrical parameters.

For immiscible solvents that have a relatively high solubility in water, it is possible to examine the effect of solvent concentration on the colorimetric response. A linear relationship exists between the colorimetric response and solvent concentration in the range of 0.05–8 wt% solvent in water.

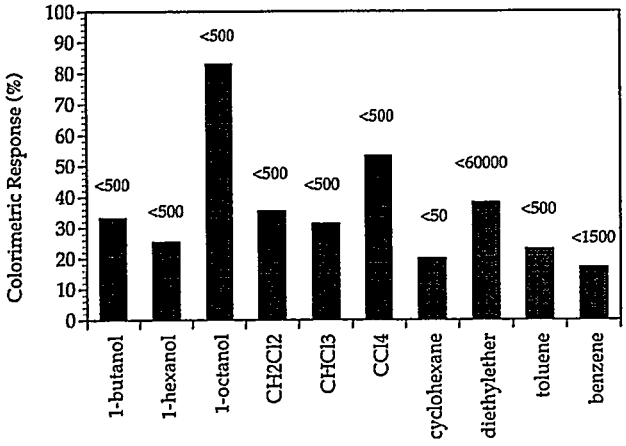

Fig. 1. Colorimetric response of polymerized membrane films toward water-immiscible solvents. Solvents are in de-ionized water as saturated solutions. A colorimetric response of >15% is easily visible to the naked eye.

We are currently investigating the interaction of solvents and their associated color responses with different lipid mixtures. Again turning to the analogy of olfaction, it is anticipated that different lipid mixtures will give rise to varying degrees of chromatic transitions for different solvent analytes. In this way, specificity will be explored using patterned arrays of thin-film sensors.

Publications

A. Reichert, D.J. Ahn, and D. Charych, "Colorimetric Detection of Solvents with Mixed Polydiacetylene Lipid Membranes," to be submitted to *J. Phys. Chem.*

Time- and Frequency-Resolved Spectroscopy of Single Nanostructures and Clusters

Principal Investigators: Shimon Weiss, Frank Ogletree, and Daniel S. Chemla

Project No.: 94015

Funding: $133,500 (FY 94)

Project Description

One of the primary challenges in modern materials science is to build and study the properties of novel mesoscopic systems that may play an important role in future electronics/opto-electronics applications. The optical, electronic, and magnetic properties of such reduced-dimensional systems are strongly altered compared to their macroscopic counterparts. Today, synthesis of semiconductor heterostructures and magnetic superlattices is carried out with monolayer control of thickness and composition. Semiconductor nanocrystals are grown with controlled diameters of a few nanometers. Understanding the properties of such novel systems requires not only the atomic-level control in fabrication and synthesis, but also the development of new spectroscopic tools to probe them. The development of the near-field scanning optical microscope (NSOM) enables one to combine superresolution ($\lambda/40$) with

various optical spectroscopies, such as fluorescence, photoluminescence excitation, Raman, and nonlinear and time-resolved spectroscopies. Moreover, the development of novel photon counting detectors with single-photon sensitivities, combined with NSOM, allows one to perform spectroscopy on a single quantum mechanical oscillator. Fluorescence from a single molecule and a single exciton have recently been reported.

The main objective of this research is to further develop the NSOM by adding to and enhancing its spectroscopic capabilities, and to use it to study the physical properties of novel mesoscopic materials systems developed at Lawrence Berkeley Laboratory (LBL). Examples of such systems are semiconductor nanocrystals, self-assembly monolayers, thin molecular films developed for biosensors, and single molecules. To enhance the NSOM spectroscopic capabilities, pulsed and continuous-wave tunable lasers spanning over the visible range of the spectrum can be used for photoluminescence excitation, photocurrent, and Raman spectroscopies. Mode-locked lasers can be used for time-resolved spectroscopies.

Accomplishments

An NSOM operating in ambient conditions was built. A fiber puller, used for making the probes, was purchased. A fiber rotation device, which is used for the metalization in an evaporator, was designed and built. A technique for making sub-wavelength probes (80-nm apertures) was devised and optimized. An He–Cd laser, used as an excitation source, was purchased. A home-made microscope, for light collection, was designed and built. The design is based on a compact piezo tube scanner for both coarse and fine positioning of the probe. Tip-sample distance is regulated using the standard shear force feedback method. Feedback signal can be monitored together with optical imaging to build a topographic image of the sample with a lateral resolution of 10 nm and height resolution of 1 nm. This topographic image is taken simultaneously with the optical image. Upon successful completion of the setup, superresolution imaging has been demonstrated. Fig. 2 shows an image of the LBL logo, patterned by electron-beam lithography. The smallest feature is a 200-nm gap between the metal lines, shown with an arrow.

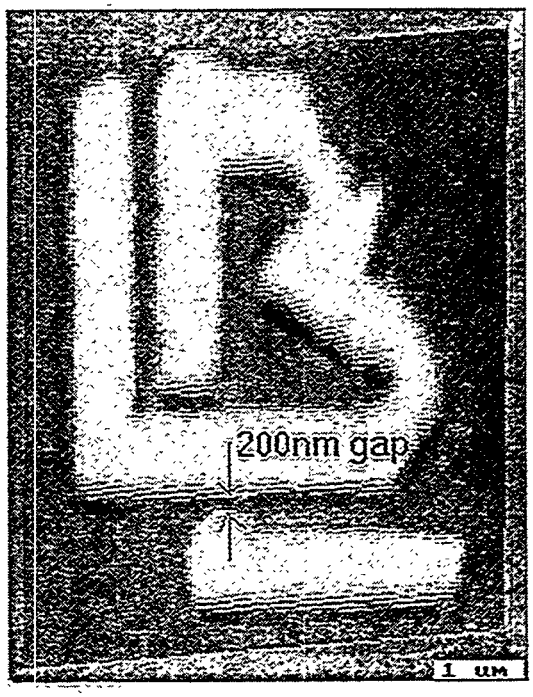

Fig. 2. NSOM transmission image of electron-beam lithographic test pattern of aluminum on glass. The smallest feature of 200 nm is clearly resolved. A conservative estimate of 80-nm resolution is inferred from the edge sharpness.

A Zeiss microscope and a Spex spectrometer have been purchased. The NSOM head was incorporated into the conventional optical microscope to allow maximum light collection efficiency. This is done with the help of an oil-immersion objective.

Two detectors have also been incorporated into the setup. A silicon avalanche photodiode detector, with single-photon counting sensitivity, is used for absorption (transmission) and integrated fluorescence imaging. Once interesting features are identified, the light path reroutes the signal through the spectrometer, onto an LN-cooled CCD camera. This setup allows one to do spectroscopy on single molecules.

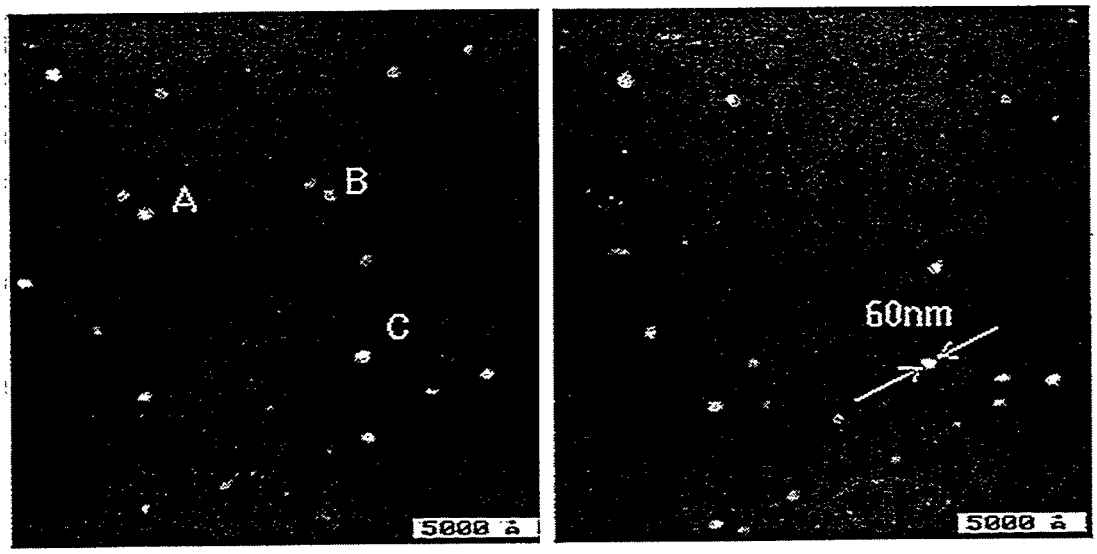

(a) (b)

Fig. 3. Fluorescence NSOM detection of individual Coumarin dye molecules dispersed on PMMA-coated glass coverslip. Individual molecules map the electric field distribution of the probe, and the resolution is determined to be 60 nm as shown with the molecule marked C. The image comprising Fig. 3b was taken30 minutes after that comprising Fig. 3a The photobleaching of single molecules is clearly observed (molecules A, B).

Recently, we demonstrated single-molecule sensitivity. Our group is the fourth group to demonstrate such sensitivity. Figs. 3a and 3b are two successive images of single-molecule fluorescence from Coumarin dye molecules. It can be seen that few of the molecules present in Fig. 3a are missing in Fig. 3b. This is most probably dueto photobleaching. We are currently studying this process as a function of the local environment. In the near future, we will study fluorescence resonant energy transfer by introducing secondary molecules that can absorb the light emitted from the primary molecules.

We have also obtained some initial results of photocurrent spectroscopy on a planar p-n diode junction and on two-dimensional electron gas constrictions. Initial attempts in nonlinear time-resolved photocurrent spectroscopy are under way.

Electron-Beam Lithographic Fabrication of Submicron Junctions for Coulomb Blockade Arrays

Principal Investigator: John Clarke

Project No.: 93015

Funding: $59,000 (FY 94)
$119,800 (FY 93)

Project Description

The goal of this project is to study dynamic critical phenomena via electrical measurements of large arrays of small metallic islands linked by sub-micron tunnel junctions. The arrays are fabricated close to a ground plane giving each island a well-

defined capacitance to ground C_g that is large compared to the junction capacitance C. Electrons introduced into such an array by application of a voltage or current bias will perceive the array as a randomly rough energy landscape, due to the presence of randomly trapped charges near each island. Because the arrays are produced by electron-beam lithography, many of the parameters of the system are under designer control. For instance, the dimensionality of the array, range of interactions of the electrons, the system size, and the amount and type of disorder present in the system can all be varied in well-defined ways. As a result, these arrays are expected to provide a good model system for the study of dynamic critical phenomena.

Accomplishments

The ground plane is a degenerately doped Si substrate; electrical isolation from the array is provided by 100 nm of thermal oxide grown on the surface of the substrate. The array pattern is defined using electron-beam lithography with a JEOL 6400 electron microscope. To produce tunnel junctions we deposit two Al films in successive, angled evaporations with an intervening oxidation step. Electrical measurements have been performed both on one- and two-dimensional (1D and 2D) arrays in a dilution refrigerator; the array sizes were 40 by 40 (2D) and 441 (1D). To make measurements in the normal state, we apply a magnetic field of 0.5 T. After electrical measurements were made, both arrays were inspected in an electron microscope and the junction areas were measured to be approximately 70×70 nm^2. Geometrical estimates of the junction capacitance give $C \approx 0.5$ fF.

As illustrated in Fig. 4, we see a Coulomb blockade region around zero voltage. A threshold voltage V_T is present, above which the current rises and eventually enters a linear asymptotic regime, as can be seen in the insets. We measure C_g by current biasing the array close to V_T and measuring changes ΔV in the voltage across the array as a function of the voltage V_g between the array and the ground plane. We expect ΔV to be periodic in V_g with period e/C_g. For the 2D array we measure a period of 0.13 mV corresponding to $C_g = 1.2$ fF. For the 1D array we obtain $C_g \sim 1.1$ fF, so that in both arrays C_g is significantly larger than C.

We interpret the I-V characteristics shown in Fig. 4 as dynamic critical phenomena. Below the thresh

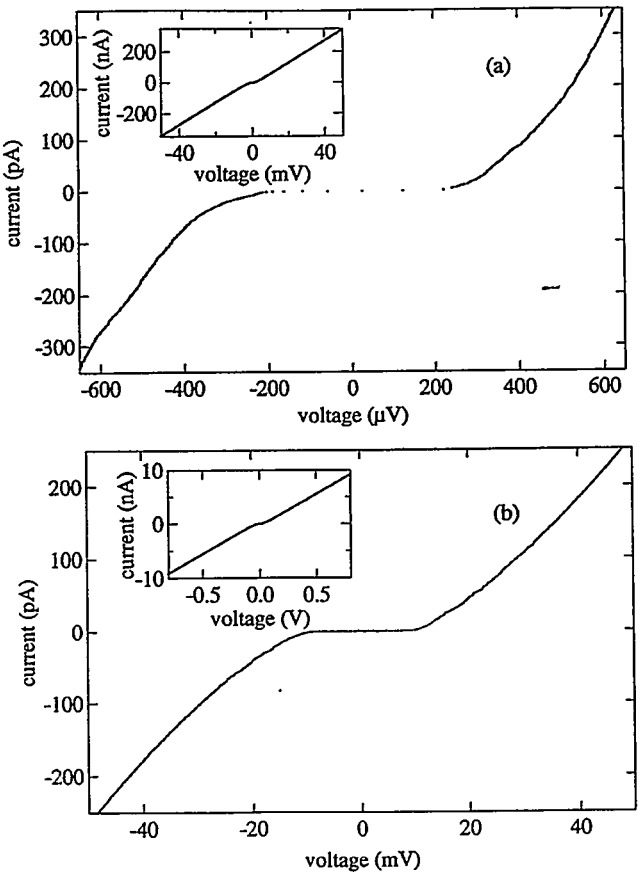

Fig. 4. (a) I-V characteristic for the 40-by-40 2D array showing the presence of a threshold voltage of 220 μV and nonlinear conduction above threshold. The inset shows the asymptotic linear regime at high current. (b) I-V characteristic for the 441-unit 1D array showing the presence of a threshold voltage of 9 mV and nonlinear conduction above threshold. The inset shows the asymptotic linear regime at high current.

old voltage V_T no current flows because electrons in the array are pinned by the inherent disorder. Above V_T the electrons become depinned and we see a transition to a conducting state in which the current is predicted to obey a scaling law $I \sim (V/V_T - 1)^{\zeta}$ for moderate values of the reduced voltage $v = V/V_T - 1$. For $v >> 1$, disorder is no longer important and I should be linear in V. Recent calculations by A.A. Middleton and N.S. Wingreen of NEC predict the exponent $\zeta = 1$ and 5/3 for 1D and 2D arrays respectively in the limit of infinite array size. The threshold voltage V_T in the same limit is predicted to be $V_T = \alpha(C/C_g)Ne/C_g$, where N is the number of rows in the array and $\alpha(C/C_g \rightarrow 0) = 1/2$ and 1/3 for 1D

and 2D arrays, respectively. Examination of the region close to the blockade indicates a threshold for positive voltage of ~220 μV for the 2D array and ~9.0 mV for the 1D array. These are somewhat smaller than estimated values of V_T = 620 μV and 9.6 mV. To look for scaling behavior we plot current versus reduced voltage in the log–log plot shown in Fig. 5. We see that for $\nu < 10$ the current is reasonably well described by the scaling form above in both the 1D and 2D arrays; the dashed lines correspond to $\zeta = 1.4$ and 1.8 for the 1D and 2D arrays, respectively. Above $\nu = 10$, the I-V curves enter the linear asymptotic regime described in the previous paragraph.

The foregoing results indicate good agreement between our experimental results and calculations based on dynamic critical phenomena. We see a threshold voltage in reasonable agreement with theory below which there is no conduction and above which we see scaling behavior. The measured exponents for 1D and 2D arrays are also in reasonable agreement with theory. Future experiments in which disorder is intentionally introduced and array size is varied are planned. Such experiments should help shed light on discrepancies between theory and measurements made to date.

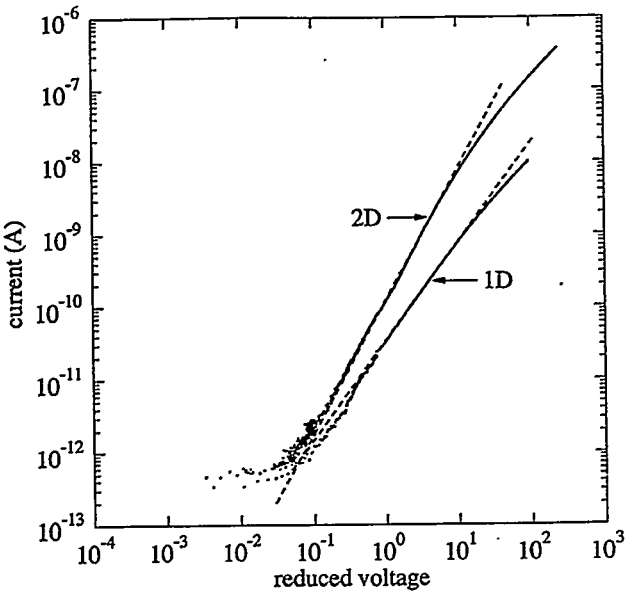

Fig. 5. Current vs. reduced voltage $(V - V_T)/V_T$ for the 1D and 2D arrays. The dashed lines follow the scaling law $I \sim (V/V_T - 1)^{\zeta}$ with V_T = 220 μV and 9.0 mV and $\zeta = 1.4$ and 1.8 for the 1D and 2D arrays, respectively.

Publications

T.R. Ho, A.J. Rimberg, and J. Clarke, "Scaling Behavior in the Current–Voltage Characteristic of a One-Dimensional Array of Small Metallic Islands," abstract submitted for the 1995 March Meeting of the APS.

A.J. Rimberg, T.R. Ho, and J. Clarke, "Scaling Behavior in the Current–Voltage Characteristic of a Two-Dimensional Array of Small Metallic Islands," abstract submitted for the 1995 March Meeting of the APS.

A.J. Rimberg, T.R. Ho, and J. Clarke, "Scaling Behavior in the Current–Voltage Characteristics of One- and Two-Dimensional Arrays of Small Metallic Islands," in preparation.

New Directions for In Situ Electron Microscopy at High Spatial Resolution

Principal Investigator: Ulrich Dahmen

Project No.: 94016

Funding: $100,400 (FY 94)

Project Description

The success of electron microscopy as a technique for materials characterization is due to its unparalleled spatial resolution. However, major limitations are posed because most observations are static, allowing only indirect conclusions about the mechanism of microstructure evolution. *In situ* microscopy overcomes these limitations through direct high-resolution observation at temperature, in a field, under stress, in ultrahigh vacuum, or in a gas atmosphere. However, *in situ* microscopy to date has been mostly a qualitative technique.

This project explores the potential of *in situ* electron microscopy, with emphasis on high spatial resolution, controlled sample geometries, and new electron optical techniques. Its goal is to examine the possibility of developing transmission electron microscopy (TEM) as a quantitative technique for the measurement of mechanisms and kinetics critical to the understanding of materials, and thereby

build a framework to prepare the National Center for Electron Microscopy (NCEM) for new instrumentation and a new focus on high-resolution dynamic investigations.

It is in the exploratory nature of this project to assess the feasibility of several different approaches to *in situ* electron microscopy, including the use of crystallographic templates to generate model microstructures, microfabrication techniques for preparation of specific sample geometries, low-drift specimen holders capable of high resolution at elevated temperature, and electron holography using field emission sources.

Accomplishments

High-Resolution In Situ Observations of Crystal Melting and Solidification

This work has shown for the first time that high-resolution electron microscopy can provide direct observations of melting and solidification of small inclusions. Nanosized Pb particles were formed in an Al bicrystal matrix by ion implantation and annealing. The Al bicrystals were prepared at LBL and alloyed with Pb by ion implantation at Risø National Labs in Denmark. The Pb inclusions were octahedral in shape and the Pb lattice was parallel to the Al matrix. Observations along <110> directions therefore provided optimized conditions for high-resolution imaging. High-resolution observations of melting and solidification of Pb particles showed extremely interesting size-dependent superheating and supercooling, thermal migration, and thermal fluctuations. The behavior of Pb inclusions at grain boundaries was distinctly different from that of bulk inclusions and is currently under detailed investigation.

In Situ Deformation Studies

An initial test has demonstrated the feasibility of *in situ* indentation experiments to be conducted using a modified version of a straining holder designed by researchers at Lawrence Livermore National Laboratory (LLNL) for the 1.5-MeV High-Voltage Microscope. Two cleaved wedges of Si, crossed at right angles, were brought into contact controllably and reproducibly. By tilting both wedges 45 degrees to the beam direction, the transition from elastic to plastic deformation could be observed and recorded on videotape. Based on the success of these initial experiments, a new holder for *in situ* micro-indentation has been designed and is under construction. The holder uses an exchangeable diamond or sapphire tip that can be positioned accurately with piezoelectric drives to indent an electron transparent thin film.

In Situ Growth and Dissolution

In situ electron microscopy using a heating stage for temperature cycling experiments has shown the importance of direct observation to understand mechanisms and kinetics of phase transformations. Using well-characterized precipitates of Ge in a matrix of Al, the difference in kinetics of growth and dissolution of different interfaces was studied by direct observation and related to the interface structures. The differential growth and dissolution rates were subsequently exploited to refine precipitate structures from a distribution of many shapes and orientation relationships to one that consists almost entirely of stable octahedral precipitates, as shown in Fig. 6. The differences between interface structures and kinetics documented for Ge precipitates in Al could also be related to metal–semiconductor interfaces where it was shown that a similar difference in interface crystallography of Al metallization on a Si substrate can lead to significant differences in spiking behavior. This is illustrated in Fig. 7, where the different depth of spikes on the two different interfaces is clearly apparent.

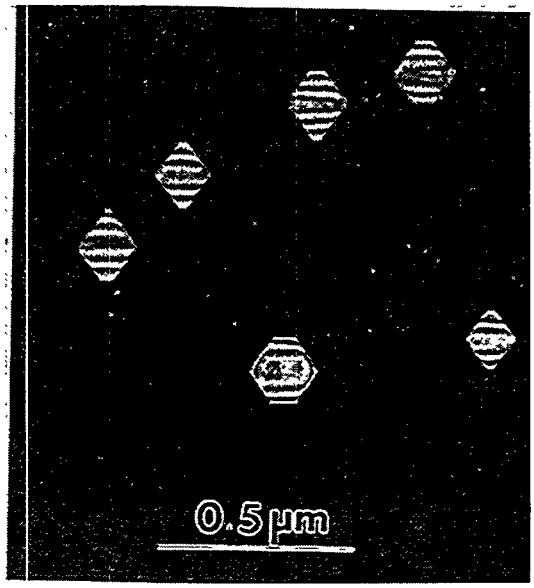

Fig. 6. <110> dark field image of octahedral precipitates resulting from shape refinement during in situ temperature cycling of an Al-Ge alloy.

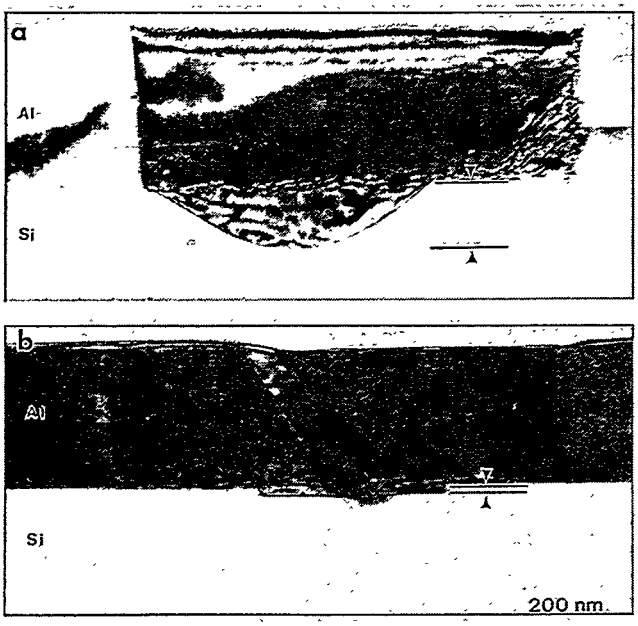

Fig. 7. Comparison of size and morphology of spikes developed by interdiffusion of Si substrate and oriented Al film. In (a) {110} Al on {100}, Si shows a deep hemispherical spike, whereas in (b) {100} Al on {111}, Si forms a shallow, flat-bottomed spike.

Publications

U. Dahmen, "HREM of Interfaces," *MSA Bulletin* 24 (1), 341 (1994); LBL-34607.

N. Thangaraj, S. Hinderberger, K.H. Westmacott, and U. Dahmen, "Thermal Stability of Epitaxial Al/Si Interfaces," *MRS Proc. ULSI in 1993*, 247; LBL-34934.

S. Hinderberger, S.Q. Xiao, K.H. Westmacott, and U. Dahmen, "Shape Training of Ge Precipitates in an Al-1.8% Ge Alloy," *Proc. MSA* 52 (1994); LBL-35361.

U. Dahmen, "Evolution of Ge Precipitate Morphology in Al," *MRS Bulletin* XIX, 22 (1994); LBL-35332.

S.Q. Xiao, E. Johnson, S. Hinderberger, A. Johansen, K.K. Bourdelle, and U. Dahmen, "*In-Situ* HREM Observations of Nanometer-Size Pb Inclusions in Al Near Their Melting Point," submitted to *J. Microscopy*..

Structural Studies of Adsorbates and Magnetic Systems with Circular-Polarized Synchrotron Radiation and Photoelectron Spin Resolution

Principal Investigator: Charles S. Fadley

Project No.: 94017

Funding: $91,500 (FY 94)

Project Description

The goal of this project is to extend the use of photoelectron diffraction and photoelectron holography, two powerful surface-structure probes, to include both the use of circular-polarized radiation for excitation and the external resolution of the photoelectron spin. These new developments will permit studying the atomic and magnetic structures of both nonmagnetic and magnetic surfaces and other nanostructures grown on such surfaces with unprecedented detail and accuracy.

Photoelectron diffraction involves exciting an electron from a core level specific to a given atomic type and then measuring its intensity modulations as a function of either the direction of emission or the energy of excitation. The resulting diffraction patterns are produced by scattering of the outgoing photoelectron wave from atoms that neighbor the emitter, and by the subsequent interference of these scattered waves with the unscattered outgoing wave. These patterns can be used in several ways to derive the local atomic structure around the emitting atom, including the recently suggested holographic inversion of large data sets to directly yield three-dimensional atomic images. If the outgoing photoelectrons further exhibit a net-spin polarization (i.e., if the number with spin up is different from the number with spin down), then *spin-polarized photoelectron diffraction* patterns can also be used to study short-range magnetic order, a topic first discussed by this group. Spin polarization in the outgoing photoelectrons can be produced in three ways: through excitation of spin-orbit split core levels

with circular-polarized radiation, through multiplet splittings of core binding energies in magnetic atoms, or through some combination of both of the prior effects. Thus, excitation with circular polarization and photoelectron spin polarization are intimately related, but only a few photoelectron diffraction studies of this type have so far been carried out. It is common in studies with circular-polarized excitation to speak of *circular dichroism* (CD), which arises whenever the intensities due to left and right circular-polarized radiation (I^{LCP} and I^{RCP}, respectively) are not identical. In the presence of a net magnetization of the specimen, *magnetic circular dichroism* (MCD) also can be measured. Circular dichroism has been observed in only a few photoelectron diffraction studies to date on nonmagnetic systems (e.g., an adsorbate and an elemental semiconductor) and magnetic systems (e.g., bulk iron and epitaxial iron overlayers).

Therefore, this project is aimed at developing both the first experimental facility to carry out such studies at the ALS, *and* accurate theoretical modeling methods to permit understanding and using the phenomena involved.

The instrumentation development involves first equipping the bend-magnet beamline 9.3.2 at the ALS with a movable slit assembly to permit selecting left-circular-polarized, right-circular-polarized, or linear-polarized radiation. Parallel to this is the development of an elliptical wiggler at the ALS that would have 10 to 20 times the brightness of a bend magnet for such studies. In addition, a new high-resolution advanced photoelectron spectrometer/diffractometer that has been developed for use on this beamline will be equipped with a spin detector to permit direct measurement of the degree of spin polarization produced for different specimens and with different excitation methods. This single-channel spin detector will be paired in an easily interchangeable way with a high-speed multichannel detector. Thus, it will be possible to accumulate high-resolution photoelectron spectra very rapidly with the multichannel detector, and then quickly switch without breaking vacuum to the much slower spin-resolved single-channel measurement when necessary to determine the photoelectron spin polarization in a given spectrum.

The theoretical aspects of the project center around the generalization of our existing multiple-scattering computer codes for photoelectron diffraction to include excitation with circular polarization, spin-orbit splitting of the core level, and spin-dependent scattering of the outgoing photoelectron.

Accomplishments

Instrumentation Development

Through a collaboration with Z. Hussain and H. Padmore of the ALS, a movable entrance slit assembly permitting the selection of circular or linear polarization has been designed, constructed, and installed on beamline 9.3.2 at the ALS. This slit will be ready for use in the coming fiscal year.

A mechanism for switching between the multichannel detector and the single-channel spin detector on the newly commissioned advanced photoelectron spectrometer/diffractometer of beamline 9.3.2 has been designed. The design of an ultracompact Mott detector for spin resolution is also being carried out in collaboration with D. Lind at Florida State University, and it too will be constructed during the next fiscal year.

Theoretical Simulations of Photoelectron Diffraction Data

Through a collaboration with M.A. Van Hove and A.P. Kaduwela of the LBL Materials Sciences Division, a new computer program has been written for simulating photoelectron diffraction data that includes excitation with circular-polarized radiation, spin-orbit splitting of the core level, and spin-dependent scattering of the outgoing photoelectrons. Our own experimental facilities for this type of work are presently under development. However, this program has so far been tested by successfully applying it to the analysis of several types of dichroism data obtained in other laboratories:

Carbon monoxide adsorbed on platinum (111): In C 1s emission from CO adsorbed on a Pt (111) surface, large circular dichroism effects of up to 75% were observed previously by Schoenhense and coworkers. We have used our new program to successfully analyze these data, and have been able to show that the cluster methodology employed represents a more generally useful

approach for describing such data than the quantum-chemical methods used previously.

Specifically, the cluster approach can include the effects of many neighbors around a given emitter, whereas the quantum-chemical methods can only include one or two neighbors.

The (100) surface of silicon: In a second study of circular dichroism in photoelectron diffraction from a nonmagnetic system, Daimon and coworkers have measured the Si 2p intensity above a Si(100) surface, using a display analyzer that directly shows the intensity distribution over a cone of about ±45° above the surface. The radiation in this experiment was incident normal to the surface. Figs. 8a and 8b show the intensities I^{LCP} and I^{RCP}, respectively, from this experiment. The maximum dichroism seen here is about 15%. Note here the seeming rotation of the main features in this photoelectron diffraction pattern in a counterclockwise direction with LCP excitation, and in a clockwise direction with RCP excitation. Figs. 8c and 8d show our theoretical simulations of these results, which are in excellent agreement with the experiment, including both the shapes of the main features and the apparent rotations associated with them. For reference, Fig. 8e shows the predicted pattern for unpolarized radiation, which is actually the sum of I^{LCP} and I^{RCP}. These rather dramatic shifts in peak position with change in polarization have not been observed previously, but are expected to be found in future studies of any crystalline substrate. Our program provides an accurate method for predicting and modeling these effects.

The (100) surface of iron: We have also modeled the magnetic circular dichroism seen by Baumgarten *et al.* in Fe $2p_{1/2}$ and Fe $2p_{3/2}$ emission from Fe(001), where the effects are much smaller at only about 3%. This involves the full generalization of our program to include both spin-orbit splitting and spin-dependent scattering, and these results also are in very good agreement with the experiment. This work thus completes the theoretical framework needed to quantitatively analyze dichroism in photoelectron diffraction from both nonmagnetic and magnetic systems.

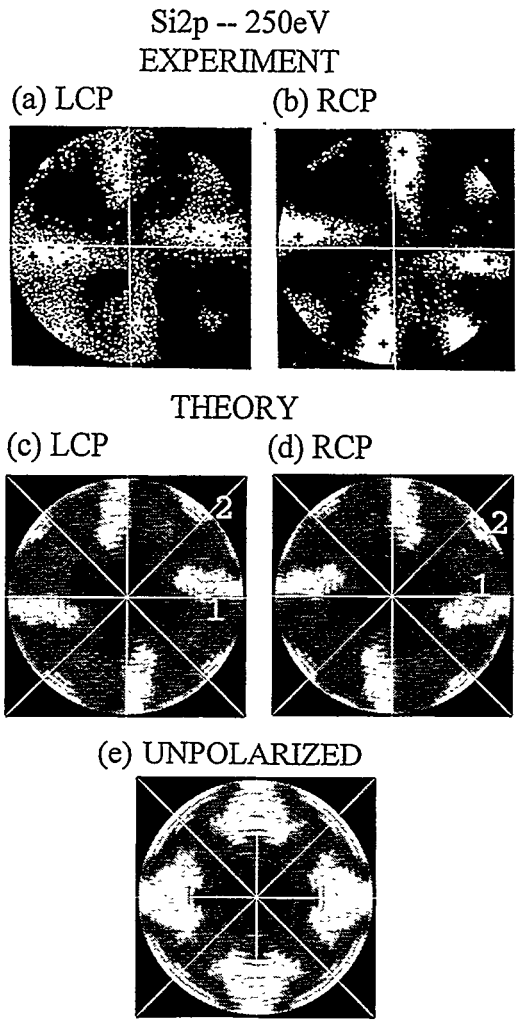

Fig 8. Circular dichroism in Si 2p core photoelectron emission from the silicon (001) surface. The experimental data shown in (a) and (b) for LCP and RCP, respectively, have been obtained by Daimon et al. in a display analyzer recording intensities simultaneously over a ±45° cone centered along the surface normal. The light also was incident along the surface normal. Theoretical simulations of these results are shown in (c) and (d), along with the predicted intensity for unpolarized excitation in (e).

Publications

C.S. Fadley, "Photoelectron Diffraction and Holography: Some New Directions," *Proceedings of the Fourth International Conference on the Structure of Surfaces: Structure of Surfaces IV*, edited by X. Xie, M. Van Hove, and S.Y. Tong (World Publishing Co., 1994); LBL-35051.

C.S. Fadley, S. Thevuthasan, A.P. Kaduwela, C. Westphal, Y.J. Kim, R. Ynzunza, P. Len, E. Tober, F. Zhang, Z. Wang, S. Ruebush, A. Budge, and M.A. Van Hove, "Photoelectron Diffraction and Holography: Present Status and Future Prospects," *Proceedings of the Fifth International Conference on Electron Spectroscopy; J. Electron Spectrosc.* 68, 19 (1994); LBL-35054.

C. Westphal, A.P. Kaduwela, C.S. Fadley, and M.A. Van Hove, "Photoelectron Diffraction Effects and Circular Dichroism in Core-Level Photoemission from Adsorbates and Ferromagnets," *Phys. Rev. B* 50 6203 (1994); LBL-35479.

A.P. Kaduwela, H. Xiao, S. Thevuthasan, C.S. Fadley, and M.A. Van Hove, "Circular Dichroism in Core-Level Photoelectron Angular Distributions from Si(001)," submitted to *Phys. Rev. B.*

A.P. Kaduwela, H. Xiao, M.A. Van Hove, and C.S. Fadley, "Magnetic Circular Dichroism in Photoelectron Diffraction from Fe(001)," in preparation.

Isotope Heterostructures Selectively Doped by Neutron Transmutation

Principal Investigators: Eugene E. Haller and Wladyslaw Walukiewicz

Project No.: 93016

Funding: $70,100 (FY 94)
$45,400 (FY 93)

Project Description

The synthesis and processing of semiconductor multilayer structures with extremely long minority carrier lifetimes required for high-efficiency photovoltaic energy conversion were proposed. These structures also allow the study of dopant-induced intermixing at very high dopant concentrations, and self-diffusion. Isotopically enriched and chemically pure ^{70}Ge and ^{74}Ge will be used to grow an undoped *isotope* superlattice by molecular-beam epitaxy (MBE). Since host atom diffusion is slower than dopant diffusion, this approach will lead to the most abrupt isotope interfaces. Doping will be achieved by the neutron transmutation process at the Missouri Research Reactor facility. The transmutation doping will produce an npnp superlattice. Photogenerated electrons and holes will be spatially separated by the internal electric fields and can be collected along the n and p layers. The spatial separation will result in reduced electron–hole recombination and thus also in enhanced minority carrier diffusion lengths.

Accomplishments

First, high-purity single crystals of isotopically pure ^{70}Ge, ^{73}Ge, ^{74}Ge, and ^{76}Ge have been successfully grown. The crystals will be used as substrates for growth of a heterointerface between two different isotopes. Several different isotope heterostrucures have so far been grown in collaboration with G. Abstreiter at the Technical University in Munich. Undoped short-period isotope superlattices with alternating layers of ^{70}Ge and ^{74}Ge with atomic layer thicknesses between 2 and 32 have been grown and studied with Raman spectroscopy. Several interesting phonon crossing phenomena were discovered. Work at LBL used structures of layers 2,000 Å thick of ^{70}Ge and ^{74}Ge on a natural Ge substrate to determine enthalpy and entropy for Ge self-diffusion. Secondary ion mass spectroscopy was used to follow the atomic concentrations of each isotope as a function of depth (Fig. 9). Because the self-diffusion was measured at the buried ^{70}Ge and ^{74}Ge interface, we have avoided any surface effects that affect most diffusion experiments in uncontrolled ways. The self-diffusion constant as a function of inverse temperature is shown in Fig. 10. The enthalpy is 3.05 eV and the entropy 9 K for Ge self-diffusion. This, we believe, is the most accurate determination of those parameters in any semiconductor. The results indicate that

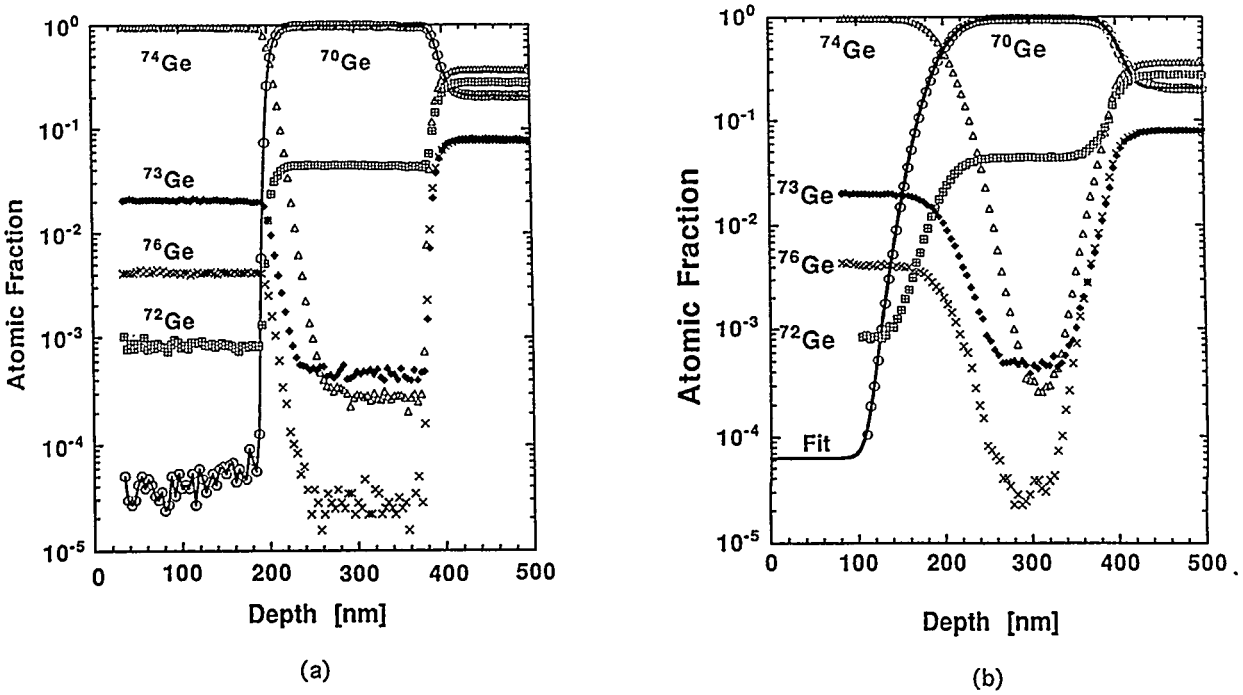

Fig. 9. Secondary ion mass spectroscopy (SIMS) profiles of different Ge isotopes for the Ge isotopic superlattice (a) as grown and (b) annealed at 586 °C for 55.55 hrs.

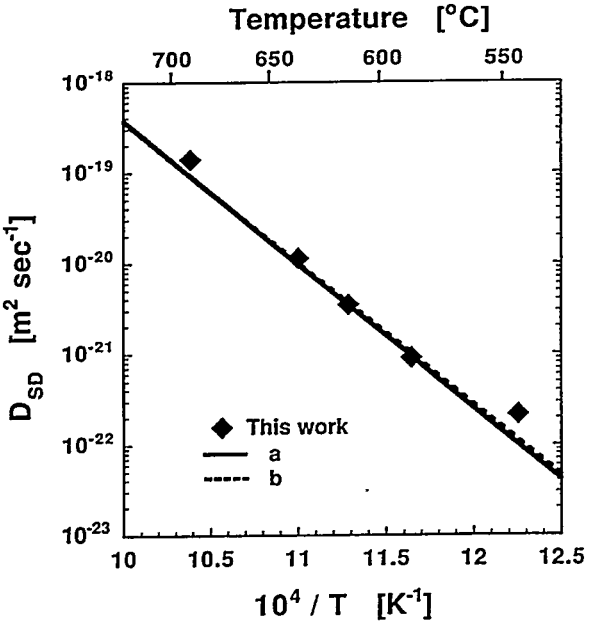

Fig. 10. Arrenius plot of the self-diffusion coefficient as a function of inverse temperature.

the method is quite general and could be used to study self-diffusion in any semiconductor system.

Secondly, during preparation of the isotope single crystals, a few crystals were doped with oxygen. In its bond-centered position, oxygen forms an infrared active center in Ge. Because of the large number of different mass combinations of the two neighboring germanium atoms, the oxygen vibrational spectrum is very complicated in natural Ge. A spectacular simplification of this spectrum is achieved through isotope enrichment. In collaboration with A. Ramdas of Purdue University, we have recorded high-resolution spectra with ^{x}Ge:O (x = 70,73,74,76) crystals. These high-resolution spectra illustrate the great simplification obtained with isotopically engineered crystals and allow the first complete and unambiguous assignment of all the features in the natural Ge:O spectrum. These results clearly demonstrate the excellent quality of the single-isotope crystals.

This project has been most successful in every aspect and has been received most positively by the international research community. One of us (E.E. Haller) shared this year's Max Planck

Research Award with Professor M. Cardona at the Max Planck Institute for Solid State Research in Stuttgart for the research performed jointly on isotope superlattices and Raman studies of the LO phonons in different isotopically controlled crystals. Over fifteen invited presentations at international meetings and prestigious institutions resulted from this work.

Publications

E.E. Haller, "Physics with Chemically and Isotopically Pure Semiconductors," *Acta Physica Polonica A* 84 (3), 395 (1993); LBL-34280.

E.E. Haller, "Semiconductor Isotope Engineering," *Proc. GADEST '93*, Klingmühle, Germany, October 9–14, 1993; *Solid State Phenom.* 32–33, 11–20 (1993); LBL-34279.

H.D. Fuchs, K.M. Itoh, and E.E. Haller, "Isotopically Controlled Germanium: A New Medium for the Study of Carrier Scattering by Neutral Impurities," *Phil. Mag. B: Cond. Matter* 70, 661–670 (1994) (M. Cardona Festschrift) ; LBL-34848.

J. Spitzer, T. Ruf, M. Cardona, W. Dondl, R. Schorer, G. Abstreiter, and E.E. Haller, "Raman Scattering by Optical Phonons in Isotopic $^{70}(Ge)_n{}^{74}(Ge)_n$ Superlattices," *Phys. Rev. Lett.* 72 (10), 1565–1568 (1994).

K.M. Itoh, W. Walukiewicz, H.D. Fuchs, J.W. Beeman, E.E. Haller, J.W. Farmer, and V.I. Ozhogin, "Neutral Impurity Scattering in Isotopically Engineered Ge," submitted to *Phys. Rev. B* ; LBL-35300.

E.E. Haller, "Physics with Isotopically Controlled Semiconductors," invited paper at the 22nd International Conference on the Physics of Semiconductors, Vancouver, British Columbia, Canada, August 15–19, 1994; LBL-35356.

K.M. Itoh, W. Walukiewicz, J.W. Beeman, E.E. Haller, J. Farmer, and V.I. Ozhogin, "Compensation Dependence of Ga Impurity Absorption Spectra in Highly Compensated Ge:Ga,As," *Proc. 6th Intl. Confr. on Shallow Level Centers in Semicond.*, Berkeley, California, August 10–12, 1994; *Solid State Comm.* (in press); LBL-35465.

H.D. Fuchs and E.E. Haller, "Germanium Isotope Heterostructures," *Bull. Am. Phys. Soc. Series II* 39 (1), 751 (1994).

E.E. Haller, "Isotopically Engineered Semiconductors," abstract submitted to MRS Symposium X, "Frontiers in Materials Science," MRS meeting, Boston, November 28–December 2, 1994; LBL-36266a.

Quantum Hall Plateau Transitions of a Two-Dimensional Electron Gas in Strong Magnetic Fields

Principal Investigator: Dung-Hai Lee

Project No.: 94018

Funding: $18,300 (FY 94)

Project Description

In strong magnetic fields, a two-dimensional electron gas exhibits the quantum Hall effect. The hallmark of this effect is that as a function of the magnetic field σ_{xy} exhibits quantized plateaus while σ_{xx} vanishes. The quantum Hall effect has completely reshaped our understanding of the electronic transport in two space dimensions. While the conventional wisdom predicts that *all* disordered two-dimensional systems are insulators, the quantum Hall effect suggests otherwise. Indeed, when the magnetic field is fine tuned to the values corresponding to the midpoints between Hall plateaus, both $\lim_{T\to 0} \sigma_{xx}$ and $\lim_{T\to 0} \sigma_{xy}$ are nonzero; i.e., the system is a metal. The purpose of our research is to understand exactly how the magnetic field resurrects the extended states, and what are the properties of these metallic critical points.

Accomplishments

Over ten years ago, Levine, Libby, and Pruisken conjectured that the long-wavelength effective theory that describes the electronic transport in high magnetic fields is a nonlinear σ-model with a topological term. Recently, in their attempt to numerically study the plateau transitions, Chalker and Coddington have constructed a network model that empirically shows all the right behaviors. What we achieved recently was to establish the link between these two models. Specifically, the network model considered by Chalker and Coddington was shown to be equivalent to a one-dimensional Hubbard model. For example, the electron localization length in the former is mapped onto the inverse spin gap in the latter, and the plateau transition corresponds to the spin-Peirls transition. It was also shown that the low-energy effective theory for the Hubbard model is an antiferromagnetic spin chain whose field theory description is the σ-model proposed by Levine, et al. Thus we have verified the Levine conjecture on the effects of the magnetic field. In addition, these results lead to a tangible representation of the σ-model so that calculations that were otherwise impossible can now be done to extract the critical properties of the plateau transitions. In addition, by generalizing this work to the case of spin-unresolved plateau transitions, we were able to study the effect of Landau level mixing on the universality class of the plateau transitions.

Publications

D.-H. Lee, "Network Models of Quantum Percolation and Their Field-Theory Representations," *Phys. Rev. B* **50**, 10788 (1994).

Z. Wang, D.-H. Lee, and X.-G. Wen, "Transitions Between Hall Plateaus in the Presence of Strong Landau Level Mixing," *Phys. Rev. Lett.* **72**, 2454 (1994).

D.-H. Lee and Z. Wang, "Hubbard Model, Spin Chain, and the Plateau Transition in the Quantum Hall Effect," in preparation.

Fundamental Investigations of the Chemical Vapor Deposition of Ge, GaAs, and ZnSe on Si

Principal Investigator: Roya Maboudian

Project No.: 94019

Funding: $42,100 (FY 94)

Project Description

This project employs high-resolution electron-energy-loss (HREEL) spectroscopy, low-energy electron diffraction (LEED), thermal desorption mass spectrometry, and Auger electron spectroscopy to investigate the interaction of atomic hydrogen and saturated (methane and ethane) and unsaturated (ethylene and acetylene) hydrocarbon molecules with the well-characterized surface of indium antimonide, as a first step toward understanding the mechanisms of etching involved in hydrocarbon-based reactive ion etching.

Accomplishments

An ultrahigh vacuum chamber equipped to use various surface analysis techniques (Fig. 11) has been designed and is currently being assembled. The key instrument is an HREEL spectroscopy system with an unprecedented energy resolution of 2 meV. HREEL spectroscopy will be used to probe the vibrations of adsorbed molecules and surface atoms and hence identify the chemical nature of surface species by means of an analysis of their vibrational modes. In addition, HREEL spectroscopy has proven to be a sensitive probe of plasmon excitations and, as such, is a means of measuring the free-carrier concentration in the near-surface region. This phenomenon will be exploited to study the effect of chemisorption on the electronic surface states that influence thenear-surface carrier concentration, and hence the plasmon frequency. Furthermore, this chamber is equipped with a low-energy electron diffraction

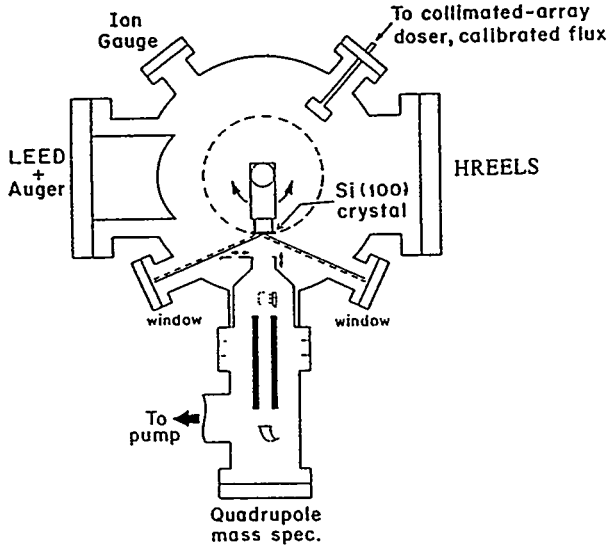

Fig. 11. Schematic of the ultrahigh vacuum chamber described in the text.

system that will be used to monitor the long-range order of the clean and the adsorbate-covered surfaces. The chamber is also equipped with Auger electron spectroscopy that will be employed to monitor surface cleanliness, the stoichiometry of the near-surface region, and the area-averaged concentration of adsorbates. Lastly, a differentially pumped quadrupole mass spectrometer (QMS) will be used for thermal desorption studies, which allows the determination of the desorption products as well as important parameters such as activation energy to desorption.

Electron Transport in Nanostructures

Principal Investigator: Paul L. McEuen

Project No.: 92028

Funding: $74,500 (FY 94)
$71,400 (FY 93)
$114,800 (FY 92)

Project Description

Learning how to controllably fabricate and probe nanometer-scale structures is one of the key challenges to modern materials science. Electron confinement in structures of this scale can dramatically alter electrical and optical properties, resulting in nanomaterials with novel characteristics. The central goal of this LDRD project is to develop techniques for creating and probing nanometer-scale systems. Of particular interest is the use of electron transport to perform novel spectroscopic measurements of nanostructures. The objectives are to deepen our understanding of nanostructures and to learn how to connect them to the macroscopic world.

The nanostructures studied were created and probed with a variety of techniques. Electron-beam lithography was employed to pattern submicron gates on the surface of GaAs/AlGaAs heterostructures. These gates were used to define narrow constrictions, or quantum point contacts (QPCs), in the underlying two-dimensional electron gas. An example is shown in Fig. 12. These devices were studied in low-temperature high-magnetic-field cryostats developed in this project. The experiments included both dc and ultrafast transport measurements. In addition to lithographic nanostructures, chemically derived nanostructures were explored using an atomic force microscope equipped with a conducting tip.

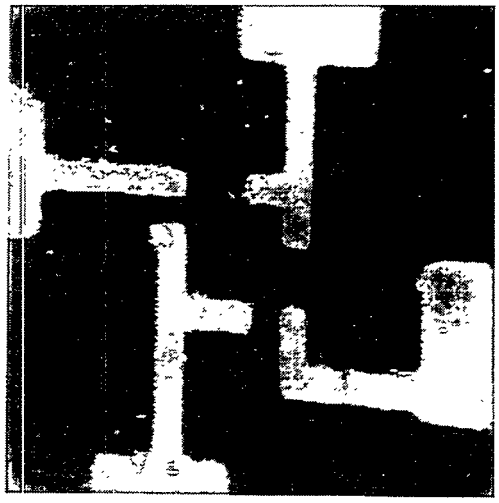

Fig. 12. AFM image of an Au gate structure on the surface of a GaAs/AlGaAs heterostructure. The narrow portions of the gate are 150 nm wide. Quantum point contacts are formed in the openings between the gates.

Accomplishments

Submicron Nuclear Spin Manipulation

Techniques were developed to create and probe nuclear spins on a submicron scale using QPCs in high magnetic fields. One QPC is used to inject spin-polarized electrons into a submicron region. The spin-polarized electrons scatter off the nuclear spins in the region, polarizing the nuclear spins and affecting the subsequent scattering rate. A second QPC is used to measure the fraction of the electrons that have spin-flip-scattered off the nuclei. This information is used to infer the local nuclear spin polarization, detect an NMR signal, etc. The results indicated that fewer than 10^8 nuclear spins could be easily studied. This project led to further experiments to examine nuclear spin diffusion and electron/nuclear spin interactions on a nanometer-size scale, along with experiments attempting to measure the flipping of a single nuclear spin.

Photon-Assisted Transport Across a Tunnel Barrier

While the dc transport properties of reduced-dimensional electron systems have been widely studied, their ac transport properties remain relatively unexplored. We have begun to study this regime, in collaboration with the Orenstein group. We have performed ultrafast measurements of electron transport across a submicron barrier in a 1D channel. Two time-delayed terahertz pulses were coupled onto the gate of a GaAs nanostructure. By examining the photocurrent generated by the pulses as a function of the time delay between them, the frequency-dependent response of the tunnel barrier was measured. The resulting spectra showed strong evidence for photon-assisted tunneling across the barrier.

Conducting AFM Studies of Tunneling Through Liquid Layers

To perform transport measurements on chemically derived nanostructures, electrical contact must be made to these structures. An attractive technique to use is an atomic-force microscope (AFM) equipped with a conducting tip, operating in a controlled environment such as a liquid. We have used such an AFM to study not only nanostructures, but also the electrical properties of the liquid itself. In particular, we have examined the tunneling between an AFM tip operating in liquid hexadecane and a graphite substrate. Both the conductance and the tip-sample separation show discrete jumps with increasing force applied to the AFM tip. These jumps result from the displacement of single liquid monolayers from underneath the AFM tip. Further experiments have shown that these liquid tunnel barriers are very stable and may be useful for tunneling spectroscopy measurements of a variety of surfaces or nanostructures.

Publications

K.R. Wald, L.P. Kouwenhoven, P.L. McEuen, N. van der Vaart, and C.T. Foxon, "Local Dynamic Nuclear Polarization Using Quantum Point Contacts," *Phys. Rev. Lett.* **73**, 1011 (1994).

C. Karadi, S. Jauhar, L.P. Kouwenhoven, K. Wald, J. Orenstein, P.L. McEuen, Y. Nagamune, and H. Sakaki, "Dynamic Response of a Quantum Point Contact," *Journ. Opt. Soc. Am B.* **11**, 2566 (1994).

D.L. Klein, P.L. McEuen, J.E. Bowen Katari, and A.P. Alivisatos, "Scanned Probe Investigations of Chemically Derived Nanostructures," submitted to *Nanotech.*

C. Karadi, S. Jauhar, L.P. Kouwenhoven, K. Wald, J. Orenstein, P.L. McEuen, Y. Nagamune, J. Motohisa, and H. Sakaki, "Evidence for Photon Assisted Transport Across a Mesoscopic Tunnel Barrier," submitted to *Phys. Rev. Lett.*

D.L. Klein and P.L. McEuen, "Conducting Atomic Force Microscopy of Alkane Layers on Graphite," submitted to *Appl. Phys. Lett.*

Infrared and Terahertz Spectroscopy of Artificially Structured Magnets

Principal Investigators: Joseph Orenstein and Stuart Parkin (IBM Almaden Research Center)

Project No.: 94020

Funding: $94,400 (FY 94)

Project Description

Synthesis and characterization of artificially structured magnetic materials is a rapidly growing field of research. Recently there has been renewed interest in thin-film structures composed of alternating magnetic and nonmagnetic layers. The interest is fueled by the discovery of huge enhancements in the magnetoresistance (MR) of these structures compared to the MR exhibited by the constituent layers in isolation. This effect, termed giant magnetoresistance (GMR), will be incorporated into the heads used to read data on magnetic disks and tapes. Further advances require the development of new materials and structures that detect magnetic fields with even greater sensitivity.

This program synthesizes novel multilayer structures and develops tools for their characterization. The structures of current interest are Cu/Co multilayers. Although these materials are grown by sputtering, their crystallinity approaches that of materials grown by molecular-beam epitaxy (MBE). The key to achieving excellent crystallinity is the use of a Pt buffer layer between the multilayer and the substrate.

The principal tools for characterization are magneto-transport and magneto-optical spectroscopy. Optical spectroscopy is performed over an extremely broad range of frequency. Time-domain terahertz spectroscopy is used to perform contactless measurements of the GMR. The capability of performing phase-sensitive magneto-optical spectroscopy in the terahertz domain is unique to Lawrence Berkeley Laboratory. Our spectrometer operates in conjunction with a superconducting magnet cryostat, permitting measurements in fields up to 8 tesla and temperatures as low as 0.4 K. The system is ideal for characterization of electron dynamics in thin films. In addition, Michelson infrared magneto-optical spectroscopy operates above the terahertz regime and is sensitive to the confinement energy of electrons in thin layers. In the visible regime of the spectrum, we are developing a Kerr microscope for imaging of magnetic domains.

Accomplishments

We have obtained results on the magneto-transport and terahertz dynamics of a series of Cu/Co multilayer films. Figure 13a shows the change in resistance due to an applied static magnetic field

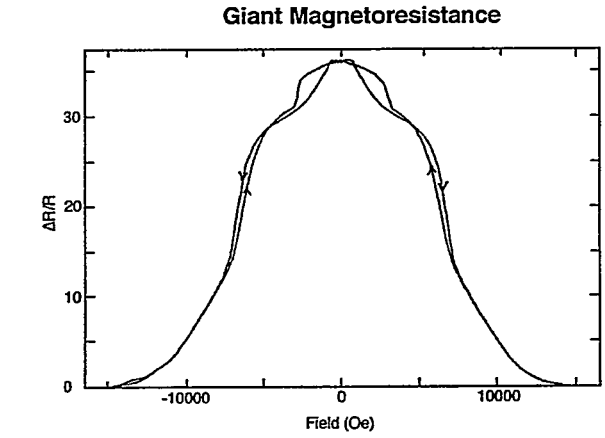

(a)

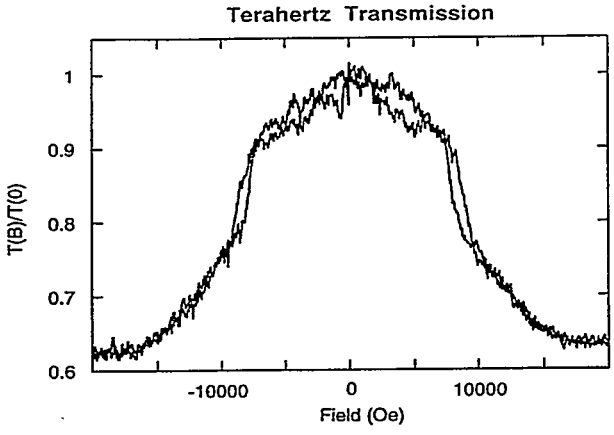

(b)

Fig. 13. Example of the use of terahertz spectroscopy as a contactless measure of resistance. (a) Change in resistance due to an applied static magnetic field in the plane of a film. (b) Transmission of terahertz radiation through the same sample.

in the plane of the film. These samples are the first to display sharp features as a function of the field. Previously studied sputtered materials show a completely smooth transition from the high- to low-resistance state. MBE samples cannot be measured because the metallic substrate shorts transport through the film. The sharp features are believed to be related to the high degree of crystallinity. Figure 13b shows the transmission of terahertz radiation through the same sample. The terahertz transmission amplitude exhibits the same features as the magneto-transport, illustrating the use of terahertz spectroscopy as a contactless measure of resistance.

Coherent terahertz spectrosocopy senses the phase as well as the amplitude of the transmitted radiation. In Fig. 14 the phase difference is shown between terahertz radiation propagating through the sample in the high-resistance state at zero-field and the low-resistance state at 2 tesla, as a function of frequency. Notice that the phase shift is linear in frequency. The Drude relation for the conductivity,

$$\sigma = \frac{\sigma_{dc}}{1 - i\omega\ \tau} \approx \sigma_{dc}(1 + i\omega\ \tau) \quad ,$$

shows that the linear phase shift is associated with the scattering time τ of electrons. The slope of the phase shift as a function of the frequency is a direct measure of the change in τ between the low- and high-resistance states. The data demonstrate

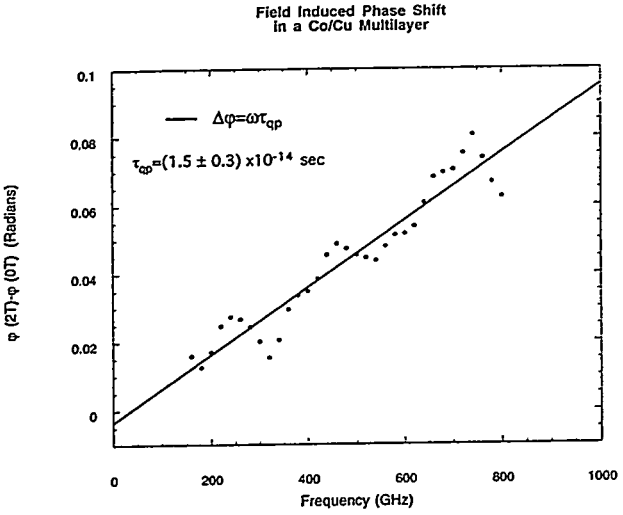

Fig. 14. Phase difference between terahertz radiation propagating through a sample in the high-resistance state at zero-field and the low-resistance state at 2 tesla, as a function of frequency.

that the origin of GMR in these samples is a change in scattering rate of 2 femtoseconds.

The sputtered films we have studied are the first to show sharp structure in GMR. Sharp structure is interesting because it implies a large local derivative of resistance versus field. Although the origin of the structure is not understood at present, the dynamics of domain reversal is suspected to play an important role. To understand the correlation between crystallinity and domain structure requires the ability to image domains. To accomplish this we are developing a scanning Kerr microscope. The microscope will image domains with 0.5-micron resolution. An interface with the beam from a Ti:saphhire mode-locked laser will permit dynamical as well as static measurements.

Establishment of the Thermodynamic Temperature Scale in the mK Region

Principal Investigator: Norman Phillips

Project No.: 94021

Funding: $76,700 (FY 94)

Project Description

There are a number of important areas of basic research in condensed-matter physics that have been hampered by the lack of an accurate, well-documented, and easily reproduced temperature scale in the mK region. The most notable examples include ^{3}He, both the normal Fermi-liquid phase and the superfluid phases, and heavy-fermion compounds, particularly heavy-fermion superconductors. Research on these materials could otherwise provide definitive tests of Fermi-liquid theory and theories of strongly correlated electron systems, which are of fundamental importance in many branches of condensed-matter physics.

In the 1970s, research at NBS (National Bureau of Standards), now NIST (National Institute of Standards and Technology), with noise and nuclear-orientation (NO) thermometers had already led to the development of a scale down to

16 mK. That scale was promulgated on "fixed-point devices"—devices that contained five superconductors with specified transition temperatures between 16 and 200 mK. These devices are generally recognized as the best available temperature standards in that region, but, because the fixed-point devices do not provide *thermodynamic* standards, the results of this research were not incorporated into the current International Temperature Scale, ITS-90.

ITS-90, the low-temperature end of which is defined in terms of the vapor pressure of ^{3}He, extends only to 0.65 K—and there is reason to suspect small but significant errors even in that scale below 1 K. It is probable that there will be international agreement on a temperature scale to lower temperatures in a few years, but the scale will be based on the melting pressure (or melting curve, MC) of ^{3}He. The MC scale offers a number of attractive features:

- Good sensitivity to below 1 mK.
- The scale is defined continuously.
- Like ITS-90, it is based on a *thermodynamic* property, but in addition there are *thermodynamic* fixed points—three between 1 and 3 mK, and one at 316 mK—that serve as both temperature and pressure standards.
- It is relatively insensitive to magnetic field.
- It is relatively free of the materials problems associated with, for example, superconducting fixed points and resistance thermometers.

The fixed points on the MC scale are an enormous advantage in comparing the realization of the scale between different laboratories and offer a striking improvement relative to the higher temperature vapor-pressure scale for which such comparisons are not reliable. Although there is research in other countries directed to the establishment of the new scale, at this time there is no significant relevant effort in the U.S. The most important element of the project is to extend the MC scale to include the thermodynamic fixed points in the 1–3 mK region.

The instrumentation for the NIST program is largely intact, the cryostat is still usable for that work, and the Director of NIST has made the facility available for our research. Thus, there would be an excellent opportunity to do some preliminary work that would be crucially important to re-establishing the temperature scale project at Berkeley. A timely and significant contribution would also be made to the extension of ITS-90 to lower temperatures.

Accomplishments

1. *Extension of the NIST MC and noise thermometer measurements to the low-temperature fixed points.* A hyperfine-enhanced nuclear cooling stage (more complicated than had been anticipated) is in various stages of design and fabrication. It uses $PrNi_5$ as the refrigerant to reach temperatures below 1 mK and a superconducting solenoid that operates at 0.7 K, and is compensated to provide a low-field region for the noise thermometer. It will carry the NIST MC and noise thermometers and a new CMN thermometer, but otherwise replaces, and is interchangeable with, the existing thermometer assembly. It will be used in FY 95 to extend the MC scale to 1 mK.
2. *20-mK to 3-K thermometry with cerium magnesium nitrate (CMN).* Two Rh–Fe thermometers, one calibrated on ITS-90 and one uncalibrated, have been obtained from NPL and compared with the NIST scale. The calibrated thermometer, unique in the world because it carries both the NIST and NPL scales, is now in use at Berkeley to calibrate secondary working thermometers. RuO_2 thermometers have been calibrated from 7 mK to 10 K, including calibrations above 0.6 K in magnetic fields to 9 T. They show excellent characteristics for use as working thermometers; a substantial improvement over the earlier performance of RuO_2 thermometers has been obtained. Some CMN thermometry that could be done most efficiently with the unmodified NIST cryostat has been carried out.
3. *Calibration of a gas-lubricated piston gauge.* Two of the three major components of the gauge have been purchased to replace the ones that had been removed from the NIST facility and are in use at NIST with a borrowed third component. That component will also be replaced in FY 95 to produce a complete gauge for use at Berkeley.

Investigation of Nanometer Magnetism by Using Surface Magneto-Optic Kerr Effect (SMOKE)

Principal Investigator: Zi Q. Qiu

Project No.: 94022

Funding: $25,700 (FY 94)

Project Description

The main objective of this project is to develop an understanding of the fundamental nature of transition metal magnetism in nanometer scale. The project consists of two efforts: (1) to develop advanced synthesis and characterization techniques for fabricating high-quality artificial structures on the atomic scale; and (2) to investigate the magnetic properties of various artificial structures by the *in situ* SMOKE (Surface Magneto-Optic Kerr Effect) technique.

A comprehensive understanding of low-dimensional magnetism requires fabricating high-quality ultrathin films with surface smoothness on the atomic scale. Molecular beam epitaxy (MBE) provides a perfect way to realize this purpose. To further explore physical quantities that vary on the atomic scale, we will develop the so-called wedged samples. With a wedged sample that has an extremely small slope (10^{-7}), detailed features within one monolayer thickness can be readily explored by measuring the corresponding quantity at different positions of the wedge. In this project, we will use the SMOKE laser as the probe beam to scan across the wedge to measure the magnetizations at different thicknesses. The basic principle of the SMOKE technique is that the magnetization of the film produces nonzero off-diagonal elements in the dielectric tensor so that the polarization plane of the incident beam will rotate upon reflection from the sample surface with a rotation angle proportional to the magnetization. The sensitivity of SMOKE can easily reach the mrad scale that corresponds to the magnetization of a submonolayer film. The unique character of the transition metal magnetism is the hybridization of the magnetic electrons with the conduction electrons of the substrate. Thus, rich phenomena are expected in the transition metal artificial structures. The particular phenomena to be studied in this project include the 2D magnetic phase transition, magnetic surface anisotropy, oscillatory magnetic coupling, and the induced magnetic moment.

Accomplishments

In the past year, we made a great effort to set up an ultra-high-vacuum (UHV) system. This system is equipped with multi-evaporation sources, high-energy electron diffraction (HEED), low-energy electron diffraction (LEED), Auger electron spectroscopy (AES), an Ar ion sputtering gun, and *in situ* SMOKE spectroscopy. The system will function with film growth, characterization, and *in situ* magnetic measurement. The vacuum chamber consists of three stages. The top stage includes an Ar ion sputtering gun to clean the substrate and a LEED/AES system to perform the structural and the chemical characterizations of the film. The middle stage includes four evaporation sources to grow the artificial structures and a HEED system to perform the structural and the growth characterizations during film growth. At the bottom stage, two pairs of electromagnets were installed inside the vacuum chamber to produce the magnetic field for the SMOKE measurement. The magnetic field is either perpendicular (polar) or parallel (longitudinal) to the film plane. A sample manipulator with five motion freedoms and a temperature range of 100–1,300 K will transfer the sample between different stages. A UHV-STM will also be added to this system next year to strengthen the characterization ability. The installation of the system was completed in the fall of 1994.

As a preliminary test, several Co films were grown onto a Cu(100) substrate at room temperature and measured by the SMOKE technique. The HEED and LEED results show that the Co overlayer film has a 1×1 fcc structure. Figure 15 shows the HEED intensity during the growth of a Co film at room temperature. The strong oscillations in the HEED intensity suggest an epitaxial growth of the film. Both polar and longitudinal Kerr ellipticity were measured by the *in situ* SMOKE technique. No polar loop was observed. The longitudinal Kerr signal (Fig. 16) shows a 100% remnant magnetization, indicating that the surface anisotropy of the

Co/Cu(100) system favors an in-plane alignment of the magnetization. The detailed relationship between the magnetic properties and the morphology of the films is being investigated.

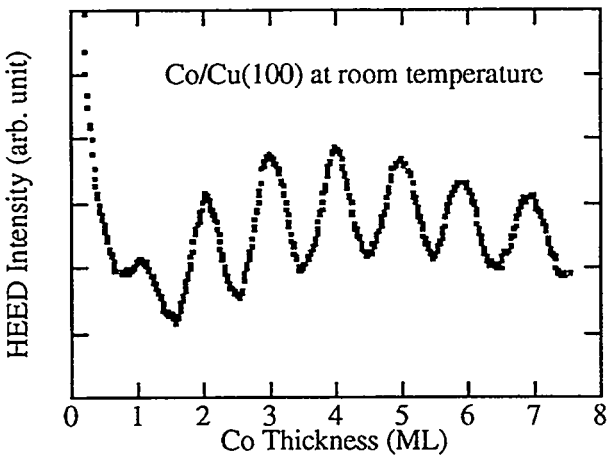

Fig. 15. HEED intensity during the growth of a Co film at room temperature.

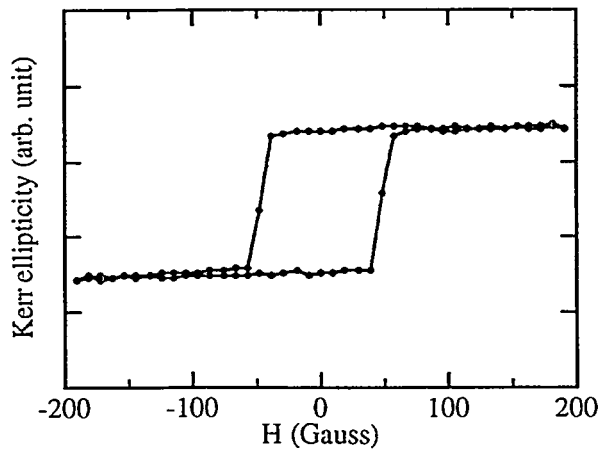

Fig. 16. A longitudinal Kerr signal showing a 100% remnant magnetization.

Publications

Z. Q. Qiu, "Effect of the Biquadratic Magnetic Coupling on the Spinwave Excitations in Magnetic Superlattice," submitted to *Phys. Rev. B.*

Fundamental Relationships Between Mechanical Properties and Structure in Diamond Films

Principal Investigator: R. O. Ritchie

Project No.: 94023

Funding: $40,500 (FY 94)

Project Description

The extreme stiffness, hardness, and thermal conductivity of chemical vapor-deposited (CVD) diamond, with its low chemical reactivity and thermal expansion, make it an attractive material for a wide range of applications, including coatings, microelectronic packaging, detector windows, and heat-sinks. Despite this broad interest, virtually nothing is known about its mechanical properties, particularly with regard to fracture and fatigue. Accordingly, this program was aimed at determining the fracture toughness and stress-corrosion resistance of diamond and diamond films by using both indentation and continuum (fracture-mechanics) testing techniques.

Accomplishments

Novel techniques of constant and repetitive indentations were used to determine the toughness and stress-corrosion cracking resistance of CVD diamond; results were compared with fracture-mechanics tests on bulk samples. The research combined the mechanical property evaluation with extensive optical/scanning electron microscopy evaluation of crack configurations beneath the indenter, using ~400-μm-thick free-standing diamond samples prepared by Crystallume Corporation of Menlo Park. The objective was to provide a basis for the toughness and subcritical crack-growth resistance of CVD diamond and to establish inexpensive techniques for determining these properties on bulk or thin-film material.

Indentation results on free-standing diamond films (typically ~200 to 400 μm thick) yielded fracture toughness values of 5.5 MPa$\sqrt{m}$, in close

agreement to values obtained by testing full ASTM Standard E399 compact-tension specimens. Fracture surfaces were distinctly intergranular (Fig. 17), the gradation in grain size from the nucleation to growth side of the film being clearly noticeable. Studies to examine the stress-corrosion cracking (static fatigue) resistance were more complex. Despite a report of the susceptibility of CVD diamond to stress corrosion in laboratory air, the present studies on subcritical crack growth under sustained loads clearly showed that diamond was essentially immune to stress corrosion in a wide range of environments. Specifically, experiments involved indenting CVD diamond samples under an oil environment and monitoring any crack growth from the corners of the indent following removal of the load. After the initial cracking on indentation, no further (subcritical) crack growth was observed. Exposing the sample to extremely active environments, including moist air, water, nitric acid, hydrochloric acid, and sulfuric acid, similarly showed no tendency for subcritical cracking.

Indentation methods were also applied to determine the structural integrity of diamond films grown on metallic substrates. Specifically, interface fracture toughness measurements were made to assess thin (<10-μm-thick) films of CVD diamond on titanium and steel; far higher interface toughness values were achieved with the former system.

Fig. 17. Intergranular nature of the fracture surface during fracture-toughness testing of free-standing diamond films.

Atom-by-Atom Chemistry and Processes by Low-Temperature (4 K) Scanning Tunneling Microscope

Principal Investigator: Miquel Salmeron

Project No.: 94024

Funding: $75,500 (FY 94)

Project Description

We are exploring the possibility of atom-by-atom chemistry at surfaces by moving one atom of a species next to an atom (or molecule) of another species, with atomic-scale control of spatial positions to induce reaction between them. Another goal has been to develop a tool where the position and chemical identity of a probe tip are preserved for long periods of time (e.g., hours) with atomic control (fractions of an Å) for studies requiring long integration times.

We are building a scanning tunneling microscope (STM) that operates at LHe temperature (4 K) and up to several hundred Ks for sample preparation in ultra-high vacuum (10^{-11} torr). Operation at low temperature eliminates low thermal drift down to the scale of Ås per day, as well as suppresses the loss/gain of atoms at the tip and surface by diffusion. The atoms/molecules to be reacted will be absorbed on the clean surface and displaced, one-by-one, by the STM tip. The feasibility of this displacement process has been demonstrated by D. Eigler at IBM-San Jose.

Accomplishments

The construction of the LHe-cooled STM to study atomic processes (chemistry, nanofabrication) atom-by-atom is nearing completion. We have built a specially designed ultra-high-vacuum (UHV) chamber with its vibration isolation stage. We have built the liquid He transfer line and cryostat that penetrates into the UHV system. At present the system is in an advanced stage of final assembly and testing. The tests and assembly milestones include:

- Pumping the new UHV chamber to 10^{-9} torr (passed successfully).

- Alignment of the cryostat-sample holder with the axis of the chamber so that when displaced the sample is within the focal length of the surface-science instruments (low-energy electron diffraction—LEED; Auger electron spectroscopy—AES).
- Assembly of the He transfer line from the LHe Dewar to the cryostat-sample holder. Status: completed and successfully tested. In the first cooling tests in the UHV chamber that were performed, we reached 6 K at the sample holder and 10 K at the sample. Work on improving the thermal shield is in progress that should decrease the temperature to 4 K.
- Completion and testing of the STM head. Atomic resolution on graphite in air was reached with very good noise level and in the absence of any vibration isolation. Tests in the cryogenically cooled sample stage in UHV are now in progress.

Publications

We are preparing a contribution to the next American Physical Society meeting to be held in San Jose in March 1995. The topic is the presentation of the new design of the UHV LHe instrument and its imaging capabilities in the case of CO on Rh(110). Later, we will submit a paper to the *Review of Scientific Instruments.*

Catalytic Atomic Force Microscopy

Principal Investigators: Peter G. Schultz and John Clarke

Project No.: 94025

Funding: $56,200 (FY 94)

Project Description

The application of the tools of synthetic chemistry to the construction of nanostructures with complex architectures and interconnections requires the development of new techniques. We propose to develop a technique whereby highly localized chemical catalysis on surface atoms or molecules can be carried out using a scanning probe device. By varying the nature of the catalyst and the chemical composition of the surface, it may be possible to construct molecular assemblies not readily accessible by existing microfabrication techniques. This methodology should, for example, make possible the construction of interconnected two-dimensional arrays of nanostructure for sensory or electronic applications.

Modern chemical synthesis has made possible the assembly of such complex molecular structures as the natural product palytoxin and the protein HIV protease. However, in comparison, approaches for the synthesis of nanostructures with comparable control over molecular composition and architecture are still in their infancy. One strategy that offers considerable promise is the adaptation of scanning tunneling or force microscopy to manipulate atoms and molecules on surfaces. These techniques allow imaging of surfaces with atomic resolution and have become important analytical tools in materials science, nanolithography, catalysis science, and, more recently, in the analysis of biomolecules. In addition, both atomic force microscopes (AFMs) and scanning tunneling microscopes are being used to directly modify surfaces, electrochemically as well as mechanically. However, the latter applications are currently limited in resolution and the complexity of structures that can be fabricated. The potential of these approaches for constructing novel nanostructures would be enhanced significantly if the resolution of these microscopes could be combined with the wide array of catalytic transformations available in chemistry.

This project intends to develop an AFM in which the scanning probe has been modified with a metal catalyst that can be used to chemically modify the surface of a self-assembled monolayer (SAM) in a spatially defined fashion. Spatial resolution will be achieved by localization of the catalyst using the scanning probe. The chemically modified surface can be further covalently modified in a second step to generate more complex two-dimensional architectures.

In principle, many different heterogeneous catalysts can be supported on an AFM tip, making possible a variety of chemical transformations, including hydrogenolyses, oxidations, coupling, and polymerization reactions. The system we are initially choosing to investigate uses a platinum catalyst to hydrogenate an azide-derivatized SAM

to generate alkyl amino groups with concomitant release of N_2. This catalytic reaction is known to have a very low activation energy and yields no byproducts that could lead to inactivation of the catalytic tip. Because metal-bound hydride is the likely reactive species, the catalytic reaction is also expected to occur only at those sites in which the tip contacts the surface, resulting in high spatial resolution. In addition, since the reaction occurs only in the presence of a hydrogen donor such as H_2, the reaction can be easily terminated by simple removal of H_2. Finally, free amino or hydroxy groups can be derivatized in high yield in a secondary reaction by a host of molecules, including acids, aldehydes, and metal complexes.

Accomplishments

Formation of a SAM surface terminating with azide groups has been achieved via self-assembly of 11-bromoundecyltrichlorosilane onto smooth glass. The resulting bromide surface groups were converted to azide groups by reaction with NaN_3. For all AFM experiments the samples were mounted to circular glass cover slips in a standard liquid cell. For the catalysis experiment, a standard AFM tip was coated with chromium as an adhesion layer followed by platinum using an electron-beam evaporator. (See Fig. 18.) Scanning was performed in H_2 saturated isopropanol. After scanning, the sample was removed from the liquid cell and reacted in aqueous buffer with aldehyde-modified latex beads derivatized with a fluorophore.

Scanning of an azide-terminated SAM with a Pt-coated AFM tip in isopropanol/H_2 and subsequent derivatization with fluorescent latex beads resulted in brightly fluorescent squares. The structures exhibit exactly the same size as the area scanned with the catalytic AFM tip (here 10 μm). To ensure that the scanning tip did not significantly damage the SAM and thereby lead to the observed fluorescence labeling, a low-force scan of the surface previously scanned with the catalytic tip was performed prior to derivatization. No difference whatsoever relative to the surrounding unscanned area was apparent from the AFM pictures obtained. Scanning of an azide-derivatized surface under exactly the same conditions with an untreated fresh silicon tip did not reveal any detectable structures after derivatization with the fluorescent latex beads or FITC. Only the non-specific background signal could be detected. These preliminary results suggest that during scanning with the platinum tip, the imaged surface azide groups of the SAM are catalytically reduced to amino groups. These groups can then be specifically labeled with the fluorescent-modified latex beads. Such labeling results in latex beads covalently attached to the surface of the SAM in a spatially defined fashion. These experiments should allow one to carry out nanochemistry using many of the tools of the modern organic chemist.

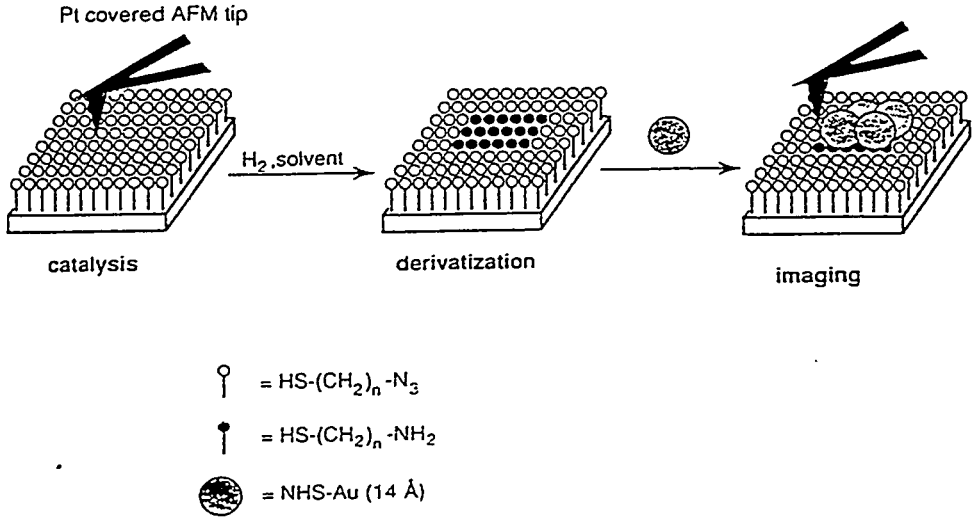

Fig. 18. Catalytic imaging with a scanning probe microscope.

Combinatorial Synthesis of High T_c Superconductors

Principal Investigators: Peter G. Schultz and Xiao-dong Xiang

Project No.: 94026

Funding: $184,800 (FY 94)

Project Description

The purpose of this research is to develop a more time-effective, systematic, and economical strategy for the synthesis of new materials. This goal will be accomplished by developing a methodology that allows the parallel synthesis and analysis of new materials with novel electronic, magnetic, optical, and mechanical properties. Such a methodology would allow one to synthesize and characterize materials approximately 10^3 to 10^5 times faster than the current rate. The ability to rapidly synthesize and analyze large libraries of materials should lead to new and exciting solid-state materials composed of previously unexplored combinations of elements. Moreover, the synthesis and analysis of large numbers of diverse chemical structures should add significantly to our understanding of and ability to predict the structural and physical properties of solid-state materials.

The discovery of new materials with novel physical and chemical properties often leads to the development of useful new technologies. Currently, there is tremendous activity in phenomena such as superconductivity, supermagnetic alloys, nonlinear optics and high-strength materials. However, even though the chemistry of extended solids has been extensively explored, few general principles have emerged that allow one to predict the composition, physical properties, and reaction pathways for the synthesis of such solid-state compounds. Consequently, the discovery of new material depends largely on the synthesis and analysis of new compounds. Given the approximately 100 elements in the periodic table that can be used to make compositions consisting of three, four, five, or even six elements, the universe of possible new compounds remains largely un explored. The question then arises whether there is a more efficient, economical, systematic way to discover new materials with novel properties.

One of the processes whereby nature produces molecules with novel functions involves the generation of large collections (libraries) of molecules and systematic screening of these libraries for those molecules with a desired property. One such example is the humoral immune system, which in a matter of weeks sorts through some 10^{12} antibody molecules to find one that specifically binds a foreign pathogen. Recently, this notion of generating and screening large collections, or libraries, of molecules has been applied to the drug discovery process. The discovery of new drugs can be likened to the process of finding a key that fits a lock of unknown structure. One solution to the problem is to simply produce and test a million different keys in the hope that one will fit the lock. Methods have recently been developed for the synthesis of large libraries (up to 10^{12} molecules) of peptides, olignucleotides, and other small molecules on a time scale of days. This approach promises to have a huge impact on the pharmaceutical industry. Biotechnology companies are being founded to pursue this new opportunity (and currently represent investments of hundreds of millions of dollars and hundreds of new jobs), and most major pharmaceutical companies are building research programs in this area.

This project is to apply this same combinatorial approach to the discovery of new materials. The design of new materials, like drugs, is largely an empirical trial-and-error process. Although theory can provide some guidance, the synthesis and characterization of large numbers of compounds remain the only way to generate materials with new properties. A combinatorial approach toward materials science should be applicable to a large number of targets, such as magnetic materials, efficient heterogeneous catalysts, and doped polymers with novel optical and mechanical properties. We have picked as our first target the combinatorial synthesis of high-temperature superconducting materials. Clearly, high-temperature superconductors represent a target of tremendous practical and theoretical interest. The development of room-temperature superconductors would have an enormous impact on modern technology and industry.

Accomplishments

Synthesis of high T_c superconducting materials is being carried out on a microscale (100-μm to 1-mm diameter samples) in a spatially addressable format. Methods are being developed for generating combinatorial arrays, processing samples, and screening the physical properties of the samples. These methods are described here.

Generating Combinatorial Arrays

Both solution-phase and thin-film methods are being pursued for library generation. For solution precursors (nitrate, acetate, or carbonate salts) of superconducting materials, a multichannel "drop-on-demand" delivery system is being developed. This system can simultaneously eject drops as small as 50 picoliters at high rates (2 kHz) from eight inkjets containing eight different precursors in any desired stoichiometry. These drops will be delivered to an array of 100 × 100 physically separated microwells fabricated in an inert substrate (e.g., MgO).

A sputtering chamber was also fabricated for generating diverse libraries of superconducting thin film. Targets consisting of different precursors (oxides and carbonates) are sputtered through a series of physical masks to generate spatially separated arrays of layered thin films. The initial experiments, which are currently in progress, involve generating 16- and 128-compound libraries (again on a MgO substrate) of PbBSCCO and BSCCO superconductors. In preliminary experiments, a library of 16 superconductors has been generated and screened using a binary masking strategy with the reactants delivered in the following order: Bi_2O_3, PbO, CuO, CaO, $SrCO_3$ (Fig. 19). The stoichiometry was approximately 1:1:1:1:1. The PbBSCCO sample was found to correspond to the 2212 phase with a T_c of 90 K.

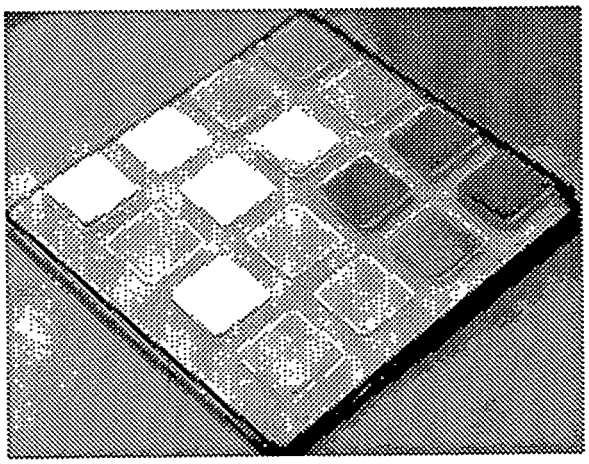

Fig. 19. Library of high-temperature superconductors containing the following compositions: Cu, CuCa, CuSr, CuPb, CuBi, CuCaSr, CuCaPb, CuCaBi, CuSrPb, CuSrBi, CuPbBi, CuCaSrPb, CuCaSrBi, CuCaBiPb, CuSrPbBi, CuBiSrCaPb.

In addition, photolithographic approaches (in which photolithography and thin-film deposition are combined), as well as ultrasonic spraying approaches, are being pursued that should allow 10^4 samples to be deposited in a 1 × 1 inch square.

Processing Samples

A single sample (1-mm diameter) has already been synthesized of the $Bi_2Si_2CaCu_2O_8$ superconductor using solution-based methods that have the expected T_c of 85 K. Importantly, microscale solution phase synthesis requires far shorter heating times ($1/1000^{th}$), probably as a result of homogeneous mixing of precursors and a larger sample surface/volume ratio. This approach should facilitate the isolation of metastable phases. In addition to high-temperature sintering, we will investigate the use of other processing conditions, including lower temperature flux and hydrothermal synthetic methods, as well as variations in atmosphere, pressure (including ultrahigh pressure), and temperature.

Screening Samples

A number of scanning detection systems are being developed for high-temperature superconductors. A nonscanning rf susceptibility probe has been designed and tested that exhibits satisfactory preliminary results for contactless measurement. We anticipate this probe will allow us to detect samples with <250-μm-diameter dimensions. Ongoing is the fabrication of two other systems for contactless measurements, i.e., SQUID (Superconducting Quantum Interference Devices) and microwave split-ring resonator detection systems. The low-temperature scanning systems have also been designed and are currently being fabricated. To detect a large number of samples efficiently, system automation will be required. In light of this, we have also been working on the interface of computers with the various measurement instruments so that all the measuring systems can be computerized.

Spin-Polarized Photoemission Studies of Magnetic Surfaces, Interfaces, and Films

Principal Investigator: Neville Smith

Project No.: 94027

Funding: $124,300 (FY 94)

Project Description

Photoemission spectroscopy with spin analysis is a valuable method for the study of magnetic systems. The electronic structure of the two spin populations can be determined separately, and one can also infer magnetic alignment in thin films. A call for a stronger research effort in magnetic technology has been emphasized in a number of national reports, and has received reinforcement from the recent discovery of magnetic mutlilayers with useful transport properties. The ALS is poised to become the world's leading facility for magnetic spectroscopies such as spin-polarized photoemission and x-ray circular dichroism.

The immediate purpose of this proposal is to foster the introduction of spin analysis technology at the ALS. Spin-polarized photoemission will be a major element of the planned wiggler beamline. The ultimate goal is to fold the developments of this project into a larger magnetic materials program. Acquisition of the spin-detection technology constitutes a stand-alone, self-contained project.

Accomplishments

Activity was devoted entirely to design work. It was determined that, even with the out-year funding, a stand-alone system for spin-polarized photoemission was not a viable option. Instead, activity was directed to retrofitting existing photoemission systems with spin-detection capability. There are two such systems at the ALS: one presently operated by C.S. Fadley; the other under construction by J.L. Tobin. The desirability of the so-called "complete experiment," combining spin analysis of photoelectrons with circular polarization of the incident photons, was a major design consideration.

Four alternatives for spin analysis were examined: (1) conventional Mott scattering at 100 keV; (2) "mini-Mott" devices of the kind developed at Rice University; (3) the low-energy (100 eV) NIST devices; and (4) the SPLEED-type devices available commercially from Germany. In terms of cost, figure of merit, ruggedness, and match to our energy range, the mini-Mott devices (option number 2) emerged as the method of choice.

An outgrowth of this design exercise was the realization that undulator beamlines 7.0, 8.0, and 9.0 could all be modified to deliver circularly polarized photons in the range below 100 eV in an extremely cost-effective manner by use of multiple reflection devices. A commercially available unit was examined but found to be inadequate in that it did not permit rapid conversion between the circular and conventional linear polarization modes. Instead, we have chosen a novel method proposed by C.T. Chen, and detailed engineering design has started. This work is in collaboration with J.L. Tobin of LLNL.

Time-Resolved Studies of VUV, XUV, and Soft-X-ray Photo-Induced Chemistry at Surfaces

Principal Investigator: Harry W.K. Tom

Project No.: 93020

Funding: $64,600 (FY 94)
$123,800 (FY 93)

Project Description

The purpose of this research is to study mechanisms by which high-energy photons (VUV, XUV, and soft x-rays) can induce surface chemical reactions. In contrast to previous work in this field, which has been limited to the study of ions that have already desorbed from the surface, our investigations probe the atoms or molecules as they react and evolve on the surface and therefore allow the study of more complex chemical behavior than desorption. The mechanisms may open new ways of manipulating surface photochemistry and improving semiconductor processing.

Laser-based pump-probe techniques are used to time resolve the surface chemical reactions on the 30–50 fs time scale. A chemical reaction is initiated by irradiating a sample with a short pulse of VUV or soft-x-ray that is made by high harmonic generation in a gas. The evolution of the chemical reaction is then probed with a second probe pulse, which is time delayed with respect to the initial pulse. The probe pulse generates either a second-harmonic or photoemission signature of the chemical species on the surface during the probe pulse. Measuring the reaction time allows us to uniquely distinguish between direct photochemical processes that occur in less than 100 fs, indirect secondary electronic processes that occur during the first ps, and lattice thermal processes that continue for several ps.

This program specifically develops the capability to manipulate XUV and soft-x-ray beams (focusing, beam splitting, beam combining, time delaying, and beam overlapping) required in time-resolved measurements at synchrotrons such as the ALS at LBL. The optics will be developed in close collaboration with D. Attwood and J. Underwood at LBL's Center for X-ray Optics.

Accomplishments

Laboratory and laser development stages are almost finished. We routinely generate 30 fs pulses at 800 nm with a mode-locked Ti:sapphire oscillator and amplify those pulses to 0.5 mJ energy in 35-fs duration at a 1-KHz repetition rate. Through the use of the amplified pulses, time-resolved photoemission and time-resolved surface second-harmonic generation experiments are performed on chemical reactions induced by short visible pulses in the ultrahigh vacuum environment. Using short visible pulses, we have generated and detected the first coherent excitation of a surface optical phonon on GaAs(100). The ability to excite giant nonthermal vibrational amplitudes on surfaces is a surprising result and opens up the possibility of controlling surface chemical reactions through manipulation of specific vibrational modes. XUV pump-pulse experiments should begin soon after the final laser amplification stage is completed.

Publications

L. Xu, Y.M. Chang, and H.W.K. Tom, "Observation of Coherent Surface Optical Phonons by Time-Resolved Second-Harmonic Generation," *Ultrafast Phenomena* **IX** (1994).

L. Xu, Y.M. Chang, and H.W.K. Tom, "First Observation of Coherent Surface Optical Phonons," submitted to *Phys. Rev. Lett.*

Laser Trapping of Radioactive Atoms

Principal Investigator: Stuart Freedman

Project No.: 92035

Funding: $140,300 (FY 94)
$185,100 (FY 93),
$99,600 (FY 92)

Project Description

The purpose of this research project is to exploit laser-trapping and cooling techniques to study the subtle effects of weak interaction at low energies. Offsetting the obvious advantages of high energies, where weak interaction effects are much larger, is the challenge of inventing experimental methods with extremely small statistical and systematic uncertainties. On the other hand, this approach is a cost-effective alternative to performing high-energy experiments. Laser-trapping techniques offer a practical method for precision experimentation, particularly when rare and radioactive atoms are involved. There are several obvious applications. One of the most precise determinations of the Weinberg angle comes from an atomic physics experiment with an atomic beam of stable cesium. At present, the cesium experiment determination is limited by uncertainties in our theoretical knowledge of atomic wave functions in alkali atoms. However, if parity mixing could be observed in a series of isotopes of the same atom, this limitation could be avoided. Accomplishing this feat with alkali atoms requires one to deal with radioactive isotopes. New tests of time-reversal symmetry invariance from searches for a fundamental electric dipole also will be possible for trapped atoms, and there are examples of attractive cases in heavy exotic atoms.

There are a number of possible applications for trapped atoms in nuclear physics. Sources of trapped radioactive atoms could be used to study time-reversal violating correlations in beta decay with unprecedented precision. New measurements of beta-decay correlations, particularly electron–neutrino angular correlations, would be feasible with laser-trapped atom sources. Up to now, measurements of these correlations were restricted to a few favorable radioactive noble gases. Atom trapping will allow new electron–neutrino correlation measurements for a number of important nuclear systems. These experiments are potential tests of the assumed symmetries of the weak current, and they could offer us the most effective probe of the physics beyond the Standard Electroweak Model.

For the first application of this new experimental tool, we are studying the beta decay of 23-second half-life ^{21}Na. A source of laser-trapped ^{21}Na will be used in a precise measurement of the beta asymmetry parameter. For this measurement, the atoms will be trapped and then polarized by optical pumping. A precise measurement of the beta asymmetry combined with the measured lifetime provides a sensitive test of the V–A structure of the weak interaction. The present experiment will not only demonstrate the value of the method we are developing but also will provide interesting information on a problem of current interest: Does the correct theory of the weak interaction contain both left- and right-handed couplings?

In the time since this project was begun at LBL, a successful technique for efficiently collecting and capturing short-lived atoms produced at the 88-Inch Cyclotron was developed. Because of our demonstration and the potential uses of trapped radioactive atoms, competing programs have been initiated at Colorado, Stony Brook, Wisconsin, LAMP has been developed, and TRIUMF. We welcome this competition and the wide interest this field now enjoys.

Accomplishments

Our present focus is the ^{21}Na experiment, but we have begun developing techniques for dealing with other atomic species. Graduate student Mary Rowe has built a system of diode lasers that can be

adapted for use in experiments with other alkalis, such as cesium, rubidium, and potassium. These lasers have been used to trap the two naturally occurring isotopes of rubidium in experiments to study cold-collision losses from magneto-optic traps. The method of atom trapping used for rubidium is similar to that used by the other groups in this field—trapping atoms from the vapor of radioactive atoms confined in a cell. Our group, however, continues to favor the method of Zeeman slowing because it seems more appropriate for most on-line accelerator experiments. The experiments at the Cyclotron use this method.

A prototype on-line radioactive atomic beam facility was built at the Cyclotron to demonstrate the feasibility of our approach. Last year, we continued to optimize the Mg-filled system, which routinely produces ^{21}Na beams with fluxes between 10^7 and 10^8 atoms/s for periods of 24 to 36 hours. In an experiment described in *Physical Review Letters*, the feasibility of our technique was demonstrated by loading about 4,000 atoms at a time into a magneto-optical trap. This accomplishment is recognized as initiating this new area of nuclear physics research, and was presented by Song-Quon Shang in a invited talk at the American Physical Society meeting in Washington, 1994.

With a similar off-line apparatus, significant progress was made in developing specific methods that will be used in future experiments. In the course of this work, a new trapping transition in sodium and the explanation of the so-called "type-2 trap" were discovered. A detailed study of collision losses from magneto-optical traps was made. A paper describing cold-collision losses in type-1 and type-2 traps was published this year. Two additional papers are being prepared for publication, and much ^{21}Na work is described in the Ph.D. thesis of Zheng-Tian Lu.

An atomic beam of francium was developed in recent runs at the Cyclotron. In this experiment, thin gold foils in a heated yttrium-coated oven were bombarded by ^{18}O. Francium is more attractive than cesium for parity-mixing experiments because the size of the effect is roughly the cube of the number of protons. Since there are no stable isotopes of francium, on-line experiments with laser-trapped francium probably are the only feasible approach. The atomic intensity obtained is already adequate for trapping ^{210}Fr atoms using our current approach. We are developing ideas for a parity-mixing experiment with francium while continuing to focus on the experimental work on ^{21}Na.

An experiment to make precision measurements of ^{21}Na hyperfine splitting is now proceeding. This experiment will be the first application of the new techniques developed last year, and it is a first step toward measuring beta asymmetry. Significant technical progress was made this year by producing a "clean" radioactive beam. Previously, a target of natural Mg was used along with the ^{24}Mg(p,α)^{21}Na reaction. Despite the significant difference in the vapor pressure of Mg and Na, the resulting beam contained 10^9 times as much Mg as Na. Recently, we used a target of MgO and a much hotter oven. The resulting ^{21}Na beam was essentially free of Mg. This is an important achievement that will allow us to use more sophisticated methods of transverse cooling to focus the atomic beam. Previously, there was a danger of coating optical components with Mg. The new oven also runs for much longer periods without reloading.

Publications

S.-Q. Shang, Z.-T. Lu, and S.J. Freedman, "Comparison of the Cold-Collision Losses for Laser-Trapped Sodium in Different Ground-State Hyperfine Sublevels," *Phys. Rev. A* **50**, R4449 (1994).

Z.-T. Lu, C.J. Bowers, S.J. Freedman, B.K. Fujikawa, J.L. Mortara, S.-Q. Shang, K.P. Coulter, and L. Young, "Laser Trapping of Short-Lived Radioactive Isotopes," *Phys. Rev. Lett.* **72**, 3791 (1994).

S.-Q. Shang, et al., "Efficient Methods of Trapping Atoms," in preparation.

New Concepts in IsoSpin Studies

Principal Investigator: J. Michael Nitschke

Project No.: 92037

Funding: $113,700 (FY 94)
$130,600 (FY 93)
$63,400 (FY 92)

Project Description

The purpose of this study is to evaluate the feasibility of establishing a new, unique tool for nuclear physics research—the IsoSpin Laboratory (ISL). The ISL will open a new era in nuclear physics with unique and exciting scientific opportunities for the nuclear physics community as a whole and LBL in particular. The ISL will facilitate nuclear reactions with beams of *radioactive* ions (in addition to stable ions) and thus expand nuclear physics research in the new dimension of isospin. There is a chance that the ISL could be built at LBL because of its outstanding record in accelerator-based nuclear science and the availability of the Bevalac complex.

Several site-specific questions related to the location and infrastructure have to be addressed, however:

- What are some constraints on producing a primary (proton) beam that meets ISL specifications?
- What are the environmental and radiological impacts of siting the ISL?
- What is the optimum method for accelerating low-velocity, low charge-to-mass-ratio ions?
- Can we develop ISL targets that are capable of operating at a power level two orders of magnitude higher than previously possible?

Accomplishments

- *What are some constraints on producing a primary (proton) beam that meets ISL specifications?* A Rapid Cycling Synchrotron (RCS) located inside the Bevatron shielding was used as a baseline. An independent consultant provided two detailed solutions to this problem, both an RCS and a conventional (large) cyclotron.
- *What are the environmental and radiological impacts of siting the ISL?* Calculations were done for radioactive inventories of several targets. The calculations include all efficiency factors, radioactive growth and decay, and accelerator transmission losses. Reliable estimates of yields of radiologically critical isotopes like ^{125}I and ^{131}I have helped establish the DOE classification of certain areas of the facility.
- *What is the optimum method for accelerating low-velocity, low charge-to-mass-ratio ions?* Post-accelerator issues were examined on this problem. As a result, several changes were made to the ISL concept that will improve its user multiplicity, beam purity, beam handling, and, most importantly, beam intensities.
- *Can we develop ISL targets that are capable of operating at a power level two orders of magnitude higher than previously possible?* This is still an open question that requires much more R&D, but a partial answer is given in the sections on targets below.

The work performed under this LDRD project has made significant contributions to the national effort toward building an ISL facility. In addition to the items noted above, other work includes:

1. *Thermodynamic target tests on a He-gas-cooled/heated-target design using a high-voltage test stand.* The operating parameters of the target can be varied over a large dynamic range, and the nonuniformity of the temperature profile has been reduced (more uniform temperatures avoid condensation of products in undesirable cooler spots in the target). The incoming He gas can be preheated to maintain target temperature even at low- or zero-beam power levels. Customizing the cooling geometry will even allow for a nonuniform power distribution in the target (as a proton beam would generate). Targets have been successfully tested at 40 kW of power.
2. *Finite-element heat-transport (FEHT) calculations.* FEHT calculations have been performed for comparison with the experimental data measured in a target test; FEHT calculations have also been made for developing improved/modified target designs. A two-dimensional computer program has been completed, and a three-dimensional program is under development.

3. *Radioactive beam calculations.* These calculations have been performed for a number of targets. The prediction of product nuclei for various targets at the ISL is extremely important for several reasons. Because of low beam intensities, the vast majority of experiments at the ISL will be beam-intensity-limited. Hence, it is important to estimate the beam intensities achievable at the ISL to determine the time required for an experiment. Additionally, safety concerns—related not only to residual dose rates due to activation and build-up of products in various parts of the machine, but also to the categorization of the facility itself—are important. A system for predicting radioactive beam intensities for the ISL is under development.

   Predictions used in an ISL white paper are based on a compilation of experimental data combined with semi-empirical extrapolations in regions where data were not available and do not include radioactive decay losses, secondary reactions, or feeding from radioactive decays. To properly predict isotopic yields, several computer programs have been developed. The LAHET Monte Carlo program transports neutrons down to 20 MeV. The MCNP program handles the transport of neutrons below 20 MeV and gives neutron fluxes. The TSAO program gives predicted yields based on experimental data and extrapolation ("semi-empirical"). "High" mass yields are the residual mass distributions given by LAHET, which do not include contributions from neutrons with energies lower than 20 MeV. "Complete" mass yields (including all neutrons) are currently not available. The program DKCHAINMKR extracts nuclear data from a database (half-life, decay mode, branching ratios, etc.) and constructs decay chains, including alpha decay, electron capture, and beta decay. The final program, GROWTHDK, calculates the growth and decay of each isotope, not only during proton-beam irradiation of the target, but also during cooling times, and gives calculated yields as a function of time. This code system is now complete. Figure 1 shows the beam intensities

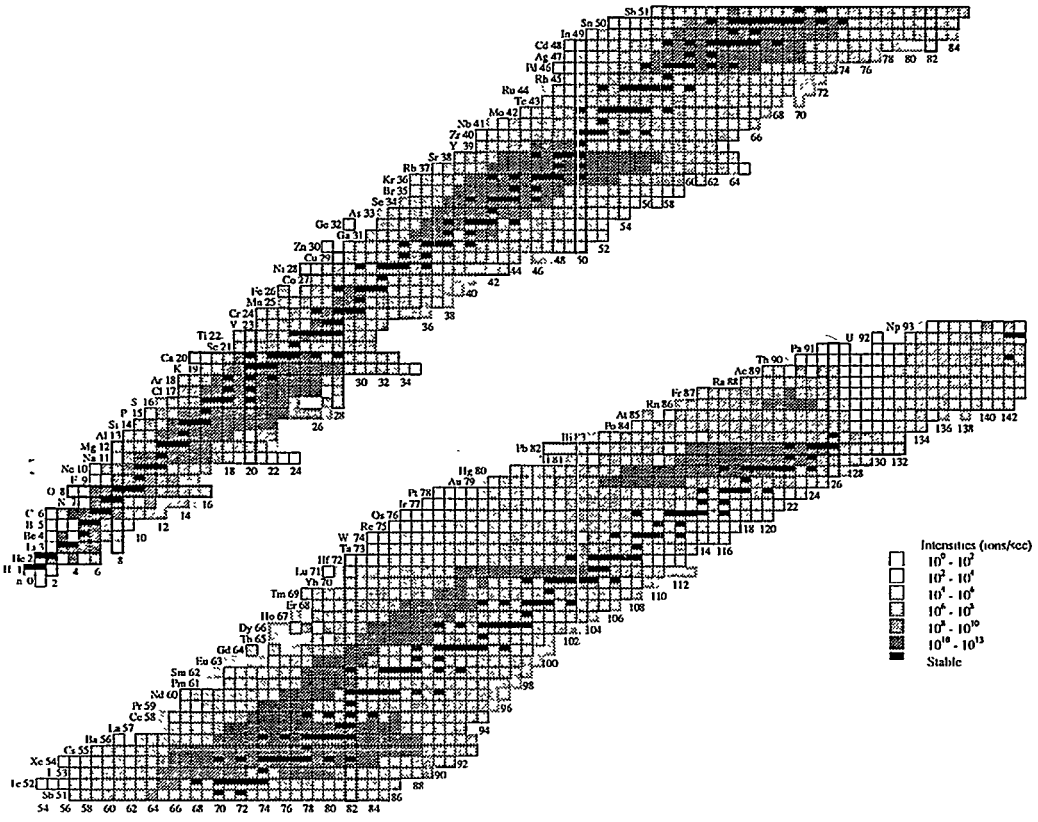

Fig. 1. Preliminary radioactive beam intensities (1,000 MeV protons, 100 μA, on various targets) after a 200-ms delay. Highest are from CaO, Nb, La, Ta, Pb, and UC targets.

one would expect for a number of targets (the highest intensity is plotted for a given isotope) after a 200-ms delay time (the time required to remove the species from the target, and ionize, separate, and accelerate it to the target). Full-color and black-and-white postscript files (UNION_1000_BEAM_3.CPS and UNION_1000_BEAM_3_BW.PS, respectively) are available via anonymous ftp from academic.lbl.gov in the /pub/ISL directory.

4. *BRAMA.* Nonaccelerated beams of radioactive nuclei can be made available to experimenters using a Broad Range Atomic Mass Analyzer (BRAMA). A magnetic sector device has been designed by George Kalnias (AFRD) that would be capable of separating isotopes in the mass range of A = 6–240 amu.

5. *Shielding calculations.* These calculations have been performed to address the all-important EH&S radiation safety issues.

Publications

R.J. Donahue, J.M. Nitschke, M.A. Stoyer, and G.C. Moeller, "Radiation Problems in the Design of a Radioactive Nuclear Beam Facility," presented at the Specialists Meeting on Shielding Aspects of Accelerators, Target Irradiation Facilities, Arlington, TX, April 28–29, 1994, and to be published in the Proceedings; LBL-35459.

S. Chattopadhyay and J.M. Nitschke (eds.), *Proceedings of the Workshop on Post-Accelerator Issues at the IsoSpin Laboratory*, Berkeley, CA, October 27–29, 1993 (May 1994); accepted for publication in *Particle Accelerators Journal*; LBL-35533.

J.M. Nitschke, "Future Prospects for Radioactive Nuclear Beams in North America," presented at the International School Seminar on Heavy Ion Physics, Dubna, Russia, May 10–15, 1993, and to be published in the Proceedings; LBL-34239.

Portions of the new mini-white paper that will be published following the January 19–21, 1995, Durham, NC, Town Meeting were supplied by the LBL ISL group.

Microstrip Gas Chambers for TPC Readout

Principal Investigators: Howard H. Wieman, Wen G. Gong, John W. Harris, and Jeffery T. Mitchell

Project No.: 93021

Funding: $45,200 (FY 94)
$103,700 (FY 93)

Project Description

Traditionally, time projection chambers (TPCs) have been read out with multiwire proportional chambers (MWPCs) located over a surface of pads that pick up the induced signal from avalanche on the wires. This MWPC technology sets a practical limit on the two-track resolution and the position resolution obtainable with a TPC. Built with microfabrication technology, the microstrip gas chamber (MSGC) offers good spatial resolution of 30 μm for minimum ionizing particles, excellent energy resolution of 11% for ^{55}Fe x-rays, and high rate capability over 10^6 particles/s/mm^2. It improves significantly over a multiwire proportional chamber. The purpose of this project is to develop suitable MSGCs for reading out a TPC that can be operated in much higher track density environments with improved position resolution.

Since microstrips are fabricated on an insulator substrate, surface charge build-up resulting from avalanches can lead to gain instability. Controlling this instability has been one of the most important issues in building a useful device. In the previous year, we successfully constructed several working microstrip gas chambers on glass and ceramic substrates. The gain stability was obtained by using either low-resistivity glass or ion implantation. However, those two approaches may be less practical for applications on a large scale. In the current year, our efforts are concentrated on exploring alternative approaches to solve the gain-instability problem. We have developed a thin-film coating technique by sputtering a layer of

Pestov glass of low resistivity onto an MSGC substrate. We have also built the microgap chamber (MGC), which achieves intrinsic gain stability through a novel design.

With the gain instability under control, we have conceived a possible application of MSGCs for vertex tracking in a future Relativistic Heavy-Ion Collider (RHIC) experiment. The conceptual design of a small TPC readout by concentric rings of microstrips was proposed.

Accomplishments

The Pestov glass with low resistivity and electronic conductivity was found to be an ideal substrate for building an MSGC with high gain stability and high rate capability. The only disadvantage may be its large leakage current (>100 nA) when used in bulky form. By using the thin-film coating technique, we reduced the leakage current to less than a few nA for a glass layer 500-nm thick. Furthermore, the thin-film technique rendered the choice of substrate less important. MSGCs built upon ceramic and quartz substrates with Pestov glass coating all showed good performance of high gain stability and good energy resolution. For a large-scale application, it can save the cost of ion implantation and use less material of the special Pestov glass. We have tested our chambers in gas mixtures of Ar–CH_4 (10%) and He–C_2H_6 (50%). Typical energy resolutions of 17–20% were measured for 6 keV ^{55}Fe x-rays. The gain variation was less than 5%. The maximum gas gain was about 2,000.

The newly invented MGC by Bellazzini represents a novel class of gas detector. The novelty lies in its three-dimensional structure of electrodes and insulator in comparison with the planar structure of an MSGC. Figure 2 shows the cross-sectional view of an MGC. It consists of a cathode pad and anode strip, separated by a quartz insulator of a few microns in thickness. With minimum insulator exposed, the problem of gain instability caused by surface charging-up is eliminated. A working prototype of the MGC was built after we solved several problems in device fabrication and testing. One needs an insulator of high breakdown strength and a large fraction of quenching gas to operate this device smoothly. We tested the MGC in both Ar–Ethane (50%) and He–Ethane (50%) gas mixtures. Figure 3 shows a typical pulse height spectrum of ^{55}Fe x-rays measured in an Ar–Ethane

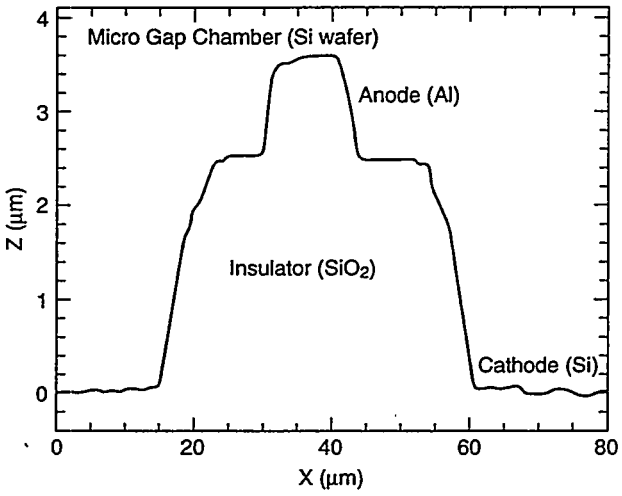

Fig. 2. The cross-sectional view of a microgap chamber.

(50%) gas mixture. An energy resolution of 20% (FWHM) was obtained. The gas gain obtained before breakdown was close to 1,000. No gain variation was observed during the operation.

Microstrip readout is not of much benefit in large TPCs where transverse diffusion is large. In small TPCs with cool gases and short drift distances, however, the high spatial resolution of the MSGC

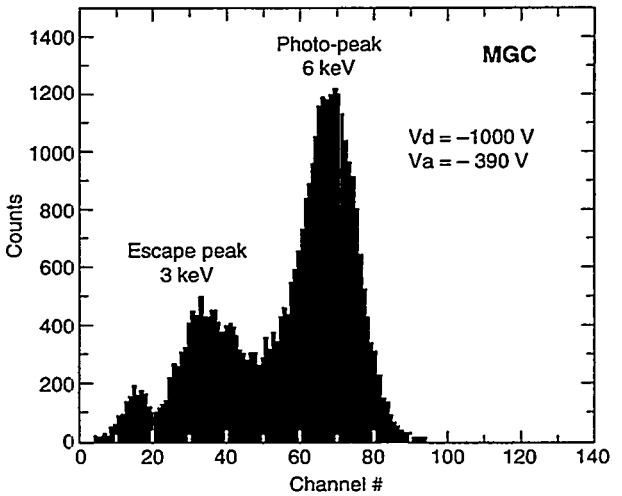

Fig. 3. ^{55}Fe x-ray spectra measured by a microgap chamber in the Ar–C_2H_6 gas mixture.

is well matched to the small diffusion widths. The advantage of using a gas detector for vertex tracking lies in its low mass, which can reduce multiple scatterings for low-momentum particles and improve their momentum resolutions. A preliminary feasibility study and conceptual design were carried out for a very-low-mass (<1% X_0) micro-TPC vertex tracking (VTX) detector in the STAR experiment. It showed that the VTX detector could perform better than a multiple-layered Si drift detector for measuring low-momentum particles produced in the high-multiplicity interactions at RHIC. To prove this concept, we are pursuing a few R&D issues. They include electron diffusion and attachment in a low-diffusion gaslike DME, mask design and fabrication of microstrips with radial structure, readout electronics integration of preamplification, shaping, and charge storage.

Publications

W.G. Gong, H. Wieman, J.W. Harris, J.T. Mitchell, W.S. Hong, and V. Perez-Mendez, "Microstrip Gas Chambers on Glass and Ceramic Substrate," *IEEE Trans. on Nucl. Sci.* **41**, 4:890 (1994).

W.G. Gong, J.W. Harris, and H. Wieman, "Fabrication and Test of a Micro Gap Chamber," *Bull. Am. Phys. Soc.* **39**, 1041 (1994).

W.G. Gong, J.W. Harris, and H. Wieman, "Microstrip Gas Chamber on Thin-Film Pestov Glass and Micro Gap Chamber," LBL-35779, July 1994; submitted for publication in *Nucl. Instrum. Methods in Phys. Res.*

H. Wieman and S. Margetis, "A Micro TPC with a Microstrip Gas Chamber Readout," internal report of STAR R&D.

Physics Division

The Portable DAQ: A Data Acquisition System for Particle Physics Based on Standardized Software Tools and Techniques

Principal Investigators: Gerald S. Abrams, Alessandra Ciocio, and Patrick LeDu

Project No.: 93022

Funding: $93,500 (FY 94)
$149,600 (FY 93)

Project Description

We have progressed in our development of reusable software tools for real-time applications. Our particular interest has been in high-speed data acquisition systems that feature a distributed multiprocessor environment based both on workstations and microcomputers. We seek to identify methods and tools that promote the reuse of software and to understand their behavior in the complex and changeable configurations that typify particle and nuclear physics experiments.

A skeletal prototype data acquisition system has been constructed to meet our criteria for reusability in different experimental configurations. This skeletal system employs our network-based table data server in an EPICS environment; the generality and reusability of these tools have been established in the FY 93 pioneering effort of this collaboration. We were able to demonstrate a simple thread of data acquisition tasks that were synchronized and controlled through a series of EPICS user interface panels. We extended this simple control model to a larger set of data acquisition tasks.

Accomplishments

Almost immediately, we encountered problems in scaling the EPICS state machine model to match the number of independent tasks found in real acquisition systems. Although the state machine model provided a convenient high-level mechanism for interacting with and controlling system tasks, it consumed huge amounts of system memory in the microcomputers. In addition, system configuration activities (for example, adding or deleting system tasks) became extremely difficult with the complex EPICS state machine tasks. It became clear that, while the EPICS state machine model may be appropriate for some process control applications, it is not a good fit for modeling and controlling large software objects. The particular source of the intractability in the otherwise reusable (for the most part) tool kit of EPICS is the hard-coded nature of the state machine implementation.

As a result, we developed a script-based control model that described various series of actions that took place in response to user requests. Unlike most command line scripting languages, this facility was integrated directly into the EPICS "push button" and process variable record environment. The result was a flexible, easily edited control model that existed within the overall data acquisition architecture at the same level as the previous EPICS state machines. The flexibility provided by replacing the coded state machines by an interpreted scripting facility proved invaluable in allowing us to reconfigure the acquisition system to meet different hardware demands.

Since the control model was interpreted, it was also possible to alter the system's control behavior without rebooting (i.e., dynamically). This feature will be especially important for applications with a premium for high data-taking efficiency in a complex detector environment. This model has been added to the STAR detector DAQ system being built to support early TPC sector testing. It has also been adopted by the BaBar On-line group as a basis for early system prototype development. The extension to a tcl (tool command language) implementation, which would incorporate a standardized scripting tool kit rather than our present custom-built version, is viewed as a natural development path.

Chemical/Hydrodynamical Computational Models for Combustions Systems

Principal Investigators: Alexandre Chorin, Paul Concus, and James Sethian

Project No.: 94028

Funding: $20,000 (FY 94)

Project Description

The problem of analyzing turbulent flow models that can also take into account the chemistry is extremely difficult, and present programs do not succeed in predicting correctly important effects such as NO emission. We intend to develop a computer model that uses a high-accuracy numerical description of fluid flow, into which a simple model of the chemistry can be reliably coupled. The program will be written so that it lends itself to experimentation with turbulence models. As a start, this program should be able to predict some of the simpler chemical consequences of various assumed kinetic mechanisms in simple model problems.

In particular, much of the combustion community uses the probability distribution function (pdf) model as an interface between the chemistry and the fluid mechanics. An analysis will be carried out of the convergence of the pdf model. Promising alternatives also will be examined, particularly various versions of Lagrangian-conserved-scalar or progress-parameter descriptions. It has been shown that a mollified (smoothed) pdf model can converge for a simple model problem. We will consider whether this mollification extends to the more complex situation in turbulent combustion.

Accomplishments

Work was done by Dr. Anne Bourlioux and members of the LBL Mathematics Department on the numerical analysis of combustion problems. We worked in particular on two of the most important problems in combustion modeling: the numerical description of interface motion (which is needed to describe the distribution of reactants and products), and the modeling of the coherent structures in turbulence (which must be connected with the subgrid resolution in the turbulence model).

Very good progress was made on the first problem. A methodology was developed, based on Sethian's level set method, for moving multiple interfaces accurately and without mass loss. The methodology was tested on several problems that involve internal and external free boundaries. We are writing several papers that describe our results.

In the realm of coherent structures and turbulence modeling, a new methodology was developed for combining a vortex-based renormalization scheme with a computed Smagorinski coefficient. This method is now being tested on several problems in which vortex motion is interacting with the effects of heat release.

New Si Microstrip Disk Detector for Vertex Reconstruction of B Meson Decays

Principal Investigator: Natalie Roe

Project No.: 92039

Funding: $80,000 (FY 94)
$135,000 (FY 93)
$178,000 (FY 92)

Project Description

This project's goal is to meet new demands for precise three-dimensional reconstruction of vertices from decays of B mesons produced at forward angles through the use of a new type of vertex detector, the Silicon Microstrip Disk. The disk consists of wedge-shaped double-sided Si microstrip detectors that are joined to form an open polygon, supported and read out at the outer radius. An engineered design for the D0 detector has already been produced; many of these concepts can be adapted to the requirements of an asymmetric B factory. A conceptual detector design was developed in FY 93. This line of research was continued in FY 94 with production of prototype detectors and the design of a suitable readout system.

Accomplishments

Substantial progress has been made toward developing a silicon vertex detector that is optimized for the physics program at an asymmetric B

factory. The most significant achievements are summarized below.

B Factory Conceptual Design

A conceptual design for a silicon strip detector was completed that is optimized for use at an an asymmetric B factory. The disk-style detectors developed for Tevatron collider applications have been modified into "lampshade"-style detectors that provide forward coverage with a minimum silicon area, while maximizing the track-crossing angle. The readout has been moved from the outer radius into the inner radius, where it is out of the active tracking volume. This greatly reduces multiple scattering and photon conversions. Double-sided wedge-shaped detectors are employed, with flexible kapton circuits to bring the strip signals to the readout electronics. The design has five layers of silicon sensors and provides coverage to within 300 mrad of the beamline in the forward direction and to within 500 mrad of the beamline in the backward direction. (See Figs. 1 and 2 below.)

Simulations of detector resolution have been carried out that demonstrate that this design is well suited for B-meson vertex reconstruction. More recently, the mechanical support was worked out. Consideration of the electronic requirements also was begun, including the choice of analog versus digital readout, tolerable electronic noise levels, and desirable features such as time stamping and sparse readout.

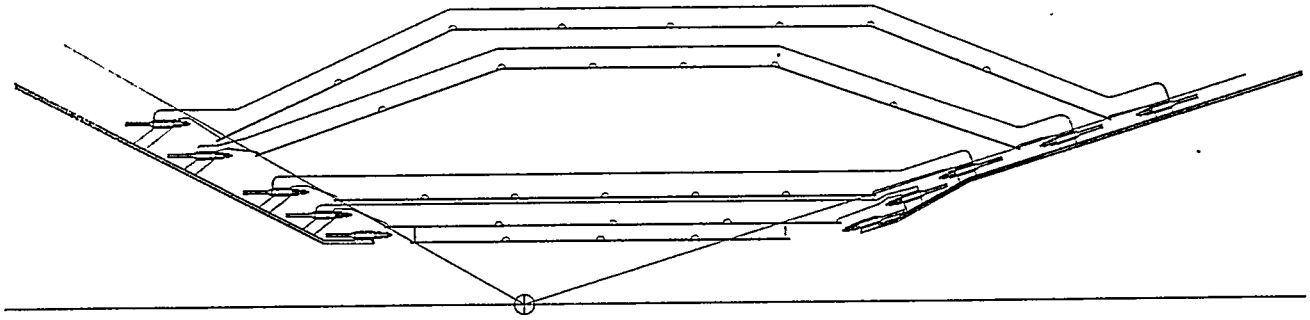

Fig. 1. Side view of the silicon vertex detector design for the asymmetric B factory.

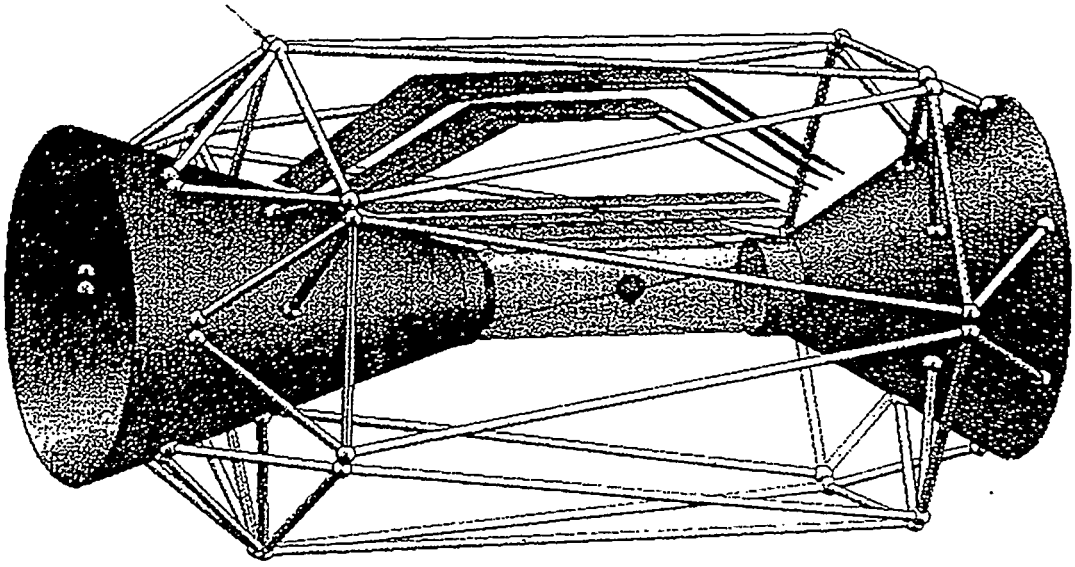

Fig. 2. 3D view of the silicon vertex detector design for the asymmetric B factory. Only one section of silicon sensors per layer is shown for clarity.

Mechanical Support

The low momenta typical of particles produced in B-meson decays on the Υ(4s) place an even greater emphasis on low-mass mechanical support. The spaceframe design that was developed in previous years has therefore been modified by replacing the aluminum tubular construction with carbon fiber tubes, which are more rigid and lower in mass. A prototype spaceframe structure was built and extensively measured for creep and deflection, and excellent results were obtained. This spaceframe will be used to provide a rigid connection between the two ends of the B factory vertex detector and to maintain alignment during installation.

Electronic Readout

A conceptual design was developed for the readout of a silicon vertex detector at an asymmetric B factory. The short bunch spacing (4 ns) and high background rate make it necessary to develop an asynchronous readout system that does not require priming prior to the occurrence of a hit. The most basic implementation would be a digital readout providing hit/no-hit information only. However, analog information was desired in order to correct for time-walk and to improve the position resolution. The conceptual design we have developed addresses these requirements by a simple and elegant technique called time-over-threshold readout. In a time-over-thresold system, a comparater is fired when the pulse height exceeds a preset threshold, and stays on until the pulse falls below this threshold. The length of time during which the comparator is on is digitized by making an AND with a clock and loading the result into a circular digital pipeline. The location of the first bit that is set in the pipeline provides the time stamp for the hit, and the number of bits that are on gives the pulseheight information.

The time-over-threshold concept is being tested in a proof of principle test chip that was designed at LBL and has been submitted for fabrication. If favorable results are obtained, we intend to pursue a full-scale time-over-threshold prototype in collaboration with UCSC and Pavia.

The conceptual design for the D0 HDI, which is now in production, also has been adapted to the needs of the asymmetric B factory. A similar flexible circuit is planned, which will be laminated to a thermal heat sink and located outside of the active tracking volume. A flexible cable will be bump-bonded to the B factory HDI to bring the signals from the readout chips outside of the detector.

Publication

N. Roe, "BABAR Letter of Intent," SLAC-443 (June 1994).

Evaluation of Trigger Algorithms for an Upgraded Silicon Microvertex Detector

Principal Investigator: Marjorie Shapiro

Project No.: 94032

Funding: $37,000 (FY 94)

Project Description

The goal of this project is to evaluate algorithms for triggering on detached vertices from *B* hadron decays using a silicon microvertex detector. The work concentrated on the following areas:

1. A study of the effect of motion of the beam position on trigger performance.
2. A study of the $J/\psi \rightarrow \mu^+\mu^-$ collected sample by CDF (Collider Detector at Fermilab) to understand issues of multiplicity and confusion in low-momentum *B* hadron decays.
3. The development of a model of the transverse spreading of charge in silicon detectors and the construction of a test-bench so we can compare the model with experimental data.

Accomplishments

To trigger on *B* decays at a hadron collider, the first issue that must be solved is that of aligning the detector to the primary interaction point. The variation of the beam position in CDF was looked at and the conclusion made that it is essential that the *x-y* beam position be determined online for each accelerator store. The *x-y* position is in general quite stable within a store, but can vary by hundreds of microns between stores. It is therefore necessary at the beginning of each store to use several hundred events to determine the beam

profile. This profile must then be downloaded to the trigger hardware. In principle, one could imagine measuring the x-y collision point on an event-by-event basis and using this information to improve the trigger. Studies of the J/ψ sample, however, show that the average multiplicity in these events is low and the overall improvement in resolution on the primary vertex position is minimal. The conclusion is that this technique is not worth the additional complexity.

The longitudinal beam profile in hadron colliders is quite long (30 cm at the Tevatron and ~7 cm at the LHC), so determination of the average beam position in z is not useful. The question arises whether an event-by-event z beam position is possible and if that information will improve the trigger. Determining the interaction point in z is less complex than in x-y because the tracks do not curve in this projection. In the CDF data, the x-y beam position varies with z, with a slope of typically 5 microns per cm. It is therefore necessary to know the z position of the interaction to determine the mean beam position in the x-y plane. The most straightforward technique to find the event z position is to use a histogram method to determine the mean intersection point(s) of all tracks in the event. I cannot study this algorithm using CDF data (since the SVX detector is not segmented in z) and I am currently working on a Monte Carlo study of this issue. There are several questions to be addressed in the study. First, how many layers of z readout are necessary for the algorithm to work? Second, how sensitive are the results to multiple interactions within the same beam crossing? Preliminary results indicate five layers of silicon should be sufficient.

At the present time, the studies have been limited to algorithms that work in the transverse plane (the z position of the primary vertex is used to determine the primary beam spot, but the trigger itself only looks at impact parameter and curvature). Once the Monte Carlo study is completed, it should be seen whether including z information at the trigger level improves the performance.

Multiplicity in B Decays

Studies of the CDF J/ψ dataset show that there are few additional tracks near the B meson decay. A cut requiring that the B meson carry at least 50% of the summed track momentum in a cone of radius

$$\Delta r = \sqrt{(\Delta\phi)^2 + (\Delta\eta)^2} = 1.0$$

keeps essentially all B candidates. This fact has several implications. First, it shows that in studies of trigger efficiencies the major source of track confusion will be other tracks from the B decay rather than tracks from the rest of the event. Second, it points to a possible way of removing non-B background at the trigger level (it might be possible to remove events with a large momentum in tracks coming from the primary vertex).

The CDF data also provide information on how many layers of silicon are necessary for reliable impact parameter determination. In a sample of events where only two silicon hits are present on each muon, there are long tails in the impact parameter resolution (these tails can be seen easily by determining the position of the J/ψ vertex and looking at events where the vertex appears to be behind the primary vertex). The fraction of events in the tails is reduced significantly if at least three layers of silicon are required. The preliminary conclusion is that four layers of silicon is sufficient (if the z position of the primary interaction is already known).

Modeling of Transverse Size of Silicon Clusters

By comparing CDF data with Monte Carlo simulations, my student (Doug Reher) and I have found that existing silicon simulations do not properly describe the number of strip channels that fire when a track traverses the detector. The poor agreement between data and Monte Carlo has important implications for studies of detector upgrades. It is impossible to properly predict the position resolution and two-track separation of a silicon system if we cannot describe the response of the silicon.

My student began work on an improved Monte Carlo for describing the motion of charge in silicon. This Monte Carlo uses a code developed by the Santa Cruz silicon group as its starting point. Added to that code is a model of dE/dx energy loss in silicon that was developed by Gerry Lynch at LBL. We worked on incorporating diffusion in the code as well. The first goal of the exercise is to be able to reproduce the CDF results. Once this is possible, the code can be used to predict silicon response in detectors more appropriate for future collider experiments. The software can also be used to predict changes in resolution for silicon that has undergone radiation damage.

Though the project ended in FY 94, we can use the equipment to test these predictions experimen-

tally. We set up a laser- and computer-controlled x-y stage to allow us to scan silicon detectors and measure the transverse profile of the electronic response. We intend to study a number of detectors with this setup. We purchased some n- and p-type silicon detectors and are also looking at a number of low-resistivity silicon detectors originally bought by the SDC (Solenoidal Detector Collaboration) group. We can study the effect of radiation on detector performance. We have successfully irradiated a number of devices at the 88-inch cyclotron and are planning further irradiation studies in the near future.

Directions for a Particle Astrophysics Initiative: Additional Observations of the Cosmic Microwave Background

Principal Investigator: George F. Smoot

Project No.: 93023

Funding: $125,000 (FY 94)
$103,400 (FY 93)

Project Description

Particle physics and cosmology/astrophysics have evolved toward each other; the cross-fertilization has reached the point where experiments in one field can be justified based upon their impact on the other. In particular, results obtained from the COBE satellite have energized the study of early-universe physics. We would like to go beyond these recent achievements to study the early universe in greater detail. The purpose of this exploratory study was to determine what is necessary to make such measurements, what are the appropriate measurements, what one could learn from them, and how well the measurements need to be made.

Inflationary models of cosmology are interesting and are the only existing models that can explain the COBE and large-scale structure observations. In reviewing the results and theory, my collaborators and I have found that inflation not only makes the local universe flat, isotropic, and characterized with a near-scale-invariant spectrum of density fluctuations, but also simultaneously produces gravity waves. The gravity waves have nearly the same spectrum as the density fluctuations but have an amplitude set by the energy scale of inflation (potential of the inflation field at the time the gravity wave was generated). However, the density perturbations amplitude is set by the ratio of the energy scale of inflation to the derivative of the energy scale (cube of the potential divided by the derivative of the potential). Thus, if one were able to measure the gravity-wave spectrum amplitude or its ratio to the density spectrum amplitude, then one would determine the energy scale of inflation and its derivative.

The ratio of inflation-produced gravity waves to density fluctuations is related to the common slope of their spectra, which is determined by the derivative of the inflation field, so the measurement of either the slope or the ratio determines the other, in conventional inflationary cosmology. The measurement of one or both can be used not only to choose between current models of inflation but also to constrain their basic parameters.

Learning about the inflation potential is clearly exceptionally interesting physics. It is likely that the energy scale is on the order of 10^{16} to 10^{14} GeV. The low level of fluctuations observed in CBR anisotropy by COBE indicates that the energy scale of inflation is below a few times 10^{16} GeV at the time current horizon-size fluctuations were generated. The need for baryogenesis set the lower bound above 10^{9} GeV. Most current models of inflation require energy scales on the order of 10^{14} GeV or greater. This is thought to be a very interesting energy range in particle physics: 10^{16} GeV is the predicted energy of grand unification in supersymmetric particle physics theories. It is likely that there will turn out to be a deep connection between grand unification, supersymmetry, and inflation.

Accomplishments

I have investigated a number of possible approaches and joined with two groups in studies of the scientific and technical criteria of potential space-based missions. One group is primarily composed of Europeans. We submitted a proposal to ESA (the European Space Agency) to obtain funding for a one-year feasibility study. The proposal was accepted and the assessment study began. We are calling our mission COBRAS (Cosmic Background Radiation Anisotropy Satellite). COBRAS is on the scale of a medium-

cost mission for ESA. In addition to the proposal, a conference proceedings was published on the mission. A proceedings for the feasibility study that covers COBRAS in more detail is in press or printed.

During the feasibility study (termed the Assessment Study by the European Space Agency) COBRAS was married to another competing proposal, SAMBA (Satellite to Measure Background Anisotropies). The Assessment Study found that COBRAS/SAMBA could be accomplished within the guidelines of the ESA medium-class missions, even with the addition of SAMBA, which helped push the cost up to the limit. However, COBRAS/ SAMBA fit into the guidelines better than any of the competing missions. COBRAS/ SAMBA was one of four missions selected for a Phase A study. The Phase A study began in November 1994 with the selection of Matra Marconi as the contractor for the mission Phase A from four proposals submitted by industry for COBRAS/SAMBA. (COBRAS/SAMBA had the most industry proposals submitted.) The Phase A study is scheduled to last for 18 months with selection of one mission to go forward to flight.

The second group is producing a conceptual feasibility study for a medium-class American space mission called PSI (Primordial Structure Investigation). Reflecting their differences, the COBRAS studies focus primarily on the instrument and its performance while the PSI study is heavily weighted toward mission feasibility. At this stage PSI falls between small- and medium-class missions. Lack of opportunity for medium-class missions has slowed development, but a preliminary report was produced. Small-mission opportunities are expected to be available every year from NASA while the next medium-class is not expected for at least two years and not for launch before the year 2000. We are continuing the engineering effort for the study with support from the Director's discretionary funds at the Jet Propulsion Laboratory.

Last year the possible use of cosmic background polarization as a useful cosmological probe and discriminant was investigated. We found that it is not likely to be as useful as the anisotropy. We worked with Paul Steinhardt and his collaborators to push forward with determining how much could be learned from the cosmic background anisotropies and polarization and experimental limitations. Our work on the polarization is summarized in an internal group note. Steinhardt and collaborators published a paper on what could be determined from the cosmic background anisotropies alone and in combination with other measurements. It was clear that the cosmic background anisotropies are still the cleanest and best cosmological probe we have available.

Additional work was done on the questions of extragalactic foregrounds and the simulation of CMB anisotropies in collaboration with Professor Diego Saez. We also worked on the question of the foreground galactic emission on a number of fronts.

The major effort was directed to work on the possible missions, particularly COBRAS/SAMBA. The group has also worked to prepare for testing prototype systems. In particular, we have begun setting up a HEMT test system and facility. For the lower frequencies of a space-borne CMB anisotropy mission, HEMT receivers—particularly MMIC HEMT receivers—are a new technology that will improve performance and feasibility. As part of the COBRAS effort we have arranged to obtain a high-frequency (94-GHz) MMIC HEMT receiver. If it performs well, we will use it in an experiment. The deployments will either involve taking it to the South Pole or piggy-backing it on a balloon-borne payload.

Structural Biology Division

Hyperthermophilic Microorganisms

Principal Investigator: Rosalind Kim

Project No.: 94029

Funding: $108,000 (FY 94)

Project Description

Fermentation is the basis of approximately 12% of Japan's gross national product, according to an article in *Nature* some years ago. In addition, the majority of pharmaceutical products are made by fermentation procedures. In the fermentation plants in this country, the major engineering challenge is keeping the fermenters from overheating, since the microbes and enzymes used in conventional fermentation are thermolabile; yet fermentation creates heat. Since most chemical reactions proceed better at elevated temperatures, a new generation of enzymes and associated microbes could usher in a new age of fermentation technology that will treat the old problems as assets. The opportunities for novel catalytic processes is as vast as the niches that these organisms occupy. Thermotolerant methanogenic bacteria would be an associated technology that could aid in the development of new sources of energy by production of methane gas through fermentation.

This project exploits the biological information resident in the genomes of microorganisms living at extreme environments and attempts to understand the ecological niches that these organisms inhabit and their adaptations to these niches. The goals include:

1. Isolating thermostable enzymes capable of catalysis at extremely high temperatures.
2. Developing a fermentation technology designed to exploit the properties of these organisms.
3. Understanding the enzymatic catalysis of unusual chemical transformations.
4. Isolating an enormous collection of patentable sequences of direct industrial utility.
5. Providing an insight into the means by which enzymes can be rendered thermostable.
6. Generating a source of protein crystals better matched to higher resolution structural studies than those of existing protein crystals.

The information needed to encode thermoresistant forms of approximately 3,000 different enzymes would be provided by the sequence of the genome of a single microorganism. Experience with other microorganisms indicates this task will require sequencing between 3 and 5 million base pairs of DNA.

Accomplishments

Lambda genomic DNA library of *Pyrococcus furiosus* was obtained from Dr. Robert Kelly of North Carolina State University. The DNA polymerase gene has been cloned using primers synthesized against the gene based on the sequence published by the Yoshizumi Inhino Biotechnology Research Laboratory in Japan. The gene has been cloned into pET16B vector and the background strain is BL21(DE3)pACYC. The protein yield is 3–10 mg/l of culture. About 50% of the DNA polymerase expressed is soluble.

Lambda gem 11 library of *Methanococcus jannaschii* was obtained from Dr. Douglas Clark of the University of California, Berkeley. We are attempting to clone the EfTu and 5sRNA genes from this organism.

A clone containing the cyclic AMP receptor (CAR2) from *Dictyostelium discoideum* was obtained from Karl Saxe of Emory University. We are cloning the CAR2 gene into the vector pMAL p2 for periplasmic expression.

Data on DNA polymerase from Pyrococcus furiosus.

The gene for the DNA polymerase was cloned downstream from the T7 polymerase promoter in the pET16b vector from Novagen. In this construction, the protein carries a His-Tag at the amino terminus and the molecular weight is 92 kilodaltons. The induction of the protein is achieved with IPTG as shown in Fig. 1.

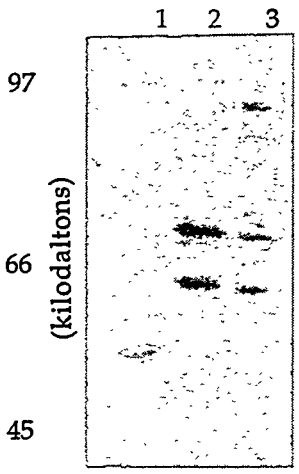

Fig. 1. 12.5% SDS/PAGE gel.
1. *Protein standard (14–97 kd)*
2. *Uninduced clone*
3. *Induced clone*

After induction of the protein, the crude extract is purified through a His·Bind metal chelation column to which the His-Tag binds, as shown in Fig. 2.

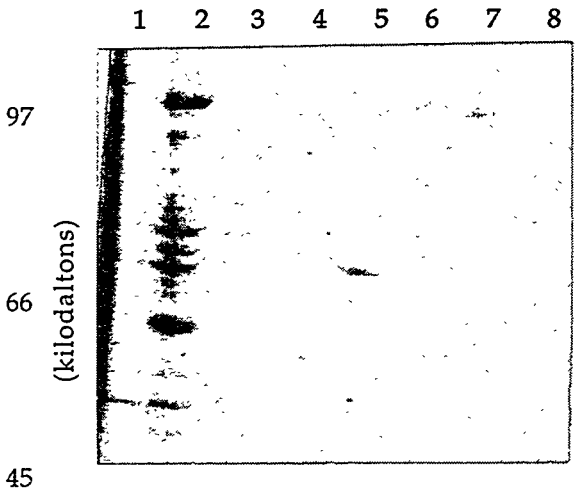

Fig. 2. 12.5% SDS/PAGE gel.
1. *Protein standard (14–97 kd)*
2. *Total crude extract*
3. *Flowthrough from the column*
4. *First wash*
5. *Second wash*
6. *Elution 1*
7. *Elution 1*
8. *Elution 2*

A Molecular Description of Transmembrane Signaling

Principal Investigator: Yeon-Kyun Shin

Project No.: 94030

Funding: $72,700 (FY 94)

Project Description

The phenomena of signal transduction have widespread implications for cell biology, physiology, and medicine. Receptors are fundamentally important proteins involved in signal transduction. This project explores a new electron paramagnetic resonance (EPR) approach to the investigation of the structure and dynamics of intact membrane receptors upon signaling. The major goal is to elucidate the mechanism of transmembrane signaling in receptors.

The recent advances in spin-labeling EPR—the site-specific spin-labeling (SSSL) method and time-resolved EPR spectroscopy—permit a new approach to the investigation of the structure and dynamics of proteins. The strategy is to site-specifically place a nitroxide spin label at any selected site in a protein using site-directed mutagenesis to replace a native residue with cysteine, which provides unique labeling sites for the nitroxide spin labels. Information on the structure and topology of a membrane protein is obtained from EPR analysis of spin-labeled mutants. Moreover, time-resolved EPR spectroscopy makes it possible to resolve the structural dynamics of spin-labeled mutants. With these methods we (1) characterize and define protein conformational changes, (2) identify all intermediates, (3) measure rate constants, and (4) interpret the kinetics in terms of structure. Experiments with a sufficiently large set of mutants would reveal the molecular mechanism. This unique EPR approach is applied to the intact bacterial chemotaxis receptor, a homodimeric membrane protein directly involved in signal transduction for bacterial chemotaxis. A startling discovery has resulted: many membrane receptors share the general structural organization. Thus it is likely that what is learned from this system will have application for other transmembrane signaling pathways.

Accomplishments

During the first year we set up state-of-the-art EPR instrumentation ready to perform spin-labeling studies on the bacterial aspartate receptor to investigate the mechanism of transmembrane signaling. The Bruker 300 E standard EPR machine was equipped with a loop-gap resonator specially designed for small-size aqueous protein samples. The microwave bridge was modified with a low-noise microwave preamplifier to improve the signal-to-noise ratio and the tuning capability.

Significant progress has also been made in preparing the mutants of the receptor for spin labeling. We have made a deletion mutant that includes only the periplasmic domain and the transmembrane domain. Now we are in the process of purifying cysteine mutants ready for the spin-labeling EPR study.

Although it was not a part of this project, as a direct outcome of this grant we have made significant progress in understanding the mechanism of flu virus entry to cells. We have described the new mechanism in a paper recently published in *Science*.

Publications

Y.G. Yu, D.S. King, and Y.-K. Shin, "Insertion of a Coiled-Coil Peptide from Influenza Virus Hemagglutinin," *Science* **269**, 274–276 (1994).

Y.G. Yu, T.E. Thorgeirsson, and Y.-K. Shin, "Topology of a Mitochondrial Signal Sequence in the Membrane-Inserted State," *Biochemistry* **33**, . 14221–14226 (1994).

Y.-K. Shin, "Influenza Virus Envelope Interaction with Host Cell Membrane May Provide a Model for HIV-Membrane Interaction," *J. NIH Res.*, in press (February 1995).

M.D. Rabenstein and Y.-K. Shin, "An Electron Paramagnetic Resonance Spectroscopic Ruler," submitted to *PNAS*.

T.E. Thorgeirsson, Y.G. Yu, and Y.-K. Shin, "A Limiting Law for the Binding of Polypeptides to Phospholipid Bilayers," *Biochemistry*, in press.

Multidivisional

SELECT, Development of a Site Remediation Analysis and Decision Support Software

Principal Investigators: Sally Benson, Nancy Brown, Joan Daisey, and Lois Gold

Project No.: 94031

Project Funding: $375,300 (FY 94)

Project Description

Efforts to safeguard human health in the U.S. by reducing environmental pollution are costly and hotly debated. One contentious issue is environmental remediation of hazardous waste sites, where cleanup is largely technology driven and expensive. It is critical that cleanup policy be based upon the best available science and be effectively communicated to risk managers and the public.

The goal of the SELECT project is to design and develop a distributed, object-oriented computer architecture to integrate, analyze, and present environmental information to help managers select cost-effective environmental remediation that maximizes health-risk reduction while minimizing costs. A salient feature of the architecture design will be the incorporation of state-of-the-art scientific advances in site characterization, subsurface and atmospheric transport processes, exposure pathway analyses, and health-hazard assessment, as well as financial analyses of environmental remediation. Comparison of estimated cancer risks from background exposures (e.g., from indoor sources or natural chemicals in the diet) with potential exposures from the contaminant site are also being incorporated.

The SELECT software tool is being designed for use by remediation project managers as well as technical experts in fields represented by each of the specialized models. The design allows for analyses performed by the experts to be saved for review by the manager. When fully developed, SELECT will accelerate the transfer to industry of state-of-the-art models and up-to-date information from the national laboratories. The project currently involves a partnership with McClellan Air Force Base, and it is being expanded to include other partners and users.

The process of SELECTing the most cost-effective and risk-reducing remediation method begins with the user providing site dimensions, pollutant choices, initial concentrations and sources, location of the affected population, and choice of remediation method (or no remediation). These data are then converted into an input file for a numerical model of pollutant transport, from which one obtains the time-dependent pollutant concentration field in soil and the time-dependent groundwater concentrations. Given these concentrations, one calculates the time-dependent exposure for the population of interest, from which the 70- or 14-year risk, beginning at any time, may be determined. After the risk has been estimated for the case of no remediation, the user may then decide that no action is necessary or may choose a remediation technology, carry out a post-remediation analysis, compare the newly calculated risk with the previous results, and determine the cost of risk reduction. By comparing the results of such analyses, the remediation manager may choose the best combination of cost and risk reduction.

Accomplishments

We have developed an initial version of a SELECT prototype. This initial prototype runs on a PC and is intended to display a simplified version of the site characterization, an animated three-dimensional depiction of the development of the concentration field over time, and graphical displays of exposure, risk, and cost effectiveness. The software allows the user to select the chemical of interest and the remediation method of choice, but it is presently developed for demonstration purposes only, and the effects of user actions are simulated.

The core of the SELECT software is the numerical model of pollutant transport in soil. We used TOUGH2 (previously developed at LBL with DOE support) to calculate the multiphase transport of volatile organic compounds. This model has been used to calculate the fate of trichloroethylene

(TCE) for the site at McClellan Air Force Base under the conditions of natural evolution, of connecting nearby residents to the municipal water supply, and of remediation, by soil–vapor extraction. The period covered by the model extends for 1,000 years from the beginning of the contamination. With the results of this model, we have made animations of the evolution of the concentration field for display in the initial SELECT prototype. Although an existing input method for site characterization data has been used for these runs, a modern interface is being developed. This interface, written in C++ and using the Motif library, is intended for UNIX workstations, but will be used in some other form for the production version of SELECT.

To calculate the exposure to humans of a pollutant in soil or water, we have used CAL TOX, a computer program created for the California Environmental Protection Agency. CAL TOX determines exposure on the basis of a simple mass-balance model of pollutant transport. Since our method of determining pollutant concentrations in soil and water is more complex and detailed, we obtained from CAL TOX only the relationships between exposure and concentration for the ingestion, inhalation, and dermal pathways. These relationships have been reduced to a simple matrix, which has been used to provide the graphs of exposure over time for the demonstration software.

The relationship between air exposure to humans in buildings and pollutant concentration in soil gas may be determined by the use of a numerical model. Such a model, STAR, has been used for many years in the study of radon entry by advective transport of soil gases into buildings. This model has been modified to determine entry rates of volatile organic compounds into buildings, from which human exposure can be found. New user-interface and graphic-output modules have been written for UNIX platforms. This software will be incorporated into the production version of SELECT, although it has not been used in the development of the initial prototype. Exposure to chemicals in outdoor air before and after remediation and treatment will also be added to SELECT.

The prototype design developed for risk-and-cost analysis uses subsurface contaminant flow through space and time, and corresponding estimates for multipath exposures. Potency values from our Carcinogenic Potency Database, from the U.S. Environmental Protection Agency, and from the California Environmental Protection Agency are used to estimate lifetime risk in the standard regulatory methodology of potency times dose. Potency values are used to compare chemical hazards at a site with hazards from background exposures. These values are also used to compare hazards for no action with alternative remediation strategies, as well as to identify the most cost-effective remediation strategy that meets user-specified risk-reduction goals. For a comparison of potential hazards from site contamination to typical or average background hazards, the HERP (Human Exposure/Rodent Potency) index is used for a variety of exposures to rodent carcinogens (both synthetic and natural chemicals) in air, food, and water. Permitted exposure levels of U.S. Occupational Safety and Health Administration and potency values for rodent carcinogens are used to estimate occupational hazards at contaminated sites. The prototype will include options for both individual and population risk, and an option for length of time exposed (e.g., lifetime or median residency time).

The SELECT module on risk plots dose versus time for each route of exposure (inhalation, oral, dermal) at the user-specified site of exposure. This plot is useful if a route-specific remediation is chosen by the user. By indicating the duration of time before any human exposure will occur, the impact of delaying remedial action can be seen. A set of carcinogenic potency values chosen by the user is displayed with potency values from the Carcinogenic Potency Database.

A histogram compares hypothetical cancer hazards from various background sources to the hypothetical cancer hazard from the no-action alternative at the chosen residence site. For no action and for each remediation alternative, a plot of risk versus time is displayed. Residence time is specified by the user. A risk curve for alternative remediation strategies, including no action, can be compared for either individual or population risk.

A comparison of hypothetical risk to projected total project cost (net present value) is plotted for each alternative, including the no-action alternative. The no-action alternative may or may not have a cost. In the case of the McClellan Air Force Base test site, we are associating the cost of well monitoring with the no-action alternative. Upon user specification of a target risk level (e.g., 10^{-6} for individual risk) and a time of interest (e.g., maximum hypothetical risk from each strategy),

SELECT responds with a plot highlighting the strategy with the lowest cost. Finally, a display of substitution risks from remediation strategies is displayed. In the SELECT initial prototype, we compare the hypothetical cancer risk from TCE in household water from wells near McClellan to hypothetical risks from drinking water chlorination byproducts typically found in the U.S.

Scientific developments have occurred in the 1990s that have important implications for the assessment of cancer risks posed by exposures to TCE that bear on potency and risk estimation in the SELECT prototype. Previous assessments of TCE carcinogenicity have been reviewed, and new developments in TCE-related epidemiology, carcinogenicity, and metabolite carcinogenicity, as well as related physiologically based pharmacokinetic models and data have been assessed. Based on this, new "no-observed-adverse-effect levels" have been hypothesized for human exposures to TCE.

Finally, cancer risks of zero predicted for exposures below those calculated for no-observed-adverse-effect levels have been compared to hypothetical risks associated with lifetime ingestive and multiroute household exposures to TCE in drinking water, at the current maximum contaminant level concentration of 5 ppb. A quantitative analysis of uncertainty in estimated cancer potency from several sources is in progress. This analysis compares TCE-related risks to corresponding risks estimated for concentrations of chlorination byproducts in household water that would be expected at the 80-ppb maximum contaminant level proposed by the U.S. Environmental Protection Agency for total trihalomethanes.

Acronyms and Abbreviations

AES	Auger electron spectroscopy
AFM	atomic force microscopy *or* atomic force microscope
ALS	Advanced Light Source
BRAMA	broad range atomic mass analyzer
CBR	cosmic background radiation
CCD	charge-coupled device
CD	circular dichroism
CDF	Collider Detector at Fermilab
CERCLA	Comprehensive Environmental Response, Compensation, and Liability Act
CFTR	Cystic Fibrosis Transmembrane Conductance Regulator
CMB	cosmic microwave background
COBRAS	Cosmic Background Radiation Anistropy Satellite
CSUMM model	three-dimensional mesoscale meteorological model
CVD	chemical vapor-deposited, *or* chemical vapor disposition
DBC	double-buffered counter chip
DOE	U.S. Department of Energy
DS	Down's syndrome
EM	electromagnetic
EMFAC	mobile source emission factor
EPICS	Experimental Physics and Industrial Control System
EPR	electron paramagnetic resonance
EPR	electron paramagnetic resonance
ESA	European Space Agency
FEJT	finite-element heat transport
FTIR	Fourier transform infrared spectroscopy
GC-MS	gas chromatography mass spectrometry
GMR	giant magnetoresistance
HEED	high-energy electron diffraction
HEMT	high electron mobility transister
HERP	Human Exposure/Rodent Potency
HREEL	high-resolution electron energy loss
HREM	high resolution electron microscopy
IC	integrated circuit
ISL	IsoSpin Laboratory
ITS	International Temperature Scale
LAHET	Los Alamos high-energy transport code
LAMPF	Los Alamos Meson Physics Facility
LANL	Los Alamos National Laboratory
LBL	Lawrence Berkeley Laboratory
LCP	left circular polarized
LDRD	Laboratory Directed Research and Development

LEED	low-energy electron diffraction
LHC	Large Hardron Collider
LLNL	Lawrence Livermore National Laboratory
MBE	molecular beam epitaxy
MC	melting curve
MCD	magnetic circular dichroism
MCNP	Monte Carlo neutron–proton transport code
MCP	microchannel plate
MGC	microgap chamber
MMIC	microwave monolithic integrated circuit
MR	magnetoresistance
MSGC	microstrip gas chamber
MWPC	multiwire proportional chamber
NBS	National Bureau of Standards
NCEM	National Center for Electron Microscopy
NIST	National Institute of Standards and Technology
NMR	nuclear magnetic resonance
NO	nuclear orientation
NSLS	National Synchrotron Light Source
NSOM	near-field scanning optical microscope
OTR	optical transition radiation
PCR	polymerase chain reaction
PDA	pentacosadiynoic acid
pdf	probability distribution function
PL	photoluminescence
PMMA	poly-methyl-metacrylate
PSI	Primordial Structure Investigation
QMS	quadrupole mass spectrometer
QPC	quantum point contact
R&D	research and development
RCP	right circular polarized
RCRA	Resource Conservation and Recovery Act
RCS	Rapid Cycling Synchrotron
rf	radio standard
RHIC	Relativistic Heavy-Ion Collider
ROG	reactive organic gases
RT-PCR	reverse-transcription polymerase chain reaction
SAM	self-assembled monolayer
SAMBA	Satellite to Measure Background Anistropies
SAW Devoce	Surface Acoustic Wave Devoce
SDC	Silicon Detector Collaboration
SIMS	secondary ion mass spectroscopy
SLAC	Stanford Linear Accelerator Center
SMOKE	Surface Magneto-Optic Kerr Effect
SNR	signal-to-noise ratio
SPLEED	spin-polarized low-energy electron diffraction

SQUID	superconducting quantum interference device
SR	synchrotron radiation
SSC	Superconducting Super Collider
SSR	simple sequence repeats
SSRL	Stanford Synchrotron Radiation Laboratory
SSSL	site-specific spin labeling
STAR	solenoidal tracker at RHIC
STM	scanning tunneling microscope
SVT	silicon vertex tracking
SVX detector	silicon vertex detector
SXPS	x-ray photoelectron spectroscopy
SXRFM	synchrotron x-ray fluorescence
TCE	trichloroethylene
tcl	tool command language
TEM	transmission electron microscopy
TIMS	thermal ionization mass spectrometry
TPC	time projection chamber
TPPE	two-photon photoemission
UAM model	three-dimensional mesoscale photochemical models
UCB	University of California at Berkeley
UCLA	University of California at Los Angeles
UHV	ultra-high vacuum
UHV-STM	ultra-high vacuum scanning tunneling microscope
UV	ultraviolet
VTX	vertex tracking
VUV	vacuum ultraviolet
XANES	x-ray absorption near-edge spectroscopy microprobe
XAS	x-ray absorption spectroscopy
XSW	x-ray standing wave
XUV	soft-x-ray and extreme ultraviolet (collectively)